Conformation-activated metal binding and oxidation in native anoxygenic photosystems

Ali Samaei

A Thesis
In
The Department
of
Physics

Presented in Partial Fulfillment of the Requirements
for the Degree of Master of Science (Physics) at
Concordia University
Montreal, Quebec, Canada

August 2018

CONCORDIA UNIVERSITY
School of Graduate Studies

This is to certify that the thesis prepared

By: Ali Samaei

Entitled: Conformation-activated metal binding and oxidation in native anoxygenic photosystems

and submitted in partial fulfillment of the requirements for the degree of

Master of Science (Physics)

complies with the regulations of the University and meets the accepted standards with respect to originality and quality.

Signed by the final examining committee:

Chair

Dr. Joseph Shin

Examiner

Dr. Valter Zazubovits

Examiner

Dr. Christophe Grova

Thesis Supervisor(s)

Dr. Laszlo Kalman

Dr. Sushil Misra

Approved by

Dr. Pablo Bianucci — Chair of Department or Graduate Program Director

Dr. André Roy — Dean, Faculty of Arts and Science

Date August 29, 2018

ABSTRACT

Conformation-activated metal binding and oxidation in native anoxygenic photosystems

Ali Samaei

In green plants oxygenic photosynthesis uses a manganese cluster to catalyze the oxidation of water molecule to molecular oxygen and protons. It is assumed that oxygenic photosynthetic organisms evolutionarily developed from their more ancient anoxygenic relatives. Until recently, the binding and utilization of manganese as a secondary electron donor in anoxygenic photosynthesis from *Rhodobacter sphaeroides* has only been achieved in genetically modified strains.

In our current work we revealed that the binding is facilitated by light-induced conformational changes. The conformationally-activated electron transfer from manganese to the oxidized bacteriochlorophyll dimer was found to be 50 % faster than that of detected in the dark-adapted conformation.

In order to characterize the accessibility of the binding site, the local dielectric constant was altered by incorporating hydrophobic molecules, such as detergents to the vicinity metal binding site. Tuning the dielectric properties of the binding site by incorporating detergent molecules diminished the observed differences between the electron transfers in the dark- and light-adapted conformations.

The EPR spectra of Cu-BTP complex at various BTP concentration and pH values were recorded. As the concentration of BTP increased, new spectral features emerged in Cu^{2+} spectra, indicating that the water molecules coordinating Cu^{2+} in the *hexa-aquo* complex are replaced by BTP molecules, forming a Cu-BTP structure. The pH dependency of Cu-BTP complex was studied by monitoring the EPR spectra of the complex from pH values of 4.0 to 9.5, and the effect of deprotonation of amine groups of BTP on coordination of copper ions was observed.

Acknowledgments

Firstly, I'd like to thank my co-supervisors, Dr. László Kálmán and Dr. Sushil Misra for their tireless guidance and help throughout my time here. The financial support was provided to me by their NSERC grants. I would have never been able to connect my knowledge of physics with the worlds of biology and chemistry if it weren't for them. Additionally, I'd like to thank my dear colleague Daniel Modafferi for his invaluable technical expertise and kindly supporting throughout my studies.

Contents

List of Figures

List of Tables

Notations and conventions

The following notations are used throughout this thesis:

ET	Electron transfer
R. sphaeroides	*Rhodobacter sphaeroides*
RC	Reaction Center
BRC	Bacterial Reaction Center
cyt c	Cytochrome c (electron donor protein)
cyt c_2	Cytochrome c_2 (BRC's native secondary electron donor)
WT	Wild Type (native strain of R. *sphaeroides*)
R − 26	Carotenoidless strain of R. *sphaeroides*
BCh	Bacteriochlorophyll
BPheo	Bacteriopheophytin
UQ_{10}	Ubiquinone Q10 (native quinone of the BRC)
P	Bacteriochlorophyll dimer cofactor of the BRC
B	Bacteriochlorophyll monomer cofactor of the BRC
B_A, B_B	Active B cofactor, inactive B cofactor

H	Bacteriopheophytin cofactor of the BRC
H_A, H_B	Active H cofactor, inactive H cofactor
Q	Quinone cofactor of the BRC
Q_A, Q_B	Primary quinone, secondary quinone
PDB	Protein Data Bank (http://www.rcsb.org)
LDAO	Lauryldimethylamine N-oxide
TX − 100	Triton X-100, or polyethylene glycol p-(1,1,3,3-tetramethylbutyl)-phenyl ether
BTP	Bis Tris Propane, or 1,3-is(tris(hydroxymethyl)methylamino)propane
Tris	Tris(hydroxymethyl)aminomethane
CAPS	N-cyclohexyl-3-aminopropanesulfonic acid
EDTA	Ethylenediaminetetraacetic acid
TEN	Solution of Tris-HCl, EDTA, NaCl
$TL^{0.X}E$	Dispersion of Tris-HCl, 0.X % LDAO, EDTA; where X varies from 0.03 to 0.1
$TL^{0.1}$	Dispersion of Tris-HCl, 0.1% LDAO
UV	Ultraviolet light
VIS	Visible light
NIR	Near infrared light
K_D	Dissociation constant
DAD	2,3,5,6-tetramethyl-p-phenylenediamine

Chapter 1

Introduction

1.1 Photosynthesis and its evolution from anoxygenic to oxygenic form

Photosynthesis is the primary process of biological energy conversion, where light energy is converted into chemical energy that sustains life on earth. In Photosynthesis the inexhaustible solar energy is exploited to fix carbon from carbon dioxide and split water, generating simple sugars used as energy sources for the living organisms. Therefore sunlight is the ultimate energy source for all biological processes. Furthermore, all of our food is based on photosynthesis and also current fossil fuels, which play key role in our modern life are the products of photosynthetic activities from millions of years ago. Our oxygen rich atmosphere, which is important for metabolic process in all respiring life forms is the consequence of realising oxygen from photosynthesis for billions of years [1].

Life began very early in Earth's history in photosynthetic organisms (Figure 1.1) and even today's life on Earth derives all its energy from this process. There are two types of photosynthesis: oxygenic and anoxygenic. Both oxygenic and anoxygenic organisms contain membrane bound protein-pigment complexes, photosystem II (PS II) and bacterial reaction center (BRC), respectively.

Anoxygenic photosynthetic organisms had already existed for about a billion years before oxygen evolving photosynthesis was developed (Figure 1.1). The main difference between anoxygenic and oxygenic photosynthesis is that anoxygenic organisms convert light energy to glucose without releasing oxygen. These anoxygenic photoautotrophs are believed to be the first examples of self-sustaining life [2]. Therefore, the development of the ability to split water into molecular oxygen and protons could be described as a key moment in the evolution of life on Earth. Ultimately, the abundance of oxygen in the atmosphere of earth provided the optimum condition for the evolution of more advanced organisms capable of using aerobic respiration.
In anoxygenic photosynthetic bacteria, BRCs are the pigment-protein complexes, which are responsible for the earliest steps in the energy conversion, while in oxygenic photosynthesis the PS II carries out the same process.

The conversion of light energy into chemical energy in both BRCs and PS II trans-membrane reaction centers is based on production of proton gradient across the membrane. PS II reaction center in algae, cyanobacteria and chloroplasts of green plants, is responsible to split water molecules into molecular oxygen, electrons, and protons, while in bacterial photosynthesis there is no oxygen in products, therefore the anoxygenic photosynthesis is used for this process [6].

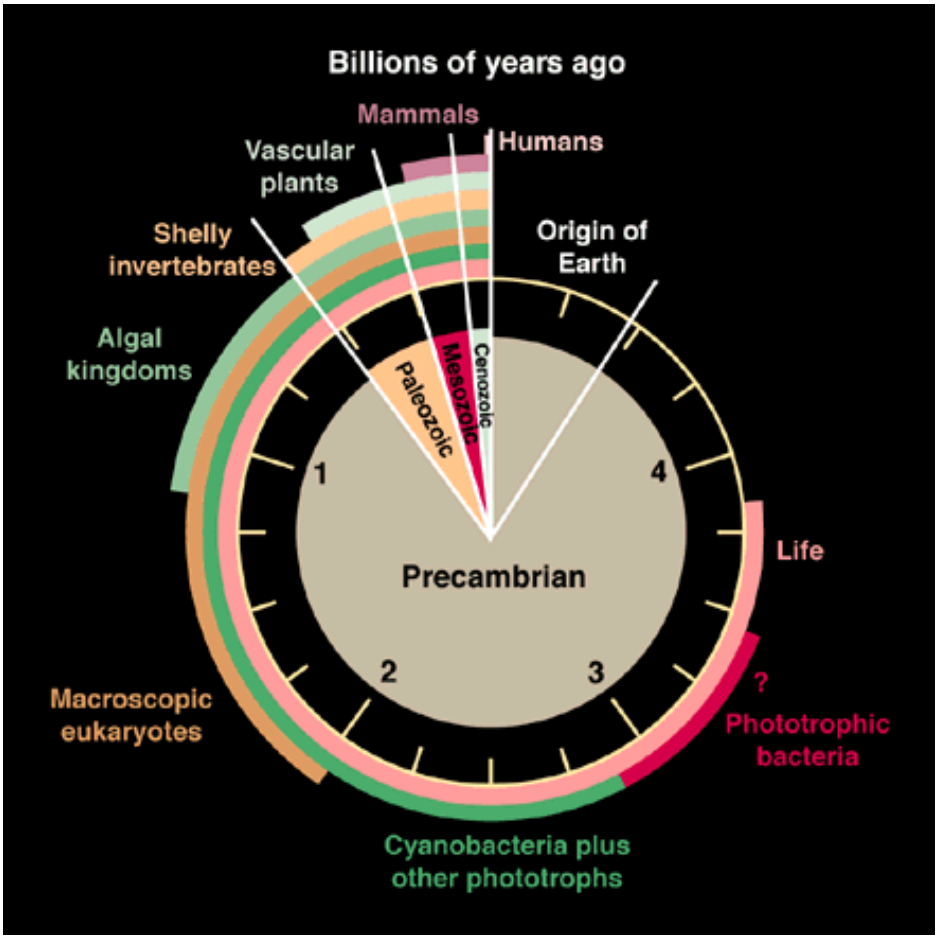

Figure 1.1 The biogeological clock of Earth. The complete history of the earth is shown in symbolic representation. Life began ~3.8 billion years ago and the primitive phototrophic anoxygenic bacteria appeared ~3.5 billion years ago. Evolution from anoxygenic to oxygenic form was occurred ~2.8 billion years ago in the Archaean oceans. Major development of the oxygenic atmosphere took place in another ~800 million years by oxygen production of cyanobacteria. The abundance of oxygen in the atmosphere was led to diversity of organisms and development of complex form of life on earth. Figure taken from [3].

In PSII water and carbon dioxide are used as the electron donor and carbon source in the conversion of light energy into chemical energy, respectively, meanwhile sugars are synthesized and oxygen is released as a by-product (Figure 1.2).By using advanced X-ray crystallography, it has been shown that the two proteins have very similar structures [4].

Based on these similarities a polygenetic study has been established to probe the share of PSII and BRC with a common ancestor [5]. Although BRCs and PS II have structural and

functional similarities, the higher complexity of PS II is an obstacle to elucidate oxygenic photosynthesis in its finest details.

The simpler BRC extracted from the anaerobically grown purple bacterium *Rhodobacter (Rb.) sphaeroides* is an excellent and simple model for studying biological energy conversion. Extensive research has been done in order to specify the characteristics of electron and proton transfer and conformational changes related to these processes in this pigment-protein complex [6,7,8,9].

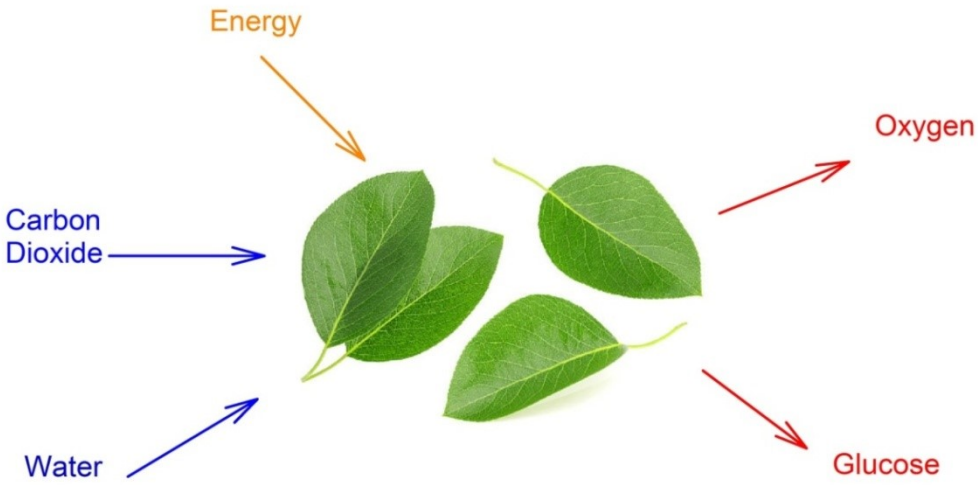

Figure 1.2: Oxygenic photosynthetic process. Carbon dioxide and water by using the energy of light are converted to oxygen and glucose in plants and cyanobacteria.

1.2 Structure of the photosynthetic reaction center

1.2.1 Comparison of BRC and PSII structures

X-ray crystallography has enabled the complete three-dimensional atomic structure of both the BRC and the PS II at a resolution of up to 1.9 Å [10,11]. The inner core of both PS II and the

BRC, are composed of multiple subunits with approximately 2-fold symmetry along a central axis normal to the membrane (see Figure 1.3).

The BRC of *Rb. sphaeroides* is composed of ~800 amino acid residues arranged in three subunits with total mass of ~100 kDa (1Da = 1g/mol). The two main subunits, L (light) and M (medium) each contain five membrane-spanning α helices. The H (heavy) subunit consists of short beta sheets and an α -helix, capping the cytoplasmic side of the L and M subunits.

The PSII has also two main subunits, D1 and D2 each contain five membrane-spanning α -helices and many other subunits surrounding its core.

The cofactors of the two photosystems are also similar and follow the same 2-fold symmetry axis, with pairs along the two main subunits. In the BRC nine cofactors are arranged from the periplasmic surface to down (top to bottom in Figure 1.1), which includes a dimer of bacteriochlorophylls (P) composed of two bacteriochlorophylls crossing the center of the protein, followed by two bacteriochlorophyll monomers (B_L and B_M), two bacteriopheophytins (H_L and H_M), two ubiquinones, (Q_A) Primary quinone and (Q_B) secondary quinone, and a divalent non-heme iron (Figure 1.3).

While PS II is much more complex protein and contains over 20 subunits and ~100 cofactors, it has a similar arrangement of cofactors with the bacteriochlorophylls (BChls) and bacteriopheophytins (BPheos) being replaced by chlorophylls and pheophytins, and having two plastoquinones, one non-heme iron and the oxygen evolving complex (OEC). The OEC is also located in this core, along the lumenal surface, near P (colored spheres in Figure 1.3B). The OEC is the site of water oxidation. It is comprised of four manganese (Mn) ions with varying oxidation states from +2 to +4, one divalent calcium (Ca^{2+}) ion, five oxygen atoms and several water molecules that help bridge the complex (Figure 1.3).

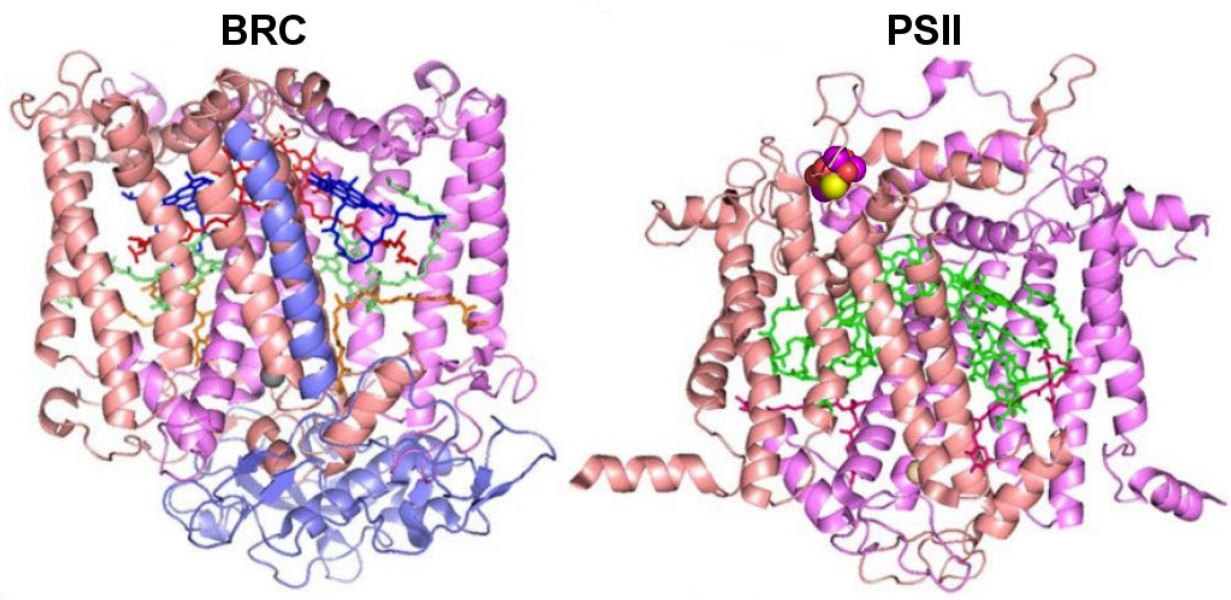

Figure 1.3 Structures of the BRC and PS II. The arrangement of subunits in BRC: M (salmon), L (purple) and H (blue). 5 transmembrane helices span the L and M subunits and 1 transmembrane helix spans the H subunit. The nine cofactors are: BChl dimer, P (red), BChl monomers, B (blue), Bpheos, H (green), ubiquinones, Q (orange) and non-heme iron (gray). The axis of symmetry for the cofactors passes vertically through the plane of the paper from the dimer to the non-heme iron. The arrangement of PSII protein: the D1 (purple) and D2 (salmon) subunits is shown, both consisting of 5 transmembrane helices. These subunits show a strong homology with the L and M subunit of the BRC with differences mainly in the C and N termini regions. The chlorophylls and pheophytins are depicted in green, the plastoquinones in purple and the non-heme iron in light brown. The OEC is also depicted as spheres, and colored by atom: Mn (purple), O (red) and Ca (yellow). Atomic coordinates taken from PDB codes 4RCR and 3WU2 for BRC and PSII, respectively.

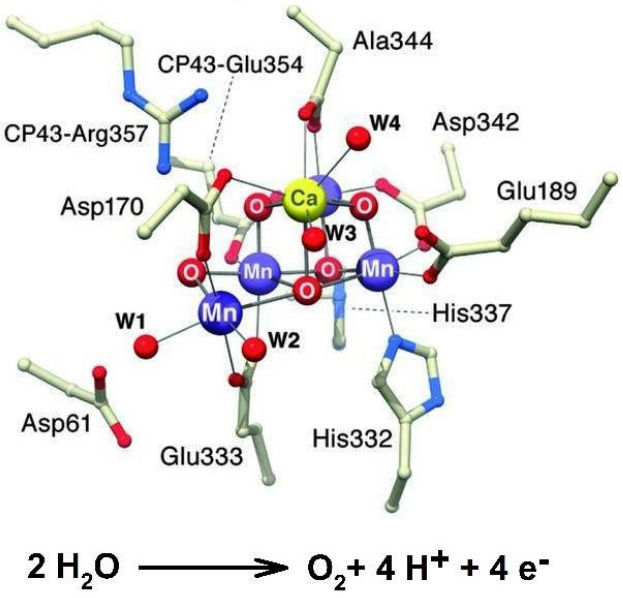

Figure 1.4:The oxygen-evolving complex and its surrounding residues. The complex is composed of four manganese ions, a calcium ion and several oxygen and water molecules (W_1,..,W_4) that bridge the complex. The manganese ions are utilised to store the electron equivalents. The chemical reaction of water splitting involves two water molecules transformed into molecular oxygen, four protons and four electrons in a four step process known as the Kok cycle. Figure taken from [12].

1.2.2 Electron transfer in the bacterial reaction center (BRC)

The overall mechanism of light-induced electron transfer in both BRC and PSII have been studied in great detail since the mid 1970s. This charge transfer process occurs with the quantum yield of nearly unity, making it most efficient biological energy conversion process in nature. Based on extensive spectroscopic studies, it was determined that upon light excitation of BRC, P acts as primary electron donor[13-15], Q_A and Q_B are primary and secondary electron acceptors,[16,17] and B_L and H_L are intermediate acceptors.

The charge transfer cycle of the BRC is illustrated in Figure 1.5. Absorption of photon excites primary electron donor, the bacteriochlorophyll dimer (P) to its electronic excited state. The electron sequentially is transferred to H of the L subunit (H_A) with the aid of the nearby B

(B_A) in ~3 ps. Then it is transferred to primary quinone (Q_A) molecule in the M subunit, in ~200 ps, before transferring to final electron acceptor, the secondary quinone (Q_B) in the L subunit which takes place from 6 - 150 μs.

Despite 2-fold symmetry in structure of BRC, Q_A and Q_B are in different dielectric environment, which lowers the energy level of Q_B relative to Q_A, thus allow electron transfer from Q_A^- to Q_B.

The electron transfer occurs completely along the L branch and the BChl monomer and BPheo of the M subunit (the Left half side of the protein) don't involve in the main photosynthetic process of the BRC, and likely serve as excitation quenchers, protecting overly excited RCs from prolonged exposure to the free radicals created from charge separation [18,19]. Electron transfer along the pigment cofactors of PS II follows a similar pathway, but with many more steps involved in the complete transfer.

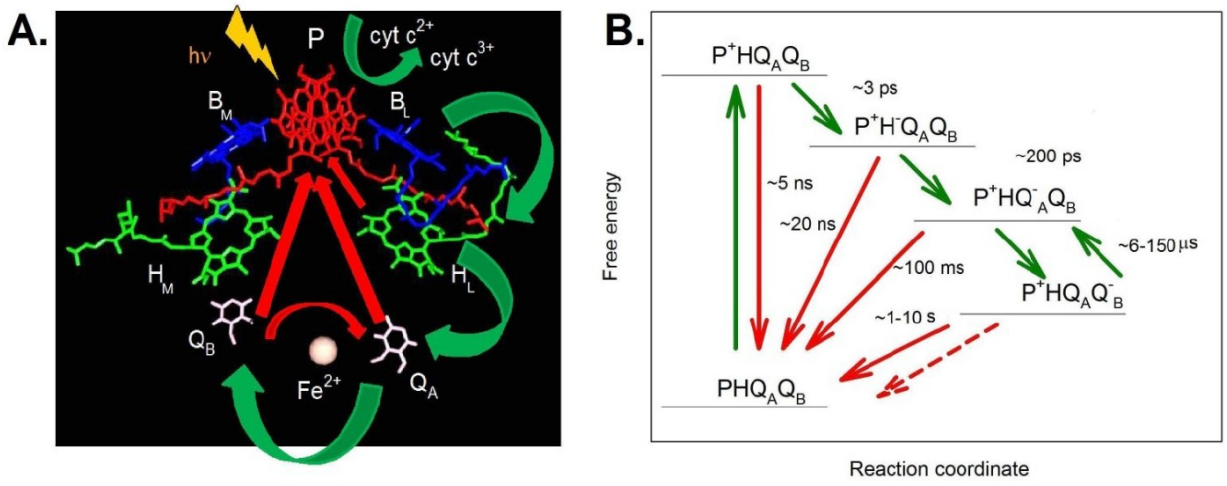

Figure 1.5: Light-induced electron transfer process in BRC. A: The light-induced electron transfer pathway. Upon light-excitation of the dimer the electron travels down in L branch sequentially from P to B, H, Q_A and Q_B. B: The free energy levels of various excited and charge-separated states formed in the electron transfer process, green arrows show the forward electron transfer while red arrows show the charge-recombination processes. The lifetimes of the forward (green) and reverse (red) reactions are presented.

In order to complete the cycle, the charge-separated state $P^+Q_B^-$ has to recover to the dark state PQ_B. In the BRC, the P^+ is reduced by a secondary electron donor protein, Cytochrome c_2 (cyt c_2) in 1-10μs [20]. Therefore the Q_B, can be reduced twice and during this process Q_B (accepts two protons from the cytoplasmic side to become quinol (Q_BH_2). The overall electron transfer cycle is shown in Figure 1.6.

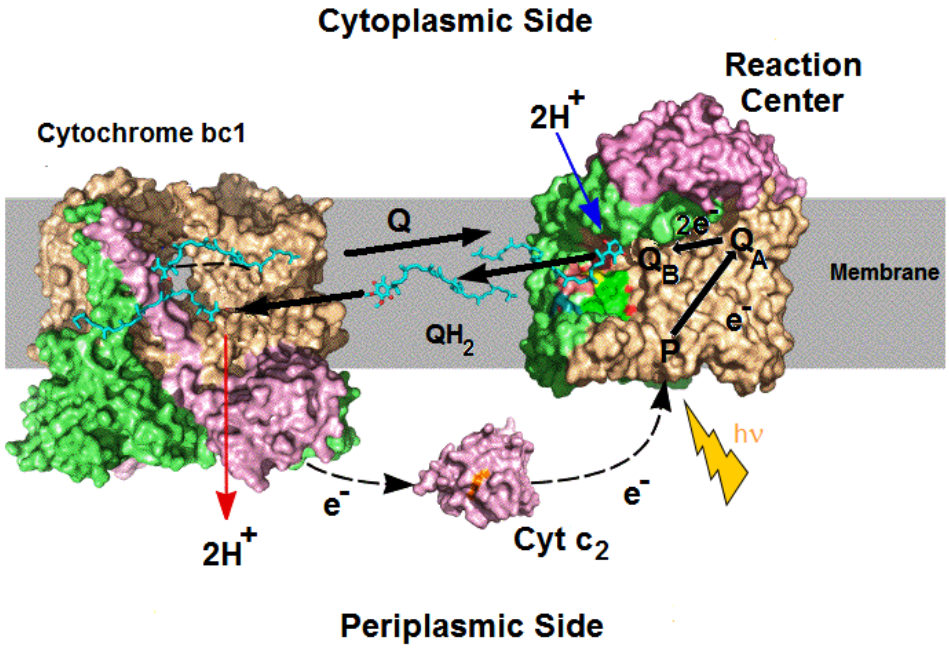

Figure 1.6: Charge transfer cycle in photosynthetic BRC. Electron and proton transfer cycle between the BRC, cytochrome bc_1 complex, and cytochrome c_2 inside the native membrane. Figure from Axelrod et al [20].

The Q_BH_2 is weakly bound to the Q_B binding site, and could be replaced by an oxidized quinone from the membrane's quinone pool. Then it diffuses to another membrane pigment-protein complex, the cytochrome bc1 complex. The Q_BH_2 will be dissociated and oxidized by cytochrome bc_1, and the cycle will continue by releasing its protons and electrons across membrane

to the periplasmic side. The generated proton gradient and electrons can be transferred by means of mobile electron carrier Cyt c_2 to complete the whole cycle.

In PS II the electron transfer process takes place in a similar way [21,22] (Figure 1.7). The light excites an electron on the special pair P_{680} and this process is followed by an electron transfer to the nearby pheophytin. The released electron is transferred to a plastoquinone in the Q_A site before arriving at the final electron acceptor, the plastoquinone at Q_B. Upon subsequent light excitation the Q_B is reduced again and this process is coupled by an uptake of two protons form quinol. Similarly to BRC the electron transfer process is unidirectional -along D1 branch- due to slight changes in the cofactor environment of PS II, which lowers the energy levels in the D1 branch as opposed to the D2 branch [21]. The exceptionally high oxidation potential of P_{680} (~1.2V) allows it to receive an electron from the nearby manganese cluster with the contribution of a tyrosine residue as an intermediate electron carrier [23]. The role of OEC is to extract four electrons from two water molecules, by splitting them into two oxygen molecules and four protons, which are released in the environment as by-products.

By comparison of BRC and PS II electron transfer processes, the presence of the multivalent manganese ions in the OEC complex is the key to understanding the mechanism of water splitting. In fact, in order to reach evolutionary transition from an oxygenic to oxygenic photosynthesis, a redox interaction must have been occurred between manganese and an anoxygenic BRC.

Actually we can emulate this evolutionary transition by studying possible interaction between manganese and anoxygenic photosynthetic reaction center in various conditions in order to develop and reproduce similar oxygen evolving cluster (OEC) to split water molecules to electrons and protons.

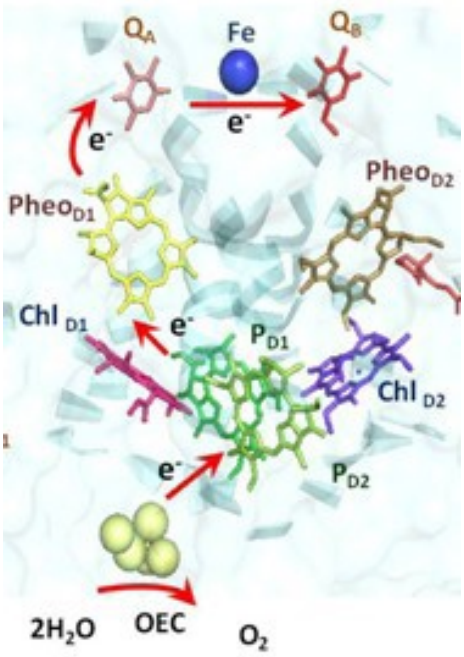

Figure 1.7: Arrangement of cofactors and charge transfer process in PS II. The PS II is composed four chlorophylls (two in the "special pair" P_{D1} and P_{D2} and two others Chl_{D1} and Chl_{D2}), two pheophytins ($Pheo_{D1}$ and $Pheo_{D2}$), two quinones (Q_A and Q_B), a non-heme iron (Fe) and the OEC. The electron resulted by light excitation of P is transferred down to PheoD1, Q_A and finally Q_B in the D1 side. Figure taken from [24].

1.3 Interaction of cofactors upon charge separation in BRC revealed by optical spectroscopy

Classically, light is considered to be a wave with an electric field component and a magnetic field component. In quantum mechanical view, light can be described as discrete particles or photons. The energy of these photons depends on wavelength (λ) through Planck's law:

$$E = hc/\lambda \qquad (1.1)$$

where the Planck's constant h is 6.63×10^{-34} J.s. Atoms and molecules have discrete energy levels. The light could be either absorbed or emitted for photons with an energy that matches the energy

difference between occupied and unoccupied levels. The electron can absorb photons and get excited to higher energy levels if the energetic difference between ground and excited state (transition energy) matches with the energy of incident photon. Since the energy is a measurable characteristic of a transition, the spectrometer measures absorption as function of wavelength, therefore the optical spectra are often plotted as function of λ [76].

Here in this study we used optical spectroscopy as a powerful tool to characterize the properties of the imbedded pigment molecules (bacteriochlorophylls, bacteriopheophytins and quinones) inside the specific protein environment. The electronic absorption spectrum of the BRC shows distinct features for each pigment due to differences in coordination and dielectric constants of their environment. (Figure 1.8 A)

The $\pi \rightarrow \pi^*$ electronic excitation due to great degree of conjugation in these molecules lowers their band gap and take them from ultraviolet (UV) spectral region to visible (VIS) and even to near infrared (NIR) regions [25]. The molecules have complex planar structures, each pigment possesses two dipole moments, Q_X and Q_Y, along which electronic excitation can occur.

The orientation of the Q_X transition dipole is in the plane of ring IV to ring II, and has absorption bands in the VIS region, at ~600 nm in bacteriochlorophylls and ~540 nm for bacteriopheophytins, while the Q_Y transition moment lies in the plane of ring III to ring I and has absorption bands in the NIR region due to a greater degree of delocalization along this transition dipole (Figure 1.8B).

In BRC the Q_Y absorption bands in NIR regime are 865 nm for the bacteriochlorophyll dimer (P), ~800 nm for bacteriochlorophyll monomers (B_L and B_M) and 760 nm in bacteriopheophytins (H_L and H_M).

The bacteriochlorophyll dimer is composed of two halves of electronically coupled bacteriochlorophyll molecules, therefore due to its high degree of conjugation the absorption band falls into the highest wavelength at 865 nm.

The Soret band due to porphyrin macrocycles has intense absorption below 400 nm, while the 280 nm band is characteristic to aromatic amino-acids such as tryptophans, tyrosines and phenylalanines, where the same $\pi \rightarrow \pi^*$ transition requires higher energy hence the delocalization of the electron in a single phenyl group is significantly lower than in the condensed aromatic systems of tetrapyrrols.

The fact that the absorption bands of the electronic transitions of the pigment molecules are sensitive to changes of their nearby protein environment such as the surrounding electric fields, optical spectroscopy is a useful technique to probe changes in the local electrostatics upon light excitation.

Upon light excitation the charge-separated state, P^+Q^- quickly forms by transferring an electron from P to Q and a local electric field across the BRC is established. The internal electric field generated by the light-induced charge separation affects the cofactors and causes detectable changes in the absorption bands in the electronic absorption spectrum of the BRC.

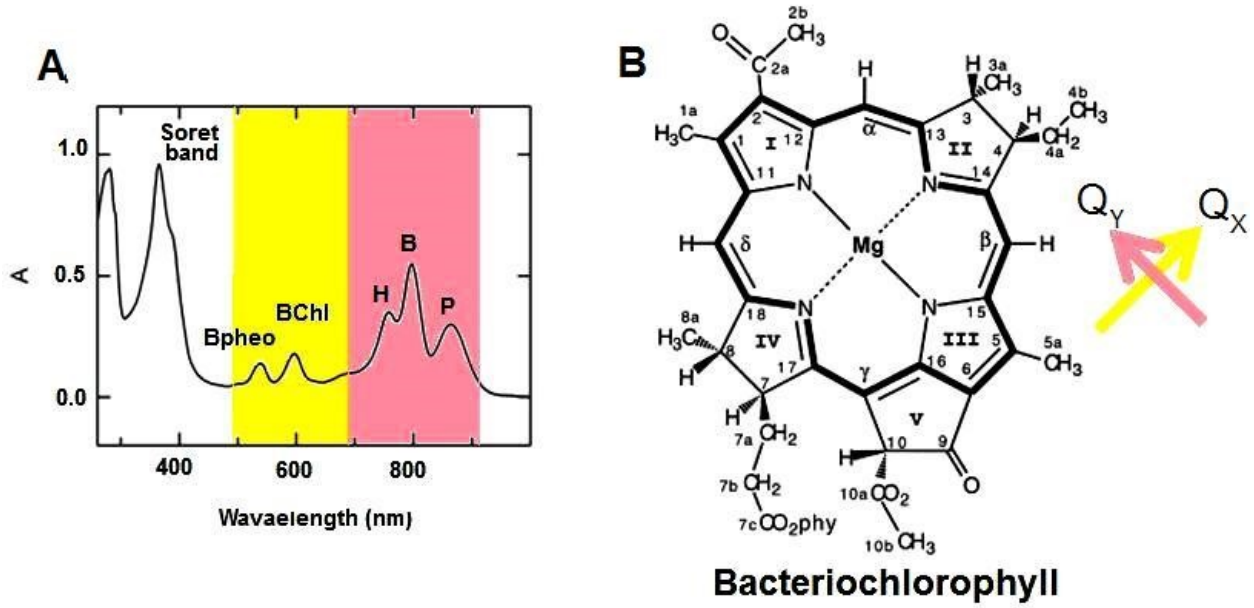

Figure 1.8: Electronic absorption spectrum of the BRC and molecular origin of these absorptions. A: UV-VIS electronic abortion spectrum of BRC. In the NIR region of optical spectrum, the Q_Y absorption band of dimer (P), two monomers (B_L and B_M), and two bacteriopheophytins (H_L and H_M) are around 865, 800, and 760 nm, respectively. In the Q_X region bacteriochlorophylls (BChl) and bacteriopheophytins (Bpheo) absorb around 600 and 540 nm in VIS region, respectively. B: The structure of bacteriochlorophyll molecule. The bacteriochlorophyll is a tetrapyrrole macromolecule with a central magnesium atom at the center. Ring I has 2-acetyl and ring V has 9-keto carbonyl group. Dipole moments of Q_X and Q_Y are between rings IV-II and rings III-I, respectively. Phy is a phytyl chain.

The absorption bands of the pigments can be bleached, shifted, or broadened upon light excitation. Bleaching is due to the change in oxidation state of a species whereas shifts are due to the changes in the polarization and broadenings are due to changes in dipole moment (Figure 1.9) [26].

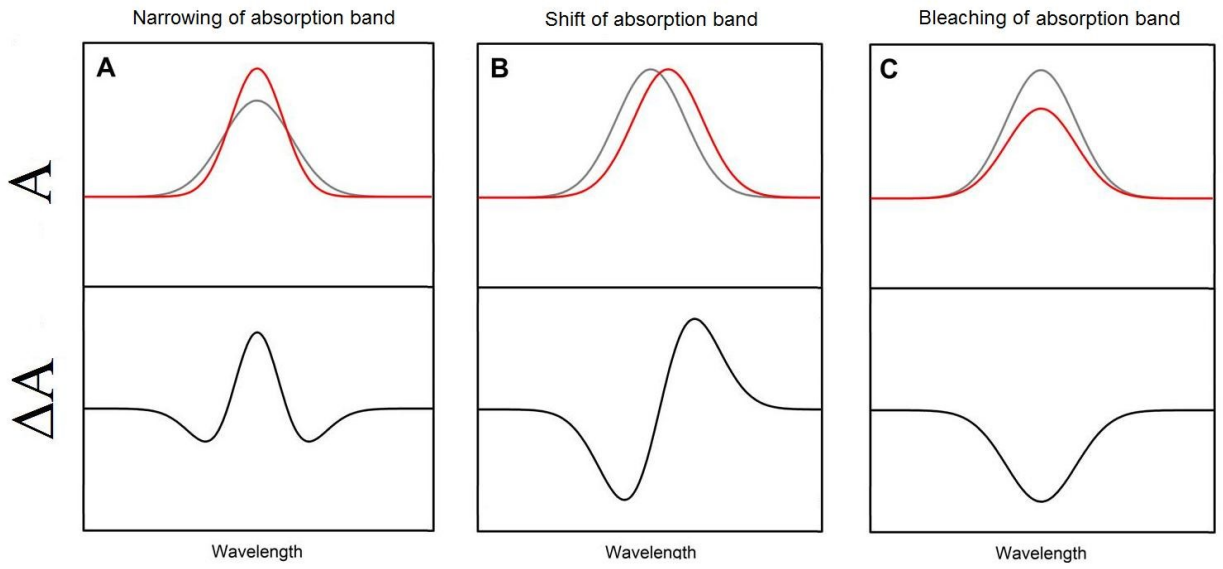

Figure 1.9: Electrochromic absorption changes. A: Shows narrowing of an absorption band due to changes of permanent dipole moment of absorbing molecule. B: the shift of an absorption band due to a change in polarizability of the absorbing molecule or disappearance of the absorbing species. C: the bleaching of an absorption band due to a change in oxidation state. Grey, red and black traces represent initial spectra, final spectra, and difference spectra between initial and final states, respectively.

The light-minus-dark difference spectrum, obtained by taking the difference between the light-induced spectrum and the dark spectrum, is useful tool to identify the subtle changes in the environment upon light excitation. This light-minus-dark spectrum can be decomposed into individual band components such as: a bleaching of the P band due to the formation of P^+ (oxidation of dimer); an electrochromic shift of the monomer band due to the presence of the positive charge on P after charge separation; and a bathochromic shift in the bacteriopheophytin bands mainly due to the nearby negative charge on the quinone. The light-minus-dark difference spectrum associated with the charge-separated state is presented in Figure 1.10 A.

The PQ^- state could be established by presence of a secondary electron donor, if the positive charge on oxidized dimer is removed by its reduction. The specific components of the light-dark absorption spectra of PQ^- state is shown in Figure 1.10 C. The remaining electric field due to the

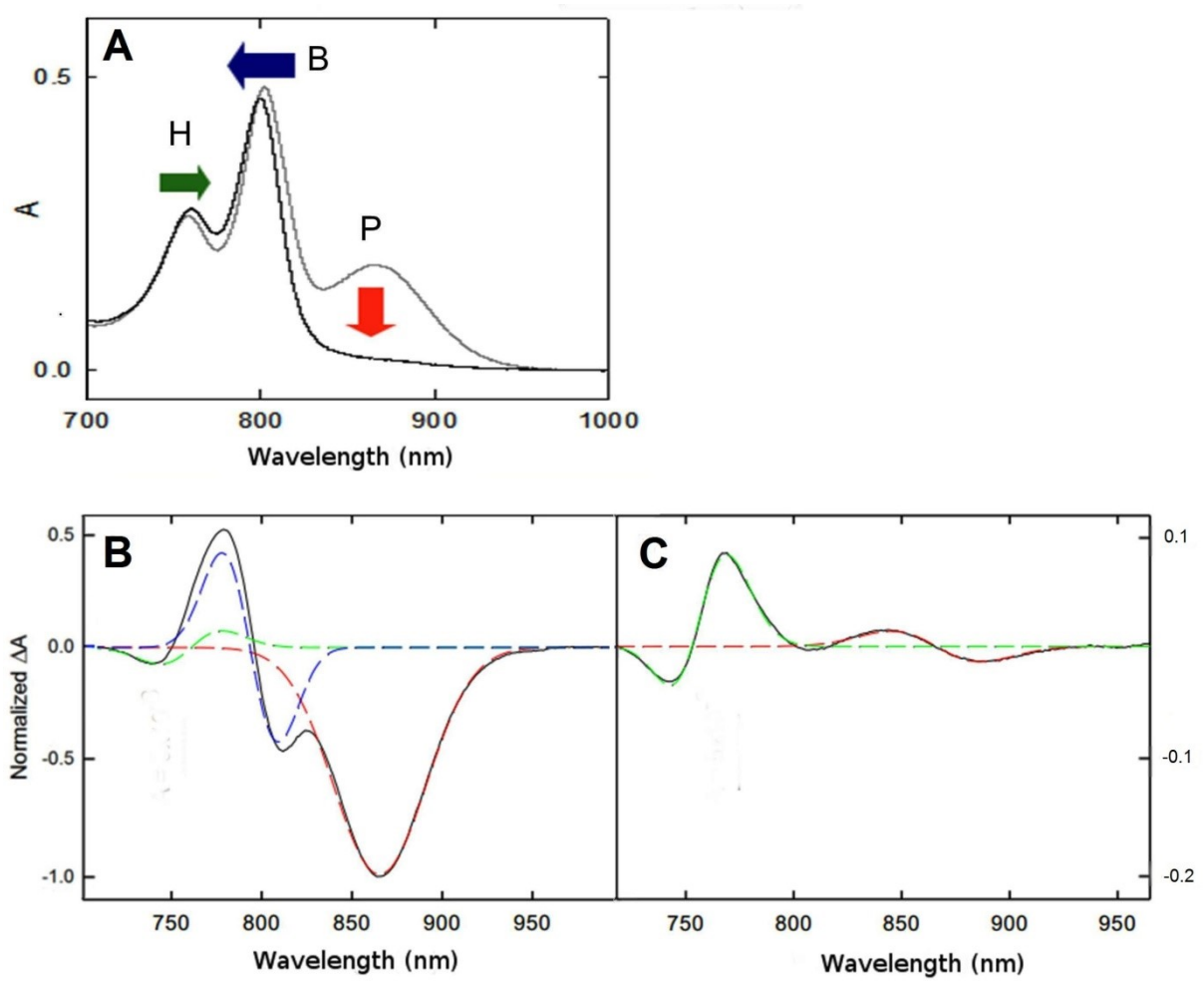

Figure 1.10: Effect of charge separation on absorption bands of the BRC. A: NIR absolute absorption spectrum (dark-adapted) of the BRC is shown in gray, and the spectrum recorded during light excitation is colored black. Light excitation causes the transfer of an electron from P to Q_B, or Q_A if no Q_B is present, (creating the P^+Q^-state). Colored arrows indicate the specific changes of each pigment, the bleaching of the P band, the blue shift of the B band, and the red shift of the H band. B: the light-dark difference spectrum corresponding to the spectra shown in panel A without presence of any secondary electron donor. The spectrum is decomposed into the individual component of each band (dashed lines), with colors matching the arrows of panel A. C: The light-dark difference spectrum with presence of a secondary electron donor, the oxidized P^+ is re-reduced to P state and only presence of Q state will affect the absorption bands.. The resulting light-dark spectrum is significantly different from P^+Q^- state, as it lacks the blue shift of B and the bleaching of the P band.

Q^- has a similar effect on the Q_y absorption bands, though the P band is no longer bleached but it does have a small blue shift due to the charge on Q^-. While the red shift of the H band is

similar, the blue shift of the B band is absent, as the corresponding transition dipole is perpendicular to the ring of dipole moment.

While the whole recovery of the P^+Q^- state takes place ~1-10 s in isolated BRCs (see Figure 1.5) and occurs through charge recombination, the recovery of the PQ^- state needs much longer time with a time constant of minutes because the reduced quinone has to find an electron acceptor from its surrounding in order to get rid of its charge.

As already mentioned optical absorption spectroscopy is a powerful tool to probe the appearance and disappearance of certain species. The linear correlation between the intensity of absorbed light and the concentration is given by the Beer-Lambert law:

$$A(\lambda) = \varepsilon(\lambda)cl \qquad (1.2)$$

where, A is the intensity of the absorption of light at a certain wavelength, c is the concentration of that species, ε is the extinction coefficient and l is the optical path length. Monitoring the kinetics of the absorption change at a characteristic wavelength is an effective method to explore reactions involving the pigments. In the present study the influence of metal ions on the absorption of the dimer was explored at 865 nm (Figure 1.11).

As it can be seen before illumination the absorption of dimer is constant. When the saturating light is turned on without the presence of a secondary electron donor (Figure 1.11 green trace) the absorption at 865 nm drops as the P is oxidized and the P^+ state is formed. Continuous illumination causes the protein to develop light-adapted conformational states. After light is turned off, a fraction of the protein that is in the dark-adapted conformation recovers instantaneously (blue trace). The fraction of the protein in the light-adapted conformations recovers at a slower pace (red trace) due to the stabilizing effect of the conformational changes on P^+.

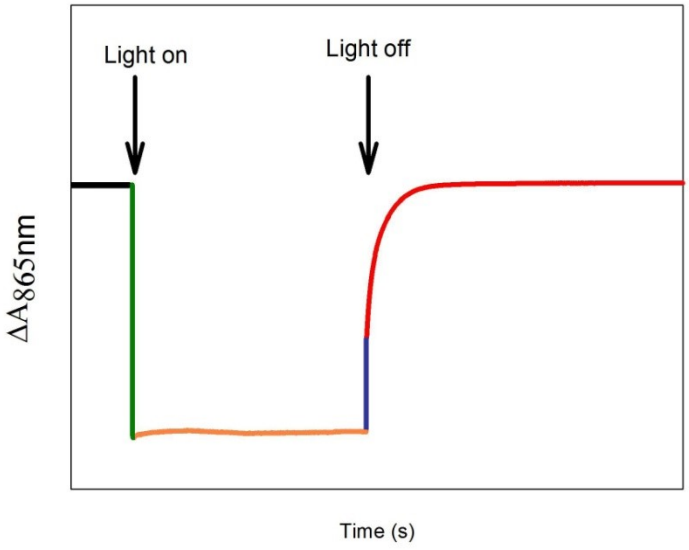

Figure 1.11: Schematic representation of kinetics of the light-induced absorption changes measured at Qy absorption band of P to identify different conformational states formed, during and after the illumination. Multiple components were identified in the kinetic traces. The green component is representative of the sudden change due to the formation of charge-separated state in the dark-adapted conformation. During prolonged saturating illumination light-induced conformational changes are occurred which can be assigned to orange constant part of the kinetics. When illumination is turned off, charge recombination from the dark-adapted conformation takes place very rapidly (~ 100 ms from Q_A and ~ 1 s from Q_B), which is represented by the blue part of the trace. The fraction of P^+ that is recovering from the light-adapted state recovers on a longer time-scale (red part of the trace). Charge-recombination kinetics can have multiple components related to different light-adapted conformational states, but only one component was shown for simplicity (pink trace).

1.4 Substitution of the natural membrane environment of the bacterial reaction center with detergent micelles

BRC is a membrane protein and in natural membrane environment it is surrounded with a large hydrophobic region with many neighboring proteins and molecules. In Nature, different membranes are classified based on different combination of phospholipids, phosphatidylcholine

and other kinds of lipids. This variation in combination mostly depends on growth condition such as temperature or aerobic/semi-aerobic growth [27].

In order to study different characteristics of BRC's, such as the energetics and kinetics of the electron and proton transfer it is necessary to isolate them from their natural membrane environment and substitute the membranes with simpler environment, for example with detergent micelles. This is also very crucial in optical spectroscopic techniques, as presence of surrounding molecules and complexes will strongly affect our measurements.

In this study the natural environment of BRCs is replaced by a detergent environment. (see Figures 1.12) These detergent micelles form a belt like structure around hydrophobic region of BRCs [35]. This micellar belt around the hydrophobic region is consisting of a layer of single molecules with their hydrophobic chains, which are pointed towards the BRC and the polar headgroups pointed to the outer surface. Micelles and liposomes are able to incorporate several BRCs. (see Figures 1.12 and 1.13).

The type and properties of the detergents also play key role on the function of the BRC [28,29]. For example, changes in hydrophobic thickness between the membrane substitute molecules and the BRC pigment, will alter the structure of both the BRC and nearby detergent molecules [30,31].

Several detergents are used as membrane substituents: lauryldimethylamine-oxide (LDAO, zwitterionic at pH 7.0 and above) [32,33], Triton X-100 or polyethylene glycol p-(1,1,3,3-tetramethylbutyl)-phenyl ether (TX-100, non-ionic), cetyltrimethylammonium bromide (CTAB, cationic), and deoxycholate (DOC, anionic).

The ionic detergent micelles have net head-group charges that repel one another so the aggregation number (the number of molecules present in a micelle) is less than 100 in aqueous

solution. Aggregation numbers of LDAO, TX-100, CTAB, and DOC detergents are 70, 140, 61, and 5 respectively in solutions without presence of any salt [34].

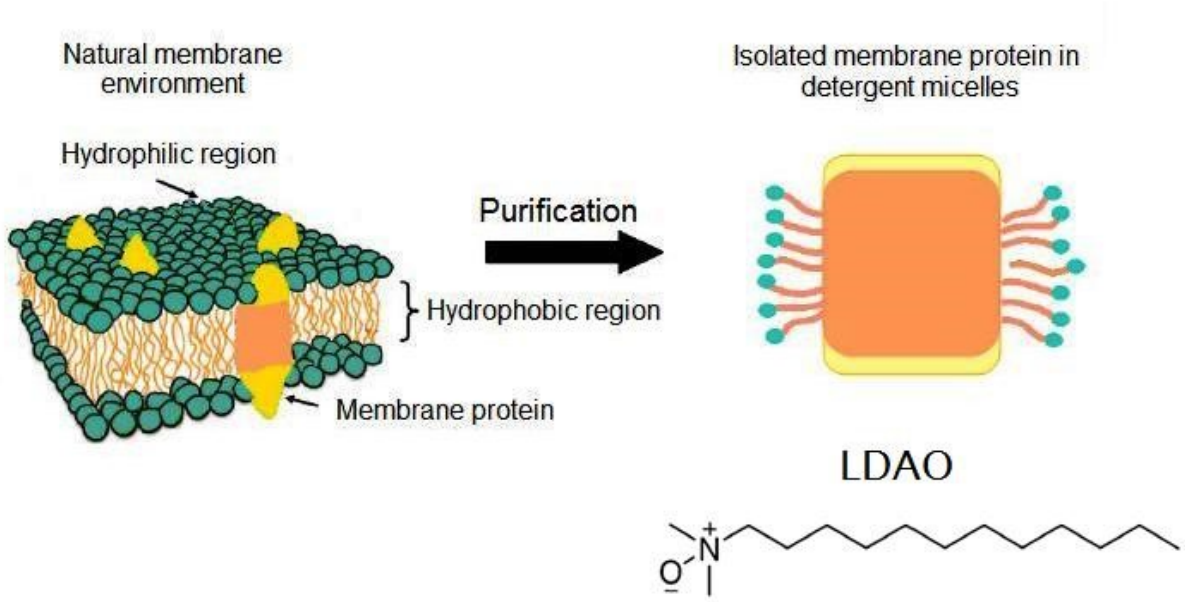

Figure 1.12: BRC in the natural membrane environment, in detergent micelles. After isolation of BRCs from natural membrane environment into membrane substituent detergent micelles, latter will form belt-like structure around the hydrophobic region of the BRC. The BRC's hydrophilic and hydrophobic regions are represented as yellow and pale orange colors, respectively. The chemical structure of typical detergent molecule, LDAO is shown. Figure taken from Deshmukh,[36].

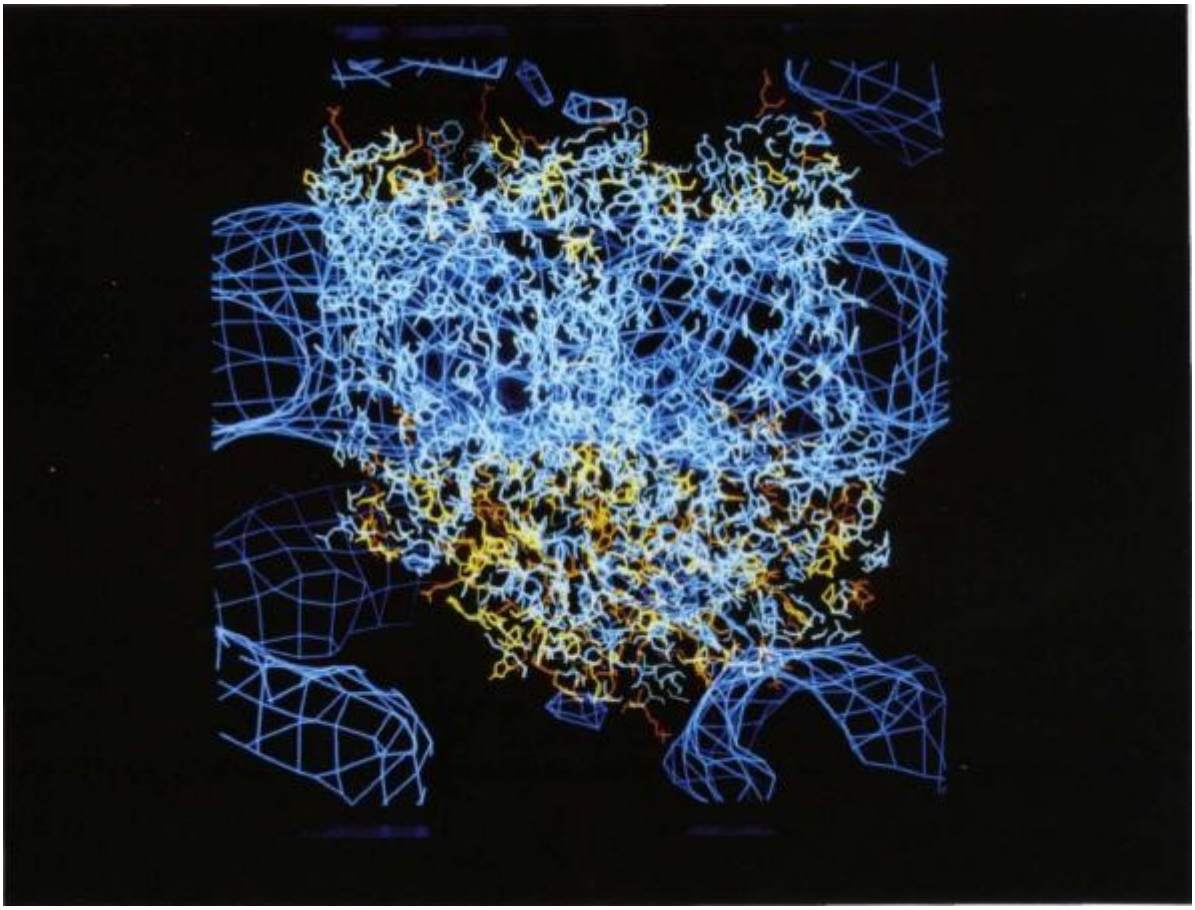

Figure 1.13: View of an RC with its detergent-phase ring. The color coding of the amino acid residues (from blue to red) according to the following hydrophobic scale are: blue, Phe, Met, lie, Leu, Val, Cys, Trp, Tyr; light blue, Ala, Gly, Thr, Ser; yellow. Pro, His, Gin, Asn; orange, Glu, Asp, Lys, Arg. The vertical axis of this picture is nearly parallel to the transmembrane axis of the molecule. This view shows that the detergent-phase ring is located exactly at the height of a more or less median region of subunits L and M, which appears completely devoid of polar and charged residues, and thus represents very likely the transmembrane region of the RC molecule. This detergent ring and the region of the detergent phase below which interacts with the H subunit belong to two different parallel detergent ring chains. Figure from Roth et al [35].

1.5 Light-induced conformational changes in BRC

In a series of work our group has earlier identified that the light-induced conformational changes observed since the mid 1980s that responsible for the extended lifetime of the charge-

separated state originate from the vicinity of P and not from the neighborhood of quinones [7-9,68]. The structural changes were sensitive to the presence or absence of the carotenoid molecule next to the inactive bacteriochlorophyll monomer (B_M) and the presence or absence of detergent or lipid molecules occupying this carotenoid binding site [9,8,68]. Briefly, the conformational changes involve the deprotonation of the M210 Tyr (Figure 1.14) that in turn depending on the conditions can either be H-bonded to the 2-acetyl group of P_M or serve as a transient 6^{th} ligand to the central Mg of P_L. The delivery of the proton from M210 Tyr increases the local dielectric constant of the hydrophobic cavity of the region and resulting in the rotation of the 2-acetyl group of B_M and up to ~80 mV decrease of the oxidation-reduction potential of P. Populating the carotenoid binding site with charged detergent molecules changed the electronic structure of P that could also be induced by the light-induced structural changes [8]. Binding of lipids and introducing hydrophobic mismatch the lifetime of the conformationally altered states could be extended to hours [64]. The structural changes could be prevented entirely if the delivery of the proton from M210 Tyr was blocked by introducing positively charged His residues nearby [7,9]. Interestingly, the manganese binding site that was discovered very recently also located at the immediate vicinity of B_B and the carotenoid binding site [36]. This coincidence presents an opportunity to link the manganese binding with light induced conformational changes.

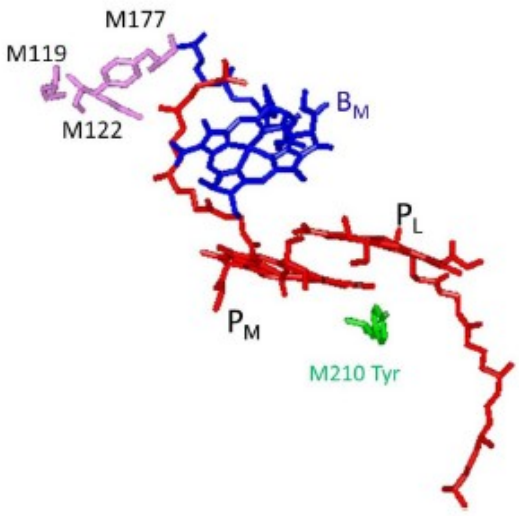

Figure 1.14: Structure of the bacteriochlorophyll dimer P. The residue with protonatable side chain Tyr M210, the bacteriochlorophyll monomer (B_M) and the residues of carotenoid binding site are also shown. The following residues make up this site: Ser M119, Met M122, and Tyr M177. Coordinates were taken from PDB entry code: 4RCR.

1.6 Metal binding sites in BRCs

Transition metals bound to BRCs can facilitate or inhibit a number of reactions. Studying the effect of metal binding on kinetics of electron transfer and charge recombination can reveal details of function of reaction centers. Several metal binding sites were identified in BRCs and few are shown in Figure 1.15. It has been reported that Zn^{2+} is able to bind RC with high affinity and can affect the rate of electron transfer from primary acceptor (Q_A) to secondary acceptor (Q_B) by changing the dynamics of protein [56,57]. It was shown that in addition of Zn^{2+}, Cd^{2+} and Ni^{2+} are able to bind the surface-accessible region on H-subunit RC, which is defined as Site 4. Due to presence of metal in this binding site a significant reduction in the rate of proton transfer was observed by providing a barrier for proton entry internal proton transfer pathway [58-60].

A site homologous to the (OEC) binding site in photosystem II (Site 3) was designed by genetic modification, where the Met is replaced to Glu at M168 and Gly to Asp at M288 positions. These substitutions led to creation of additional hydrogen bonds between P and the surrounding protein, therefore the stability of the positive charge on P^+ decreased and the P/P^+ potential has been elevated by 60 - 125 mV for every single hydrogen bond. By these mutations the P/P^+ potential of BRC was elevated from ~500 mV to up to~770 mV [37].

Fe^{2+} with dissociation constant ~1 μM in presence of sodium bicarbonate can bind to Site 3 and reduce the oxidized dimer [61]. Bound Mn^{2+} at Site 3 could reduce P^+ at pH 7.0 in presence of bicarbonate but at pH 9.0 presence of bicarbonate was not necessary for redox activity of Mn^{2+} [62]. The manganese in hexa-aquo complex forms a perfect octahedral complex six symmetrically arranged water molecules. Hence the Mn^{2+}/Mn^{3+} midpoint potential in hexa-aquo complex is 1.2 V, the substitution of one or two bicarbonate $(HCO_3)^-$ ions with water molecules, the potential of the manganese in such complexes can be lowered by ~300 mV and ~600 mV respectively [38,39].

By manganese coordination with bicarbonate and by elevating the pH the Mn^{2+}/Mn^{3+} potential was lowered to ~620 mV which is below the P/P^+ potential of mutants (modified BRCs) [38]. However, due to low binding affinity between manganese and modified BRC, the low yield ET between Mn^{2+} and P^+ was observed [38]. In other study the amino acid residues with carboxylic acid groups were added, with total six mutations, allowed 1st order ET from Mn^{2+} and oxidized P of modified BRC [41].

Metal binding Site 2, is located on the periplasmic surface of the BRC, where the natural secondary electron donor, cyt c_2 binds to BRC. Metal binding Site 1 is totally different in nature from other metal binding sites, since it is not solvent accessible, and located in the hydrophobic cavity of BRC, at the inner opening of the carotenoid binding site. The binding of Mn^{2+} at two other different location, Site 1 and 2 was predicted and then confirmed experimentally [43]. The

light-induced conformational changes described in Section 1.5 above have been shown to be blocked by the presence of Mn^{2+} at Site 1 [36].

In another study the BRC was exposed to Hg^{2+}, about 500 mercury ions binding to RC with low affinity ~50 mM^{-1} was observed. The high number of sites is due to that mercury only requires one ligand as opposed to Zn^{2+} Cd^{2+}, Ni^{2+}, and Mn^{2+} that require six ligands to form a restricted geometry dictated by the splitting of the d orbital energies. While the primary quinone was not perturbed upon mercury (II) presence, with low affinity the mercury (II) at binding site close to the secondary quinone caused inhibition of the interquinone electron transfer. Additionally the proton gate at the cytoplasmic site had the highest affinity for Hg^{2+} binding and blocked the proton uptake [63].

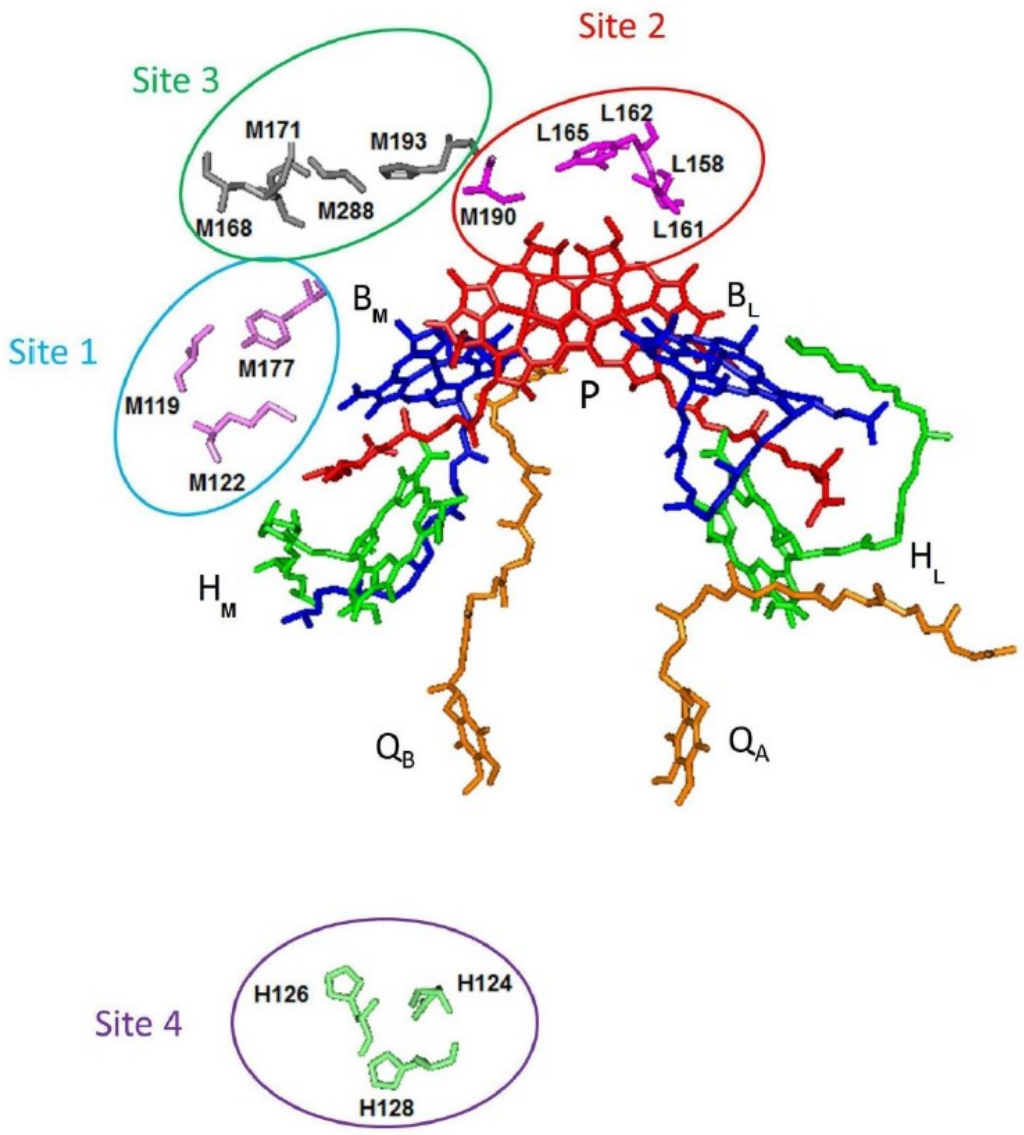

Figure 1.15: Structural views of the BRC showing probable identified metal binding sites. Coloring of the cofactors is the same as in Figure 1.3. The first site is predicted to be in the hydrophobic cavity near the inactive bacteriochlorophyll (B_M). The following residues make up this site: Ser M119, Met M122, and Tyr M177. In carotenoid-less strain (R-26) the LDAO molecule (cyan) have been observed to bind precisely to Site 1. The second site is on top of the dimer (P) at the periplasmic surface, where the natural electron donor, cyt c_2 also binds. This site consists of Ser L158, Gly L161, Tyr L162, Gly L165, and Ser M190. Binding Site 3 is also on the periplasmic surface, designed by mutation at the site homologous to the (OEC) binding site in photosystem II. In M2 mutant metal ion at this site is coordinated by His M193, Glu M173 and two genetically modified residues: Glu M168 and Asp M288. Metal binding Site 4 is on the surface of BRC, near Quinone (Q_A) binding site, and is consist of His H126, His H128 and Asp H124. Atomic coordinates taken from PDB code:1RG5

1.7 Research perspectives

To mimic the incorporation of transition metals, such as manganese with ancient anoxygenic RCs in order to involve them in charge transfer is considered an evolutionary milestone that can help us to unravel possible obstacles, which ancient RCs would have had to overcome in an evolutionary process.

Previous studies were based on two approaches to model this transition, either recreating changes in the native BRC that the high potential electron donors being able to reduce the P^+ or trying to lower the oxidation potential of electron donors to the vicinity of the reduction/oxidation potential of P.

1.7.1 Manganese as secondary electron donor in native BRCs

The incorporation of manganese to serve as an electron source to native BRC is done by changing environmental factors such as coordination of manganese with other compounds. Upon using high concentration of bicarbonate to coordinate manganese, Mn^{2+}/Mn^{3+} midpoint potential was lowered to ~ 520 mV. Although this potential still higher than unaltered P/P^+ potential in native BRC, electron donation from Mn^{2+} to P^+ was observed with very low yield [42].

By spontaneous coordination of manganese with bis-tris propane the redox potential of manganese (II) to manganese (III) transition was lowered to ~ 400 mV at pH 9.4, below the P/P^+ potential, and allowing the reduction of P^+ by this complex with a rate that competes with the charge recombination reactions.

Bis-tris propane (BTP), $C_{11}H_{26}N_2O_6$, is an organic molecule with six hydroxyl groups and two secondary amine groups placed symmetrically.(see Figure 1.16) It has a wide buffering range,

from 6 to 9.5 due to its two pK_a values, 6.8 and 9.0. Above pH 9 both amine groups of BTP are deprotonated, providing an additional ligand to coordinate manganese and lowering the manganese potential at high pH values. The maximum accessible pH for Mn-BTP complex is 9.4, which above this range the solution is not stable due to auto oxidation of Mn^{2+} to Mn^{3+} [48].

Additionally upon binding manganese to BRC, the P/P^+ potential elevates from ~500 mV to ~600 mV. Once the manganese incorporation is occurred, the electron transfer between Mn^{2+} and P^+ takes place iteratively [43].

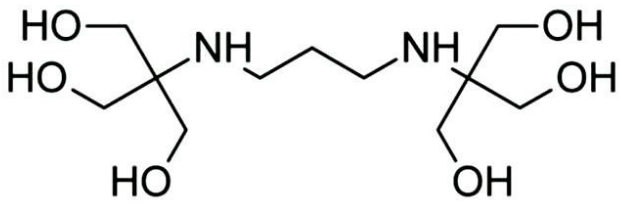

Figure 1.16: The molecular structure of bis-tris propane (BTP). There are two amine groups and six hydroxyl groups present in the molecule.

1.7.2 Objectives

The evolution from anoxygenic photosynthesis to oxygenic photosynthesis occurred by the incorporation of a transition metal complex by primitive photoautotrophs over 2.8 billion years ago. The development of this ability to split water molecules into molecular oxygen and proton and the harvesting of the resulting high-energy electrons had profound impact on life and earth.

Uncovering the details of this evolutionary transition is not only important in terms of enhancement of our knowledge about the history of life on earth, but it could also be used to design artificial energy converting device on the basis of oxygen producing photosystems.

In order to achieve this goal the mechanism of metal binding and oxidation in BRC must be understood, then attempt to improve it.

One of important step of this improvement is tuning the driving force for electron donation from manganese to oxidized dimer. The interaction of Mn^{2+} with BRC must be thermodynamically tuned by mapping energy levels of oxidation/reduction potential of manganese and oxidized dimer.

On the other hand the binding of metals to BRC must be modified electrostatically, since interacting entities are in entirely different dielectric environment. The dielectric control of metal binding in addition to the well- electrostatic control, increases the affinity of binding and leads to electron donation with high yield.

The organization of this thesis is as follows. The samples investigated and the techniques used to characterize them are described in Chapter 2. The data are included in Chapter 3. The analysis of the data is given in Chapter 4. The conclusions are summarized in Chapter 5.

Chapter 2

Materials and Methods

2.1 Growth of *R. sphaeroides* bacterium

Cell growth and purification of the BRCs from carotenoid-less strain R-26 and wild-type (WT) of *Rb. sphaeroides* were done according to the protocol outlined by Feher and Okamura [44]. The whole process involves preparing and sterilizing growth media, inoculation cells and finally photosynthetically growing bacteria. In first step the growth media was prepared with 4 g of casamino acid, 4 mL of growth factor (vitamin solution), 80 mL concentrated base, 40 mL potassium succinate solution, 80 mL phosphate buffer (1 M), and 25 mL of ammonium sulfate. Then the volume was adjusted to 4 L. The media was then bottled in 1 L Pyrex bottles and the solution was autoclaved for 1 hour at 121 C, in a SV-12 scientific pre-vacuum sterilizer. Then the bottles cooled to room temperature before doing inoculation. The inoculations were performed by adding approximately 110 mL of fully grown bacteria stored from previous growths culture to the prepared media. To avoid any external contamination, all inoculations process was done on a sterilized bench near to electric burner in dark room.

Right after inoculation step the bottles were placed in chamber which is equipped with six 60 W tungsten light bulbs and reflective siding and were kept in the dark for maximum 6 hours in order to consume the oxygen and promote the anaerobic metabolism of any oxygen in the media. After 6 hours the light bulbs were turned on and a thermometer was placed inside the chamber to control the temperature and prevent over heating the bottles. R. *sphaeroides* utilizes visible and near infra-red light and to fulfill this wide spectrum the incandescent lighting was chosen. *Rb. sphaeroides* was grown under anaerobic conditions in the presence of light for two days.

Once the cells were completely grown, the bacteria suspension was centrifuged using Beckman J2-HS centrifuge with a JA-10 rotor at 7000 rpm, and 4 ˚C for 20 minutes. Then the supernatant was discarded, and the cells were collected, weighed, and stored at -20 ˚C.

The solutions used for bacterial growth media are prepared as follows:

Vitamin solution: The growth factor or vitamin solution was prepared by mixing 2 mg of biotin, 50 mg of sodium bicarbonate, 100 mg of nicotinic acid, 50 mg of thiamine-hydrochloride, and 100 mg of para amino benzoic acid in distilled water. The solution was boiled to dissolve all the ingredients and the final volume was adjusted to 100 ml. Once it is dissolved, the solution was autoclaved for 1 hour at 121 **ºC** ˚C, and cooled for storage.

Concentrated Base: Concentrated base was prepared by mixing 12 g of potassium hydroxide and 20 g of nitrilotriacetic acid in 1 L of distilled water. The solution was stirred with a magnetic stirrer for 20 minutes. This process leads to sediment and then only the supernatant was used. Then 58 g of magnesium sulfate heptahydrate, 6.8 g of calcium chloride dehydrate, 200 mg of ferrous sulfate heptahydrate, and 4 ml of ammonium molibdenate solution in the portion of 1 mL were added slowly, waiting for completely dissolving after each addition. All contents should be dissolved

before addition of the next. Finally the 'metals 44' solution was added, pH adjusted to 6.7 by using 5 % m/v KOH at a rate of 2 mL per minute and the final volume was adjusted to 2 L.

Metals 44 solution: "Metals 44" solution was prepared by mixing 200 mg of ethylenediaminetetraacetic acid (EDTA), 1.1 g of zinc sulfate heptahydrate, 500 mg of ferrous iron sulfate heptahydrate, 150 mg of manganous sulfate monohydrate, 40 mg of cupric sulfate pentahydrate, 20 mg cobalt chloride, 12 mg of boric acid, and 150 μL of 6 N sulfuric acid in distilled water. The volume was adjusted to 100 mL. When the color of the solution turns from green to yellow it means the Metals 44 solution is properly prepared. The color of the solution will become amber weeks later.

Potassium succinate solution with 20 % concentration: 200 g of succinic acid was added to 250 mL of distilled water. To dissolve these contents, in another beaker 200 g of potassium hydroxide was dissolved in 250 mL of distilled water and cooled. While the succinic acid beaker is in an ice water bath, the potassium hydroxide solution was added slowly. The final volume was adjusted to 1 L with distilled water and final pH was brought to 6.8-7.0 by adding HCl.

1 M Phosphate buffer: To prepare the 1 M phosphate buffer 274 g of dibasic potassium phosphate trihydrate was added to 1.2 L distilled water. Then 136 g of monobasic potassium phosphate in 800 ml distilled water was dissolved and finally two solutions slowly combined. Final volume was made to 2 L at and the final pH adjusted of 7.0.

10 % Ammonium sulphate: The ammonium sulfate solution with 10% concentration was prepared by dissolving 50 g ammonium sulfate in 500 ml of distilled water and the final pH was adjusted to 7.0.

All the final solutions were stored at 4 °C.

2.2 BRC purification

The BRCs were purified and dispersed in LDAO detergent micelles according to previously described standard procedure [45-47]. Briefly, 100 g of frozen cells were suspended in 200 mL of distilled water and 2 mL of 1 M Tris buffer by stirring them for 1 hour, until a homogenized solution was attained.

After this 2 ml of EDTA, 1.25 g sodium chloride (NaCl) salt and 1.7 ml of LDAO detergent were added. The mixture was sonicated in Mandel Scientific Company's ultrasound processor (Model XL2020, Farmingdale, New York, USA) to lyse the cells. This was done in an ice bath to avoid excessive temperature for 40 minutes in intervals of 10 seconds on and 10 seconds off intervals. Once the cells are lysed all following steps should be done with limited light exposure because of photosensitivity of BRC.

The final volume of sonicated dispersion solution was adjusted to 210 mL, which was filled in 8 polycarbonate tubes and centrifuged at 4 °C for 2 hours in Beckman Optima XL-100K ultracentrifuge (Fullerton, California, USA) with Ti-70 fixed angle rotor at 45 000 rpm.

After the first centrifugation, pellets were collected inside dark room and re-suspended in 205 ml of TEN buffer and 4.66 mL of LDAO. TEN buffer contains 15 mM **T**ris-HCl, 1 mM **E**DTA, and 0.1 M **N**aCl. The solution was allowed to stir for 10 minutes at room temperature. Centrifugation of this solution was done again with same parameters as the above-mentioned ultracentrifuge procedure to solubilize BRCs in detergent micelles.

Crude BRCs in detergent micelles were now in the supernatant .In order to isolation of crude BRCs, for 220 ml of supernatant 72 g of ammonium sulfate and 7.3 ml of 30% LDAO were used. The mixture was left to stir for 15 minutes at room temperature and then centrifuged in the Beckman J2-HS centrifuge with a JA-17 rotor at 10,000 rpm (10 000 g's) and 4 ◦C for 15 minutes.

The obtained solution which contains BRC micelles were re-suspended in TEN buffer and dialysed overnight to remove the ammonium sulphate in 15 mM Tris-HCl, 0.1% LDAO, and 1 mM EDTA (TL0.1E). The BRC micelles were poured in dialysis membranes with a molecular weight cut off (MWCO) of 12-14 kDa and after clipping both sides was floated inside slowly stirring TL0.1E solution inside fridge at 4 °C in the dark.

In order to further purify the BRCs to remove antenna complexes and free pigments, diethylaminoethyl (DEAE) ion exchange column chromatography was used.

First the Toyopearl 650 M beads were first washed with TL0.1E buffer and then mixture loaded into column. After couple minutes the will lose TL0.1E buffer and be packed due to gravity. To reach further equilibration at least 250 mL of TL0.1E was flowed through a peristaltic pump. Then BRC was loaded onto the column with the pump, where it promptly binds to the column material.

Then column material was washed with TL0.1E (15 mM Tris-HCl, 0.1% LDAO, and 1 mM EDTA) buffer until no more free pigment be detected in the column waste. To verify whether the free pigment was coming, optical spectrum of eluate was recorded every 10 minutes in 260 to 1000 nm range. A linear salt gradient from 0.03 to 0.25 M NaCl was applied to the column.to elute the protein.

As the BRCs are able to bind column beads with a different ionic strength than the other impurities, we can separate and purify BRC samples by collecting the column elute with an automatic fraction collector.

The purity of the collected BRC protein with automatic fraction collector was checked spectroscopically by taking the ratio of the absorbance at 280 nm and 800 nm (A280/A800). This ratio theoretically should be 1.2 and in practice it was kept below 1.6. The reason is at 280 nm absorbance band aromatic amino acids have absorbance 1.2 times of the bacteriochlorophyll

monomer at 800 nm. In order to have pure BRC, the ratio of amplitude of absorption bands of bacteriochlorophyll dimer, Bacteriochlorophyll monomer and bacteriopheophytin should be 1:2:1.

After the column chromatography step, the gathered fractions were pooled and dialyzed overnight to remove excess salt from the BRC protein. This step was done in similar manner as before with TL0.1E buffer. Afterwards the column material was washed with 1M NaCl and stored at 4 ˚C.

The following day the purified BRC was further concentrated in order to easy use and storage. This was done by using a millipore ultrafiltration unit having a nominal molecular weight limit (NMWL) of 30 kDa under 5 psi of nitrogen.

The concentration of BRC protein was measured with optical absorption spectroscopy by determining absorption at 800 nm where it has extinction coefficient of 288 mM^{-1} cm^{-1} [47]. Purified BRC were concentrated to approximately 100 μM and then stored in black tubes at -20 °C.

2.3 Sample preparation

In all experiments the concentrated and frozen BRCs were thawed and diluted to 1 μM final concentration in different buffers immediately before the experiments. Different buffers were used depending on pH and used metal ions. In modified BRCs buffer solution prepared from distilled water by using 15 mM HEPES, 25 mM sodium bicarbonate, 0.05% Triton X-100 at pH 7.0.

For native BRC (R-26) the buffer contains 80 mM Bis Tris Propane (BTP) and 0.03 % LDAO at various pH values. These buffers were chosen as result of previous studies which

outlined the necessary conditions for binding of metal ions to modified BRCs and optimal ET from manganese to the BRC [48,36].

All sample preparation and experiments were done in the dark with only weak orange-filtered light to avoid any BRC pre-illumination before experiment.

Cupper and manganese solutions were prepared from copper (II) sulfate and manganese(II) acetate, >98 % pure, from Sigma Aldrich,. These were dissolved in the buffer at 1 M concentration and vortexed until they completely dissolved. The copper sulfate solutions were prepared at 1 M concentration the pH dropped to ~ 3.8. In order to adjust the pH the solution was diluted to 10 mM concentration. Manganese solutions were prepared fresh before experiment because Mn^{2+} needed for electron donation and it would auto-oxidize to Mn^{3+} under ambient conditions [48]. Therefore all samples with exposed manganese were measured no more than 2 hours after preparation.

2.4 Biophysical characterization

2.4.1 Optical absorption spectroscopy of BRCs in neutral and charge separated states

Measurements of light-induced difference optical spectra and Steady-state kinetics were performed on a Cary 5000 UV-VIS-NIR spectrophotometer from Agilent (formerly Varian, Mulgrave, Victoria, Australia). In order to form light-induced states continuous and white light excitation was provided by a 1000 W mercury xenon arc lamp (Oriel 6140) powered by an Oriel 8550-5 power supply, for high and low intensity experiments.

The light was delivered to assay samples through liquid-filled light guide which is coupled to the spectrophotometer. The used flux intensities were 0.5 W/cm^2 as low intensity and 1.05 W/cm^2 as high intensity depending to experiment conditions.

All measurements were done in 3 mL quartz cuvette. Kinetic measurements were performed at 865 nm with 1 nm spectral bandwidth and 0.033 s temporal resolution. Light-induced difference spectra were measured with following parameters:

Scanning wavelength: 700-1000 nm

Spectral bandwidth: 2 nm

Spectral resolution: 1.1 nm

Scanning rate: 2000 nm/min

Spectra without BRC and excitation illumination were recorded to track the changes of cupper and sodium bicarbonate complex from 200 – 1000 nm at 2000 nm/min, with 1.1 nm spectral resolution and 2 nm spectral bandwidth. Baseline correction was done for all spectra measurements before measuring the spectra.

2.4.2 Electron paramagnetic resonance spectroscopy

2.4.2.1 EPR basic principles

The Electronic paramagnetic resonance (EPR) **spectroscopy** is a technique to study materials with unpaired electrons such as free radicals, transition metals with odd number of electrons. Molecules with all pared electrons have no electron magnetic moment and have no EPR spectroscopic signatures. Electron has magnetic moment and spin quantum number s=1/2, with magnetic components $m_s=\pm 1/2$.In absence of any magnetic field there is no difference between the

energy levels of electron's magnetic moments. However in presence of external magnetic field with strength B_0, the electron's magnetic moments align either parallel (m_s=-1/2) or antiparallel (m_s=+1/2) to the field, and the energy levels of them linearly increase (see Figure 2.1) due to Zeeman effect:

$$E = m_s\, g_e \mu_B B_0 \qquad (2.1)$$

where the g_e is the so called g-facor(for free electron g_e=2.0023) and μ_B is Bohr magneton. The difference between the energy levels of upper and lower state is $\Delta E = g_e \mu_B B_0$ for unpaired free electron, which g_e and μ_B are constant. An unpaired electron can move between the two energy levels by either absorbing or emitting a photon of energy $h\upsilon$ such that the resonance condition $\Delta E = h\upsilon$ is obeyed. Generally the EPR measurements are made with microwaves in the 9–10 GHz region. The EPR spectra can be generated by either varying the photon frequency incident while the magnetic field is held constant or doing the reverse. In practice usually the frequency is kept fixed and magnetic field varies [77].

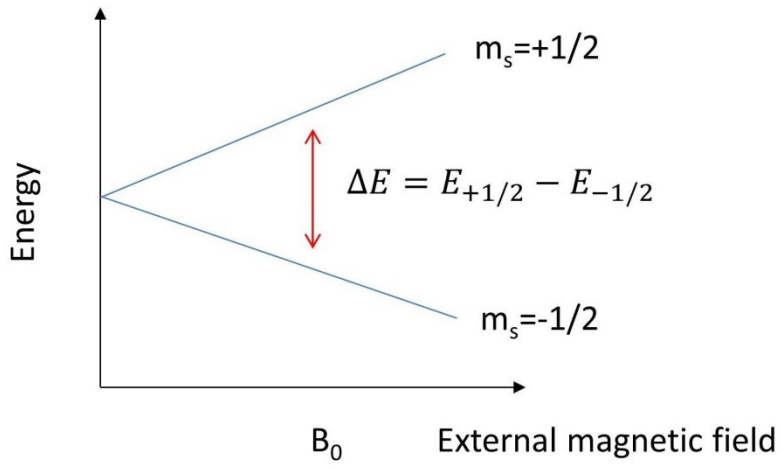

Figure 2.1: Scheme of splitting the energy levels of upper and lower state in presence of external magnetic field.

Upon increasing the external magnetic field the energy levels of upper and lower state is increased until it matches with the energy of the applied microwaves, as indicated by the double headed-arrow in Figure 2.1. At this point the unpaired electrons can move between their two spin states. Due to the Maxwell–Boltzmann distribution more electrons are existed in lower energy state, net energy absorption occurs and this absorption is converted into a spectrum. In Figure 2.2 the upper spectrum shows the simulated absorption for a system of free electrons in a varying external magnetic field. However the first derivative of the absorption spectrum is the most common way to record and represent continuous wave EPR spectra [77].

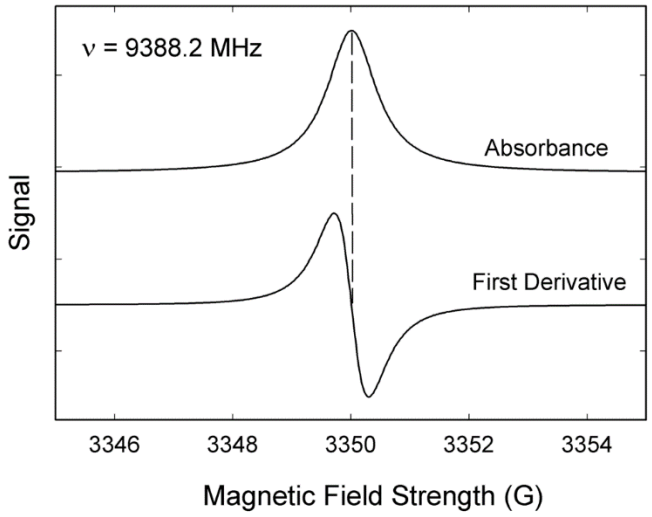

Figure 2.2: The simulated absorbance and first derivate EPR spectrum for a system of free electrons in a varying magnetic field

2.4.2.2 EPR spectrometer

Measurements of Electronic paramagnetic resonance (EPR) **spectroscopy** were performed on an X-band MS-5000 Magnettech by Freiberg Instruments spectrometer at a microwave frequency of ~9.41 GHz. Samples of ~300 μL were prepared at concentrations of 10 mM Mn^{2+} and Cu^{2+} in various concentrations of BTP between pH 4.0 and 9.4, in order to reveal the effect of BTP at

different pH regimes in Mn-BTP and Cu-BTP complexes. Similarly to sample preparation in Section 2.3, manganese and cupper solutions were prepared fresh before experiment.

2.5 Data analysis

2.5.1 Analysis of kinetic traces

One of the main methods to determine the rate constant of manganese oxidation by BRC is monitoring the kinetics of light-induced changes at Q_y absorption band of dimer at 865 nm. The studying of these changes due to formation of P^+ and its recovery could reveal other features of BRC interaction with surrounding ions and molecules.

This kinetics produced by continuous illumination were decomposed into 1 or 2 different exponential decays, associated to different processes, depending on the conditions being probed. The decomposition was done according to the following equation:

$$A(t) = Be^{k_1 t} + Ce^{k_2 t} \qquad (2.2)$$

Where,

$A(t)$ ≡ total signal amplitude at any time t

B, C ≡ amplitudes of the different decaying kinetic components

t ≡ time

k_1, k_2 ≡ rate constants of the decaying kinetic components

The time constant, or lifetime is defined by $\tau = 1/k$, the inverse of the respective rate constant (k)

2.5.2 Ligand binding

The dissociation constants were determined for ligand binding by assuming equilibrium condition,

$$nL + s \leftrightarrow nL{:}S$$

where,

$L \equiv$ the ligand (generally manganese or copper in our case)

$n \equiv$ the number of ligands active in the binding,

$S \equiv$ the substrate (generally R-26 BRC or modified BRC)

$nL : S \equiv$ substrate with bound ligand(s).

The binding equation based on this equilibrium is:

$$A = \frac{B}{1+(\frac{K_D}{[L]})^n} \qquad (2.3)$$

Where,

$A \equiv$ the fraction of occupied binding sites; in our case this is generally the fraction of BRCs exhibiting reduction by manganese

$B \equiv$ total amplitude or maximum fraction of binding attainable

$K_D \equiv$ dissociation constant of the binding

$[L] \equiv$ free ligand concentration; (generally Mn^{2+} or Cu^{2+} in our case)

2.5.3 Determination of proton dissociation constant

The pH dependencies of the manganese oxidation were fitted with a Henderson-Hasselbach equation (2.3). The yielded fit used to explain *pK* shifts of the protonatable amine residues of the BTP that are associated with the Mn^{2+} ions as ligands.

$$f(H) = \frac{1}{1+10^{(pH-pK_a)}} \qquad (2.4)$$

The Henderson-Hasselbach equation was extended to the involvement of two protonatable residues as following:

$$f(H) = \frac{1}{1+10^{2(pH-pK_a)}} \qquad (2.5)$$

Where,

f(H): fraction protonated

pKa: acid dissociation constant for protonatable residues

Chapter 3

Results

As explained in Section 1.5 of the Introduction, BTP coordinated manganese ions at certain conditions are able to bind native BRCs and act as secondary electron donor. The Mn^{3+}/ Mn^{2+} potential is pH dependent, and much remains unclear about the interaction between manganese ions and the BRC including; diffusion limits and accessibility of binding sites of BRC to manganese ions, and the rate of electron donation to oxidized dimer at different pHs.

3.1.1 Reaction scheme for manganese oxidation by BRC

As it has been shown the observed kinetics of oxidized dimer of BRC following flash light excitation is not the evidence for ET from Mn^{2+} to the dimer because the charge separated state does not provide enough life time for electron donation [43].

The reaction scheme of manganese and BRC complex can be expressed with the rate constants of each process as:

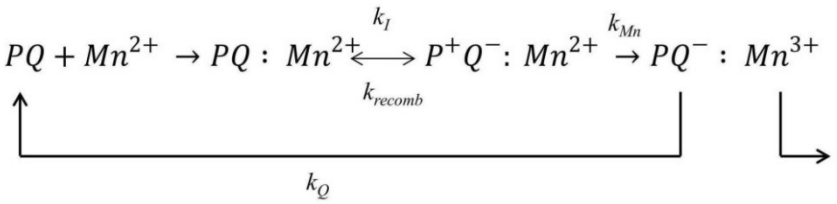

(3.1)

In order to determine the real ET rate constant between Mn^{2+} and P^+ by monitoring absorbance changes at 865 nm, the effect of each reaction and its rate must be distinguished. As we see from the equation the Mn^{2+} oxidation reaction (k_{Mn}) and charge recombination (k_{recomb}) are two opposite and competitive processes. The rate constant of electron transfer from Mn^{2+} to P^+ after generation of charge separated state (P^+Q^-) is only observable if its rate (k_{Mn}) is higher than that of the charge recombination ($k_{Mn} > k_{recomb}$).

Under saturating continuous illumination, when the rate constant of charge separated state creation k_I is much higher than the rate of charge recombination ($k_I >> k_{recomb}$) the steady state approximation can be considered, and k_{Mn} can directly be measured. Additionally the rate of recovery of quinone should be much lower than the rate of manganese oxidation in the steady state approximation ($k_Q << k_{Mn}$). After electron donation from Mn^{2+} to P^+, the Mn^{3+} is replaced by a fresh Mn^{2+} from nearby pool and new cycle can start again once Q^- loses its electron. Saturating continuous illumination is dependent upon the light intensity and it was determined ~0.95 W/cm^2, yielding maximum ET rate constants of 1.3 s^{-1} and 0.8 s^{-1} for R-26 and wild type (WT) BRCs, respectively [43]. In present work all the kinetics of P^+ reduction in presence of manganese has been performed by 0.95 W/cm^2 light intensity.

3.1.2 Metal binding sites in bacterial reaction centers

As explained in Section 1.5 of the introduction, many sites in RCs are identified as plausible candidate for metal ions binding but only two are within the distance of effective

biological electron transfer. These two binding sites were predicted by ligand binding site modeling software (Q-SiteFinder, University of Leeds [49]) One of these sites (Site 1) is located at the inner opening of the carotenoid binding site, in a large cavity in the membrane-shielded region of the protein. The other (Site 2) is located on the periplasmic surface of the BRC at the approximate location of the docking site of the native electron donor, cytochrome c_2 (cyt c_2).The location of these two metal binding sites of the BRC are shown in Figure 3.1.

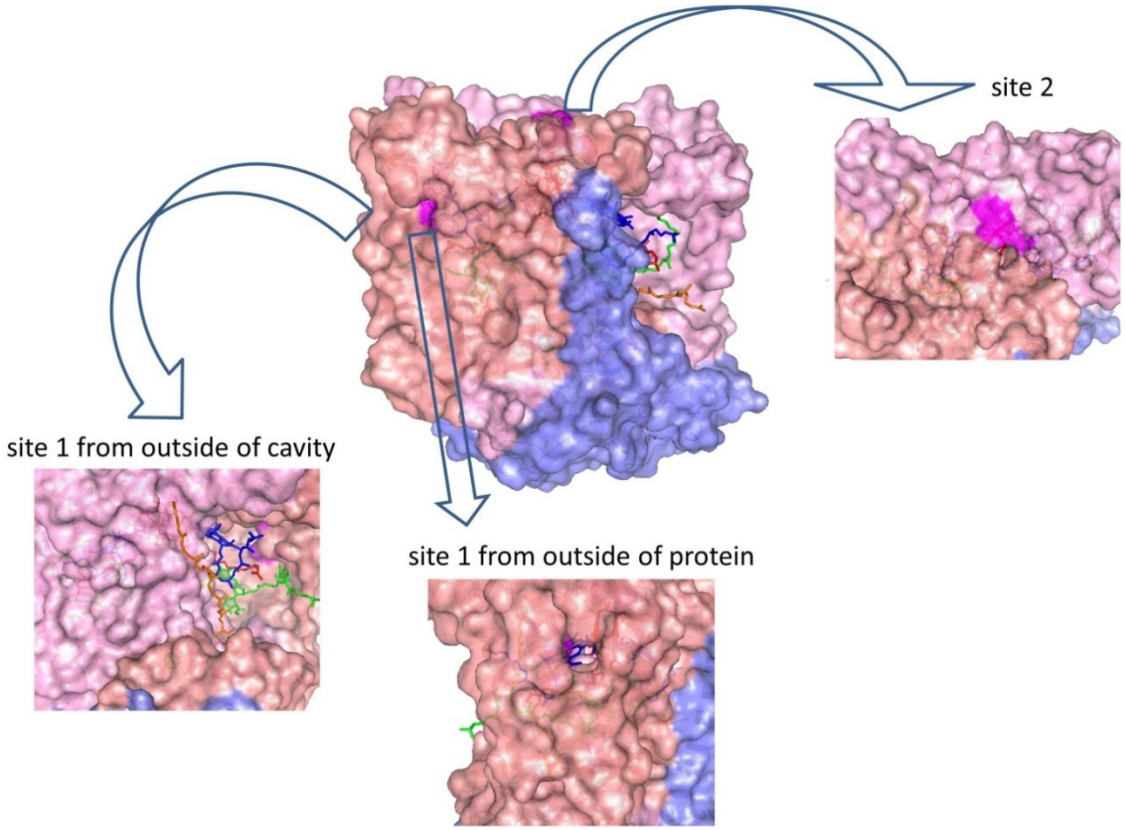

Figure 3.1: Predicted metal binding sites of the R-26 BRC. BRC represented as semi-transparent surface. Binding sites are shown as bright pink regions. Coloring of the subunits and cofactors is the same as in Figure 1.1. Atomic coordinates taken from PDB code: 1PCR

These two sites are located in different environment and have different binding characteristics. Carotenoid binding site or site 1 is like cavity inside hydrophobic region of membrane which ends to the cofactors of M-subunits. The direction of this cavity is in alignment

with the direction of Qy dipole moment of bacteriochlorophyll dimer (P) and monomer (B), therefore presence of any charged ions will affect the absorption bands of these dipoles.

The electrochromic absorption changes at ~865 nm and ~800 nm both in the dark and upon illumination suggest that manganese is present at the hydrophobic site along the direction of the Qy transition dipoles of P and of $BChl_B$ [43]. The presence of bound manganese to site 2 was confirmed by using Dual Polarization Interferometer (DPI) [43].

The other binding site (Site 2) is located at periplasmic surface of the BRC, the site which the native electron donor cyt c_2 binds there. As the distance between Site 2 and bacteriochlorophyll dimer is 13Å, the bounded manganese at this site has the potential to involve in redox activity with oxidized dimer.

3.2 Effect of light-induced conformational changes on the accessibility of binding site to Mn^{2+}

As explained in Section 3.1.2, the two predicted binding site of BRC have very different nature. The binding site1 is located at periplasmic surface located in region with very high dielectric constant and instantaneously is accessible to polar molecules and ions of solvent. On the other hand the binding site 2 at the hydrophobic cavity of BRC membrane region has very small dielectric constant and possibly has limited–diffusion accessibility due to its geometry. The affinity of these two binding sites to ions and polar complexes could be probed energetically as well. The energy of ion can be expressed as:

$$E_s = \frac{q^2}{2DR_s} \qquad (3.2)$$

which E_s is the self-energy, q is the charge of ion ze (which z is the number of charge, e is the elementary charge constant, 1.6 $\times 10^{-19}$ C), D is dielectric constant (D is equal to $4\pi\varepsilon\varepsilon_0$, ε_0 is the electric constant also known as "the absolute permittivity of free space", ε_0= 8.85×10-12 C^2 m^{-2} N^{-1}, ε is the dimensionless relative permittivity of the material in which the charges are immersed), R_s is the Stocks radius (The Stokes radius or Stokes-Einstein radius of a solute is the radius of a hard sphere that diffuses at the same rate as that solute). It can be seen that the energy of ion, which charge is distributed in large molecule is smaller than a point charge. Also we know that the ε is small in hydrophobic region of the protein, therefore it is very difficult to bury a charge inside the membrane shielded region of the protein due to unfavorable energetic enhancement. The accessibility of binding sites to manganese electron donor was tested by addition of Mn^{2+} to BRC, allowing to incubate for various time and measuring the rate content of P^+ reduction in certain times [50]. Although the experiment was not performed in optimum condition in terms of manganese concentration and light intensity, the diffusion rate of Mn^{2+} coordinated by BTP complex to binding site 1 was observed. The Fick's first law relates the diffusive flux to the concentration under the assumption of steady-state conditions is expressed as:

$$J = -D\nabla c \qquad (3.3)$$

Which J is the diffusion flux or diffusion rate (mole per unit area per unit time), D is the diffusion coefficient (area per unit time) and c is the concentration (mole) of diffusing substance (manganese in our case).

In order to reveal the Mn^{2+} diffusion to binding site, the dependency of the kinetics of manganese oxidation by P^+ was measured different times after metal addition in R-26 BRC with pre-illuminated and dark-adapted samples at various pH values. The dark-adapted samples were prepared by addition of manganese without any exposure to illumination. For pre-illuminated

samples the BRC was illuminated for one minute under saturating continuous illumination with 0.95 W/cm^2 intensity. The samples were allowed to recover (~10 minutes), and then Mn^{2+} from fresh solution was added.

The kinetics of P^+ reduction and the rate constants of these kinetics as function of manganese incubation time for pre-illuminated and dark-adapted samples in various pH is shown in Figure 3.2 and 3.3, respectively. It can be seen that in each probed pH the rate constants of ET from Mn^{2+} to P^+ are increased with increasing Mn^{2+} incubation time. Since the Mn^{2+}/Mn^{3+} potential is pH dependent, as it was expected the rate constants were found to decrease by lowering the pH. The considerable increase in ET rate constants by manganese incubation time confirms the diffusion-limited accessibility of the buried binding site to the hydrophilic manganese ions.

First, we hypothesise that since at pH 9.4 the rate constants of ET from Mn^{2+} to BRC is so high only the manganese at binding site 1 is involved in ET process, but at low pH the contribution of manganese at periplasmic binding site could be detectable. Being at the surface binding site 2 is instantaneously accessible for Mn^{2+} ions, therefore a constant component should be observed in decomposition of kinetic traces. While the kinetics of P^+ reduction in presence of manganese for both pre-illuminated and dark adapted samples in all pH ranges were well fitted with single exponential function, the probability of any redox activity of Mn^{2+} at site 2 was rejected.

For pre-illuminated BRCs the rate constant increased by 57 % to a maximum rate of 1.2 s^{-1}, and increased by 82% to maximum of 0.85 s^{-1} for dark-adapted BRCs at pH 9.4. The role of Mn^{2+} incubation time on the enhancement of rate constants was highlighted by lowering the pH. For example, at pH 8.4 the rate constant increased by 316 % and 180 % to a maximum of 0.25 s^{-1} and 0.1 s^{-1} for pre-illuminated and dark-adapted BRCs, respectively. The rise in rate constant with manganese incubation time took ~20 minutes to reach saturation for pre-illuminated samples, while dark-adapted samples needed ~60 minutes.

The insufficient dependency on Mn^{2+} incubation time and large rate constants to attain the saturation condition for pre-illuminated samples suggest that light-induced conformational changes of BRC increase the accessibility of manganese ions to binding site.

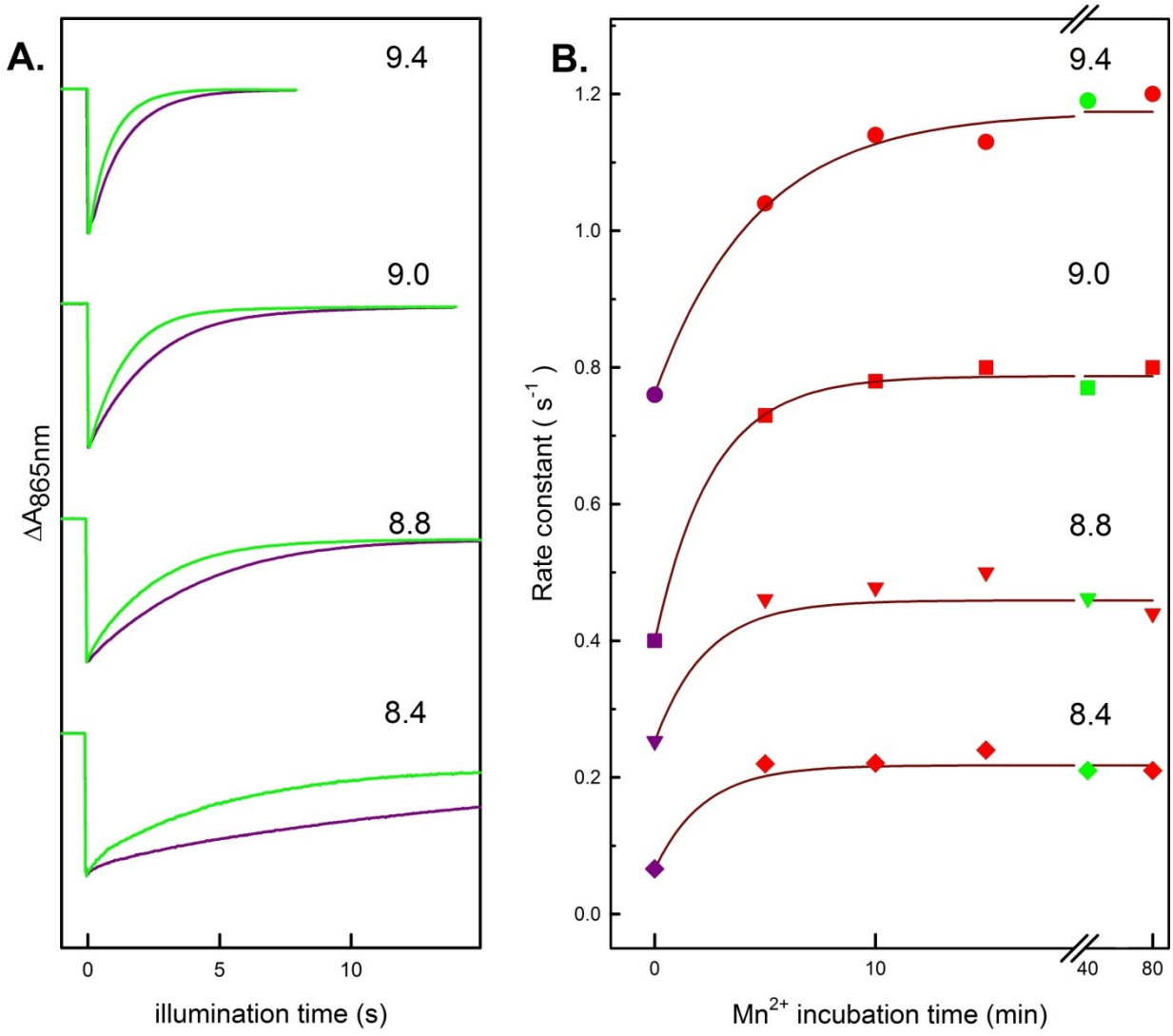

Figure 3.2: Electron transfer from Mn^{2+} to P^{+} in light-adapted conformation of the BRC at different pH values. A: Representative traces of P^{+} recovery kinetics soon after manganese addition (purple traces), and 40 minutes after manganese addition (green traces) in various pHs. B: rate constants as a function of Mn^{2+} incubation time for pH 8.4 to 9.4. Solid lines represent exponential fits to the increasing rate constant with time. Conditions: 1 μM R-26 in 0.03 % LDAO, 80 mM BTP 30 mM Mn^{2+} at various pH. Continuous illumination excitation of 0.95 W/cm^2 with xenon lamp. Pre-illuminated BRCs were prepared by exposure of the samples to 0.95 W/cm^2 continuous illuminations for 1 minute, 15 minutes prior to manganese addition.

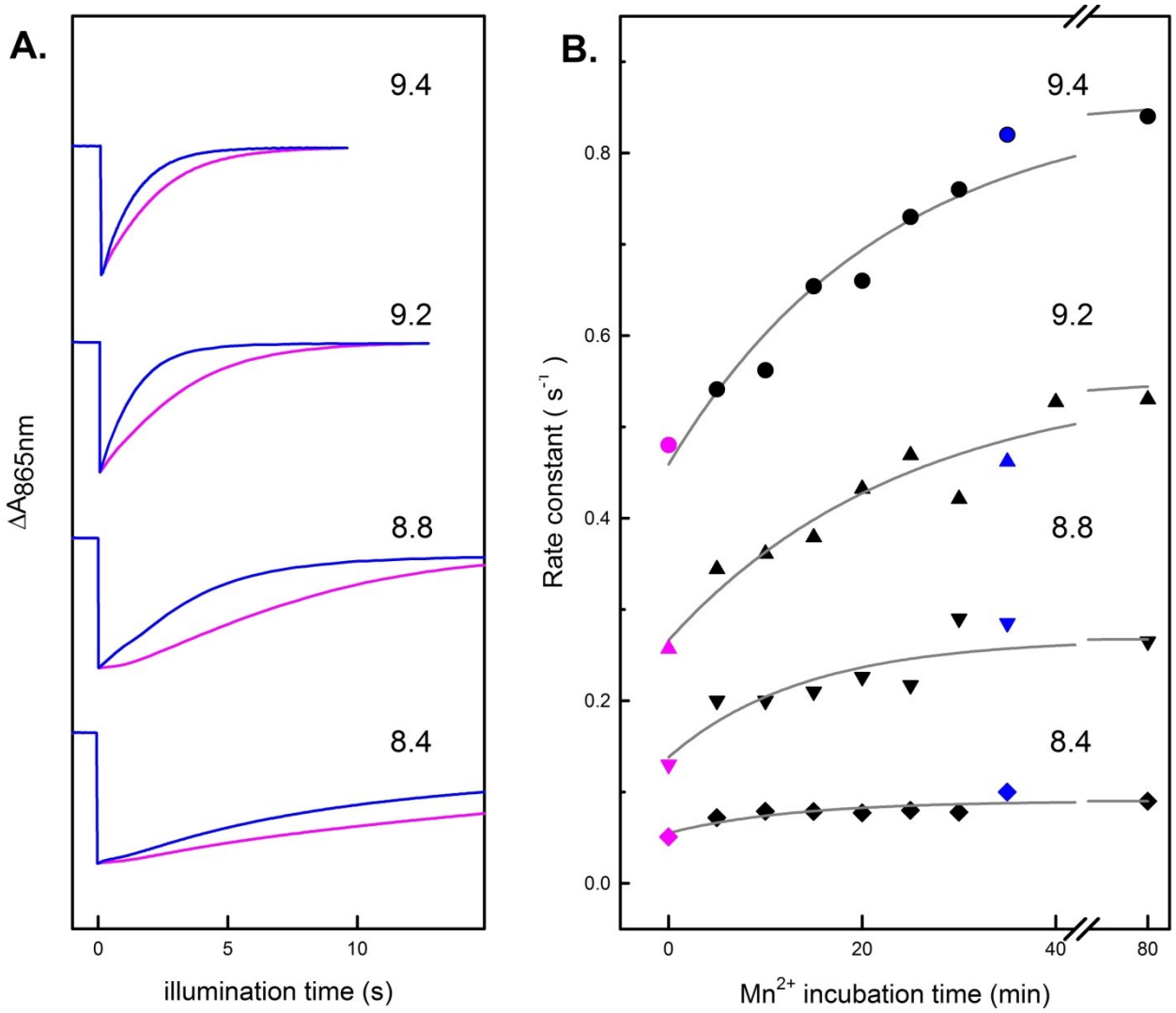

Figure 3.3: Electron transfer from Mn^{2+} to P^{+} in dark-adapted conformation of the BRC at different pH values. A: Representative traces of P^{+} recovery kinetics soon after manganese addition (pink traces), and 40 minutes after manganese addition (blue traces) in various pHs. B: rate constants as a function of Mn^{2+} incubation time for pH 8.4 to 9.4. Solid lines represent exponential fits to the increasing rate constant with time. Conditions as for Figure 3.2.

Under strong continuous illumination that corresponds to a quasi-equilibrium condition the rate of manganese oxidation in wild type (WT) BRC which contains carotenoid near binding Site 1 is reported 0.8 s^{-1}, which is similar to the value observed in dark-adapted R-26 BRC [43].

3.3 Effect of LDAO molecule on the accessibility of binding site to Mn^{2+}

It has been reported that many molecule with different dielectric properties are present inside the hydrophobic cavity of the BRC, such as water, glycerol, lipids and detergents [7,51]. Presence or absence of these molecules can be used as a useful method to probe various aspects of manganese ions binding to BRC and their function as a secondary electron donor to P^+.

In order to identify the influence of changes in dielectric constant of metal binding site of BRC on the accessibility of binding site to manganese ions, LDAO molecule was chosen to probe the cavity. The kinetics of the absorption changes at 865 nm in the presence of manganese in R-26 BRC were reported 1.3 and 0.6 s^{-1} at low (0.03%) and high LDAO (1%) concentrations [43]. High LDAO concentration in wild type (WT) BRC did not cause any further change in the rate of manganese oxidation, since the carotenoid is present in the cavity near the metal binding site.

Upon finding evidence of LDAO molecule affecting the rate of ET from Mn^{2+} to oxidized dimer, the effect of excess of this molecule on accessibility of binding site of BRC to Mn^{2+} ions was probed by performing a manganese incubation while the reduction of P^+ under sub-saturating continuous illumination was monitored. The result of rate constant of manganese oxidation as function of manganese incubation time in pre-illuminated and dark-adapted BRC in high and low LDAO concentrations at pH 9.4 and 8.4 is shown in Figure 3.4.

While in agreement with previous studies the ET rate constants at both pH 9.4 and 8.4 were dropped upon addition of high LDAO in pre-illuminated BRC, dark-adapted BRC was particularly interesting because excess of LDAO increased the ET rate constants. A huge effect from presence of LDAO molecules at high concentration on the rate constant of Mn^{2+} incubation was observed

for pre-illuminated samples, which was decreased from 13 s^{-2} to 3.5 s^{-2} and 27 s^{-2} to 4.5 s^{-2} at pH 9.4 and 8.4, respectively.

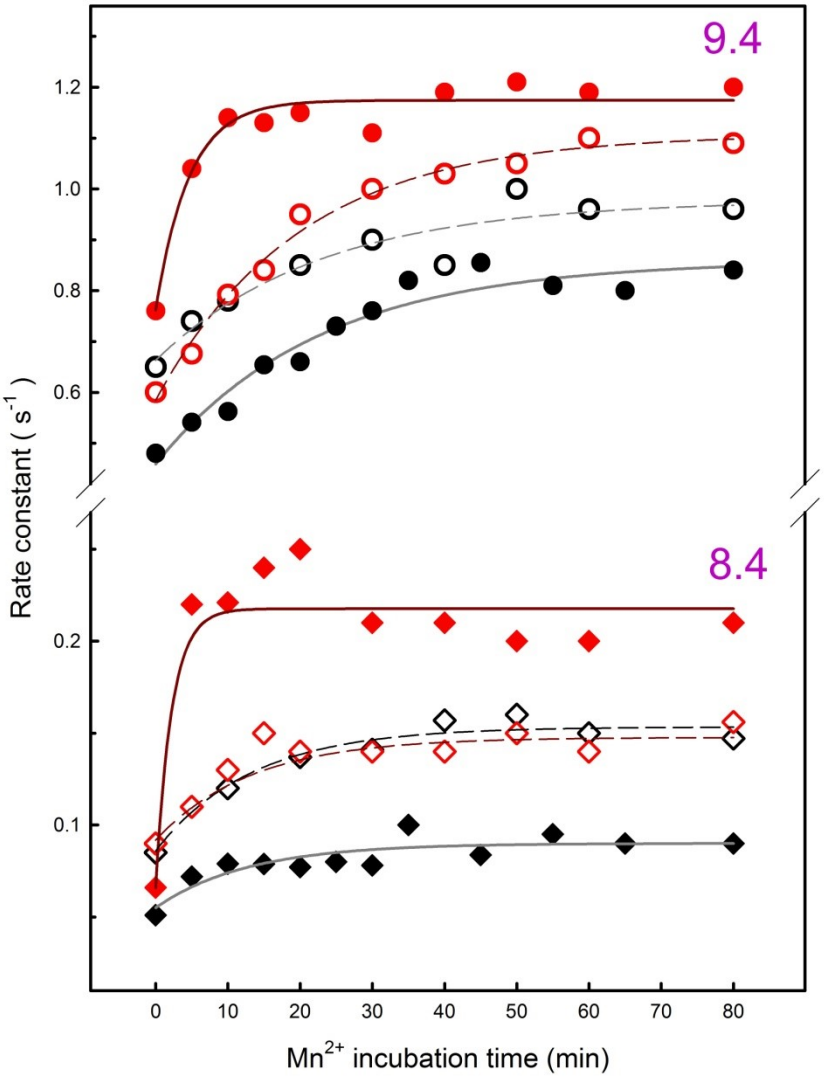

Figure 3.4: Influence of excess of LDAO molecules on accessibility of manganese ions to metal binding site of BRC. The rate constants of electron donation from Mn^{2+} to P^{+} as a function of Mn^{2+} incubation time is shown for pH 8.4 and 9.4. Solid and dashed lines represent exponential fits to the increasing rate constant with time for low and high LDAO concentration. Red and black symbols represent pre-illuminated and dark-adapted R-26 samples, respectively, while open circles and diamonds represent high LDAO concentration, closed circles and diamonds represent low LDAO concentration. Conditions as for Figure 3.2, except 0.03% and 1% LDAO were chosen as low and high concentration.

For dark-adapted BRCs elevated LDAO concentration did not cause any further changes in the rate constant of Mn^{2+} incubation, since 4.6 s^{-2} , 4.5 s^{-2} at pH 8.4 and 2.4 s^{-2} , 2.5 s^{-2} at pH 9.4 were observed with low and high LDAO concentrations, respectively. As it was shown in section 1.4 the LDAO molecule is composed a hydrocarbon chain and a charged headgroup due to presence of negative and positive charges of oxygen and nitrogen, respectively. Presence of charged complexes can alter the dielectric constant of the environment which complex is immersed, and can increase the hydrophilic property of the membrane-shielded region of the protein. As explained in Section 1.5 Introduction the structural changes are sensitive to the presence or absence of detergent or lipid molecules occupying this carotenoid binding site next to the inactive bacteriochlorophyll monomer (B_M). These light induced structural changes take place by deprotonation of the M210 Tyr, and resulting in the rotation of the 2-acetyl group of B_M. Therefore due to presence of LDAO molecule the rotation of the 2-acetyl group of B_M could be restricted, and light-induced conformational changes are not able to provide the optimum conditions for manganese ions to access deep into cavity binding site.

3.4 Decomposition of manganese oxidation kinetics: first and second order reactions

With the evidence of diffusion of redox active manganese to Site 1, we next characterized the kinetics manganese oxidation as function of manganese concentration in Mn-BRC system. This was accomplished by probing the strong saturating continuous light-induced kinetics of P^+ reduction by Mn^{2+} in various manganese concentrations.

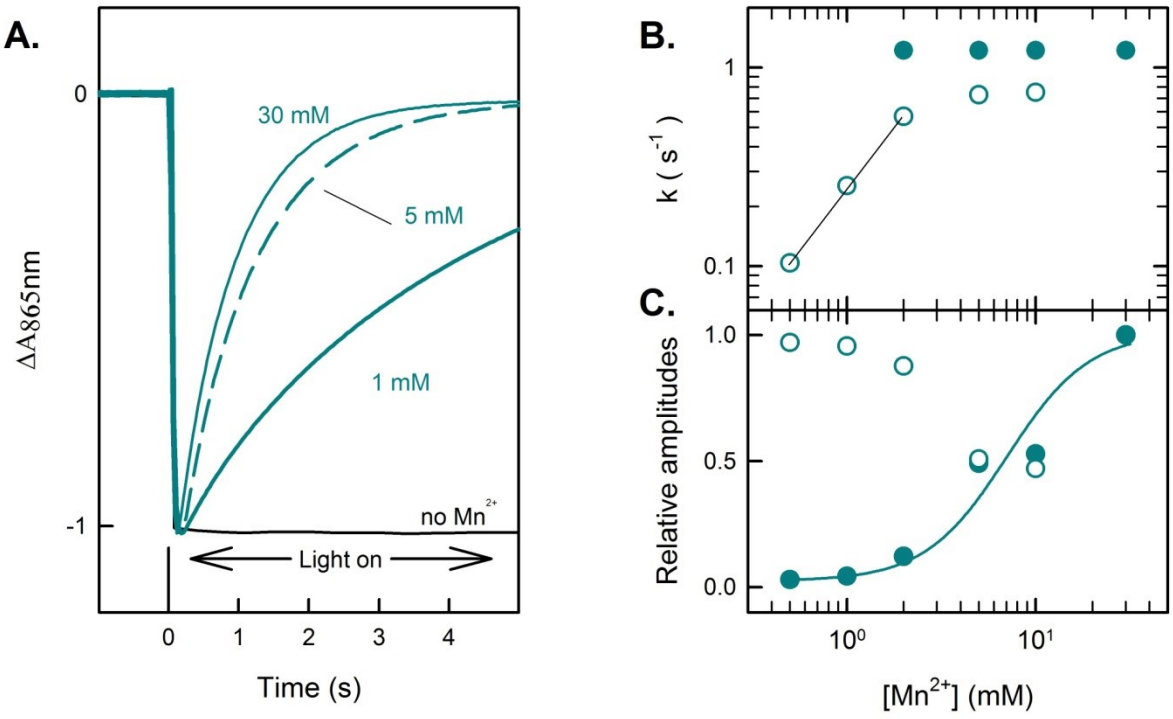

Figure 3.5: Evidence of first and second order reactions in manganese oxidation. A: The kinetics of continuous light-induced manganese oxidation from R-26 BRC at low and high concentration of Mn^{2+}. B: rate constants of fast (closed circles) and slow (open circles) kinetic components of Mn^{2+} oxidation as function of manganese concentration. C: relative amplitudes of fast and slow kinetics component. Solid line represent fitting to binding equation (2.3) for two Mn^{2+} ligands, yielding K_D of 6.6 mM. Conditions: 1 μM R-26 in 0.03 % LDAO, 80 mM BTP, pH 9.4 and varying concentration of Mn^{2+}. Continuous illumination excitation of 0.95 W/cm^2 with xenon lamp.

A titration of Mn^{2+} was performed while monitoring the continuous light-induced kinetics in R-26 BRC. This experiment allowed us to observe second order rate constant of P^{+} reduction at low Mn^{2+} concentration, which is assigned to be a collisional process and a first-order kinetics observed at high manganese concentration where the strong binding is established. The results can be seen in Figure 3.5. The kinetics was found to be biphasic at intermediate concentrations, the fast component due to oxidation of bound Mn^{2+} to BRC, and the slower component due to oxidation of free Mn^{2+} ions.(see Figure 3.5 B) The amplitude of the slower component fell, in favor of the faster component, as the concentration of Mn^{2+} increased. The behaviour of amplitude of the fast component was fitted to binding equation (2.3) with two manganese ligands, yielding K_D of 6.6 mM. The rate constant of fast component in the presence of 30 mM Mn^{2+} was 1.2 s^{-1} and was kept constant for lower Mn^{2+} concentration. Below 2 mM Mn^{2+} concentration the relative amplitude of the fast component is less than 5%, therefore its contribution could not be measured accurately. The rate of slow component was elevated by the presence of 0.5 mM Mn^{2+} from 0.1 s^{-1} to 0.75 s^{-1} at 10 mM Mn^{2+}concentration.

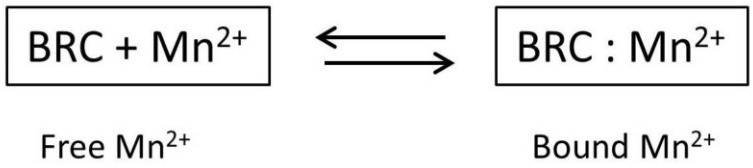

Figure 3.6: Simplified mechanism of Mn^{2+} ions interaction with BRC. At low manganese concentration, Mn^{2+} ions are unable to bind BRC. Upon addition of Mn^{2+} concentration, due to increasing of the driving force, Mn^{2+} ions diffuses to metal binding site of BRC, and Mn-BRC system forms. The ET from bound manganese and free manganese represent first order process, respectively.

At low concentration of Mn^{2+}, metal ions are in free state and rate constant of ET from Mn^{2+} to BRC was slow. The minimum concentration of 1 mM Mn^{2+} was needed to observe the

contribution of Mn^{2+} at bound state in ET process. As the concentration of Mn^{2+} increased, the population of Mn^{2+} in bound state raised, at maximum 30 mM Mn^{2+} concentration, the whole electron donation originates from Mn^{2+} at bound state. At 5 mM Mn^{2+} concentration, approximately 50 % of reaction centers are in bound state. In Figure 3.5 B, a linear relationship between the rate constants before saturation (below 5 mM) and the concentration of added Mn^{2+} was observed. This relationship indicates a second-order, collisional process and its measured rate constant is 3.5×10^2 $M^{-1}s^{-1}$.

3.5 Effect of pH on manganese interaction with BRC

3.5.1 Influence of pH on electron transfer from manganese to oxidized dimer

Figure 3.7 A shows the pH dependency of Mn^{2+} oxidation rate constants as function of pH for both pre-illuminated and dark-adapted samples. As it can be seen the rate constant of ET from Mn^{2+} to P^+ increases by increasing the pH of assay solution until to reach maximum rates at pH 9.4. This observation is in line with previous results since the Mn^{2+}/Mn^{3+} potential is ~400 mV at pH 9.4 and increases as the pH is lowered [43]. Also in Figure 3.7 A there is linear relation between rate constant of Mn^{2+} oxidation and pH. The steepness of lines shows 0.7 and 0.98 order of magnitude difference per pH in the rate constants in the light-induced and dark-adapted conformations, respectively.

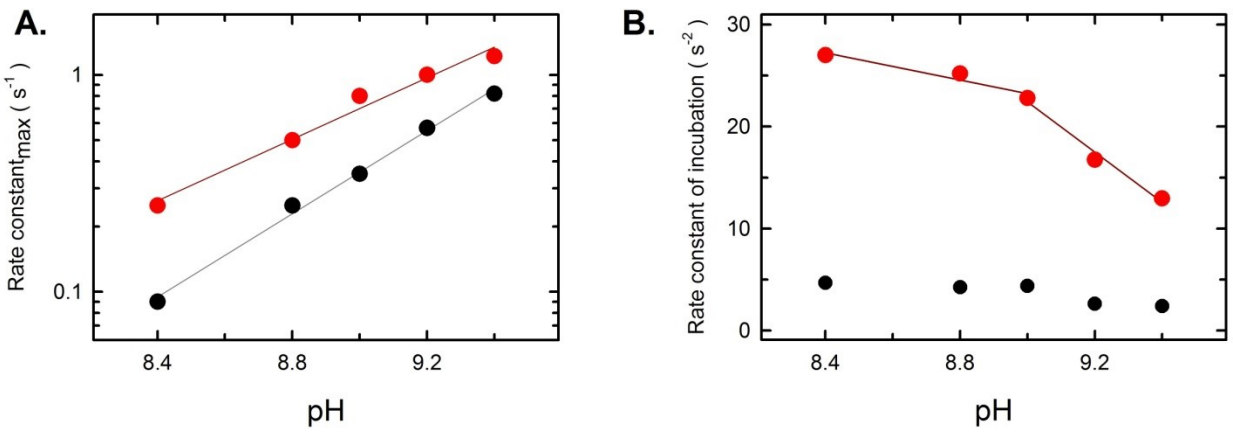

Figure 3.7: Effect of pH on ET rate constants from Mn^{2+} to oxidized dimer and rate constants of manganese ions incubation. Red and black circles represent pre-illuminated and dark-adapted R-26 BRCs, respectively. A: Rate constants of electron transfer from Mn^{2+} to P^{+} during light excitation as function of pH. The linear dependence of ET rate on pH indicates second order diffusion-limited process. The steepness of lines shows 0.7 and 0.98 order of magnitude difference in rate constant per pH for pre-illuminated and dark-adapted BRCs, respectively. B: Rate constant of Mn^{2+} incubation as function of pH, indicating the rate of diffusion of Mn^{2+} to metal binding site of BRC. Conditions as for Figure 3.2.

Also we found that the rates of increasing in ET rate constant to reach saturation state were strongly pH dependent. This change in rate of ET with respect to Mn^{2+} incubation time can be modeled by exponential function, and the rate constants of incubation are obtained. Figure 3.7 B shows the rate constants of Mn^{2+} incubation as function of pH for pre-illuminated and dark-adapted BRCs. While changes in rate constant of incubation for BRCs that are kept in the dark-adapted state were negligible, the pre-illuminated BRCs showed complex pH-dependence.t manner.

Between pH 8.4 and 9.0 in dark-adapted BRCs the rate constants of incubation approximately are independent of pH, decreasing from 4.7 s^{-2} to 4.4 s^{-2}, and slight drop was observed above pH 9.0, where the rates were 2.6 s^{-2} and 2.4 s^{-2} at pH 9.2 and 9.4, respectively. For pre-illuminated BRCs the maximum rate constant of incubation was observed at pH 8.4 and up to

pH 9 it had only a moderate dependence (nearly horizontal line in Figure 3.7 B), while above pH 9 it showed stronger dependence.

This pH dependence can be explained with the deprotonation of the second amino group of BTP molecule that can become available as an additional ligand to coordinate manganese. Similarly at this step the increased role of light-induced conformational changes on the accessibility of binding site to metal ions was observed. The manganese ions in pre-illuminated BRCs could reach to saturation rates ~5 and ~6 fold faster than in dark-adapted BRCs, below and above pH 9.0, respectively.

Therefore this observation suggests that despite variation in pH, light-induced conformational changes cause the manganese ions to access optimum position in binding site in shorter timescale, even though the rate constant of electron donation from Mn^{2+} to BRC strongly depends to pH due to different Mn^{2+}/Mn^{3+} potential.

3.5.2 Influence of pH on reduction of oxidized dimer

It has been reported that the coordination of Mn^{2+} ions by BTP is essential for manganese ions to serve as secondary electron donor to oxidized dimer of BRC [48]. The two protonable amine groups of BTP molecule appear to coordinate the manganese ions when the maximal electron transfer rate was observed. In aqueous solutionthe two pK_a, values of BTP were reported to be 6.9 and 9.0, which were assigned to deprotonation of first and second amine groups of the molecule, respectively. Spectroscopic studies showed that at pH values below the first pK_a there is no coordination of manganese ions by BTP. At pH values between the first and second pK_a (semi-deprotonated region), the Mn-BTP complex was showed signatures of manganese ion coordination [43]. Above pH 9.0 further spectral features appeared that were assigned to

deprotonation of second amine group. Two coordinating BTP molecules per Mn^{2+} ion were identified [48,43].

In this study we determined the *in situ* pK_a of Mn-BTP complex when in association with BRCs. We also explored the ability of Mn^{2+} ions to serve as secondary electron donor and reduce P^+ under suboptimal conditions. The influence of pH on P^+ reduction kinetics of R-26 BRC with presence of Mn-BTP complex using saturating continuous illumination was studied for both pre-illuminated and dark-adapted samples. The samples were exposed to 1.5 minute illumination and steady state values of P^+ prior to end of light excitation were recorded. Figure 3.8 A shows the kinetics of electron donation from Mn^{2+} to P^+ at different pH values for pre-illuminated BRCs. The amount of P^+ remained at the end of the illumination varies with pH: minimum is at pH above 9.0 and increased by lowering the pH. The fraction of this residual P^+ as function of pH is plotted in Figure 3.8 B and the data was fitted by using Henderson-Hasselbalch models involving 1 or 2 protons. Assuming the involvement of two protons fits the data significantly better. The obtained pK_a value is ~8.2 for both pre-illuminated and dark-adapted BRCs.

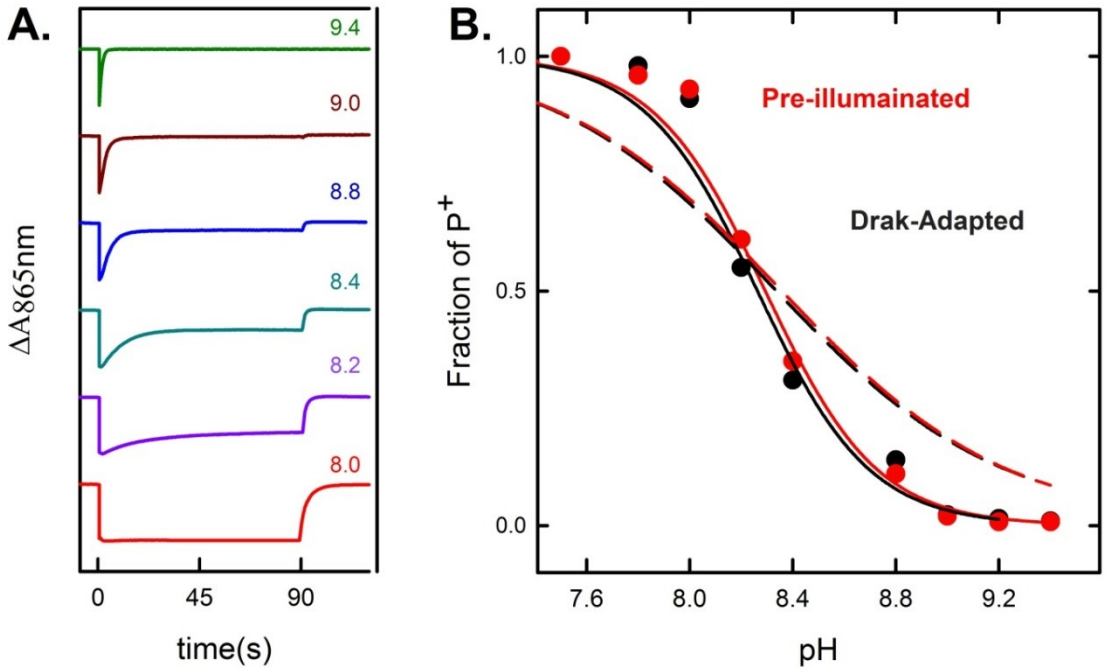

Figure 3.8: The effect of pH on the population of P^+ during continuous illumination. A: representative kinetic traces of light induced absorption changes recorded at 865 nm at different pH. Only pre-illuminated BRC kinetic traces has been shown. The light was on for a period of 90 seconds with start at t=0. The formation and disappearance of P^+ during continuous illumination is monitored at various pH values. B: The fraction of P^+ available at 90 s illumination is plotted against pH, black and red circles represent dark-adapted and pre-illuminated BRCs, respectively. Solid and dashed line represent fitting to Henderson-Hasselbalch model with 2 H^+/pH and 1 H^+/pH, respectively. Black and red curves for dark-adapted and pre-illuminated, respectively. The apparent pK_a obtained was 8.2 ± 0.03 for both BRCs. Conditions: 1 µM R-26 BRC, 30 mM Mn^{2+} in 80 mM BTP, 0.03% LDAO.

3.6 Spectroscopic signatures of dielectric tuning

The product spectrum in the NIR region after the manganese ion donated an electron should have two contributions: The spectrum characteristic to the presence of a negative charge trapped on the quinone (PQ^- state) and possible signatures of the presence of the Mn^{3+}. The former is a spectrum containing a small blue shift of the dimer peak around 865 nm (with a peak at ~835 nm and a trough at ~885 nm) and a red shift of bacteriopheophytin peak around 760 nm (with a peak

at ~770 nm and a trough at ~745 nm). Both of these are due to charge-dipole interactions, namely the charge on the quinone interacting with the dipoles of the nearby Bpheo and the distant (24 Å) P. The differences in distance are consistent with the larger shift in the Bpheo-band than in the P-band. If the oxidized Mn^{3+} is localized at the binding site, it is much closer to P (15 Å) than the quinone, therefore a stronger charge-dipole interaction is expected that can be monitored by a magnified shift on the P-band. The position of the Mn^{3+} must be sensitive to the presence or absence of carotenoid or LDAO molecule that was reported to interfere with the metal binding [50]. To understand the influence of LDAO molecules on accessibility of binding sites to manganese ions and their influence to modulate the conformational changes we monitored the recovery of the dimer shift relative to recovery of the electrochromic signals associated to the PQ^{-} state in both low and high LDAO concentration.

The peak-to-trough amplitude of two main spectral features of the PQ^{-} state in R-26 strain, namely the blue shift of the dimer peak around 865 nm with a peak at ~835 nm and a trough at ~885 nm) and the red shift of bacteriopheophytin peak around 760 nm (with a peak at ~770 nm and a trough at ~745 nm) after the first and second illumination is plotted as function of time at low LDAO concentration, in Figure 3.9.

After the first illumination at pH 9.4 the electrochromic shifts recovered in 12 minutes with a rate constant of 4×10^{-3} s^{-1} with respect to Q^{-} that recovered with a twice slower rate, 2×10^{-3} s^{-1}. However, this was not found to be the case after the second illumination, as all spectral features of light-dark spectrum recovered with same rate constant of $\sim2\times10^{-3}$ s^{-1} in ~15 minutes,

This recovery kinetics corresponds to reaction scheme for manganese oxidation, which is described equation (3.1). The system starts with $PQ:Mn^{2+}$ state and upon light excitation, manganese is oxidized. The oxidized manganese is being replaced by Mn^{2+} while the Q- recovers

to Q. Finally, the Mn^{2+} returns to same binding position and the system restores to PQ:Mn^{2+} state. This means that the recovery of PQ^{-} to PQ state and replacement of oxidized Mn^{3+} with Mn^{2+} can occur in two different rates.

The observed difference for earlier recovery of the electrochromic shift of P with respect to Q- state after first illumination does not necessarily mean that these spectral features are originated from different sources. It could, therefore, be possible that after first illumination the position of Mn^{3+} is not properly in line with the Qy dipole of P and as the quinone recovers to its neutral state, leaving the Mn^{3+} from effective arc of the dipole takes place faster than and recovery of reduced quinone.

These PQ^{-} spectra lack the large electrochromic shift of dimer because the BRCs were in the dark-adapted conformation before the addition of manganese. After first and second illuminations the BRCs are still predominantly in the dark-adapted conformation. The lack of pre-illumination prevents manganese to occupy the most advantageous position. Pre-illumination prior to addition of manganese is mandatory to observe the highest electron transfer rate. Upon addition of manganese the subsequent illuminations will not help the BRCs to turn to conformationally altered state, and the manganese will occupy somewhere further away from P and no interaction with P is obvious from the spectrum (inserts in Figure 3.9).

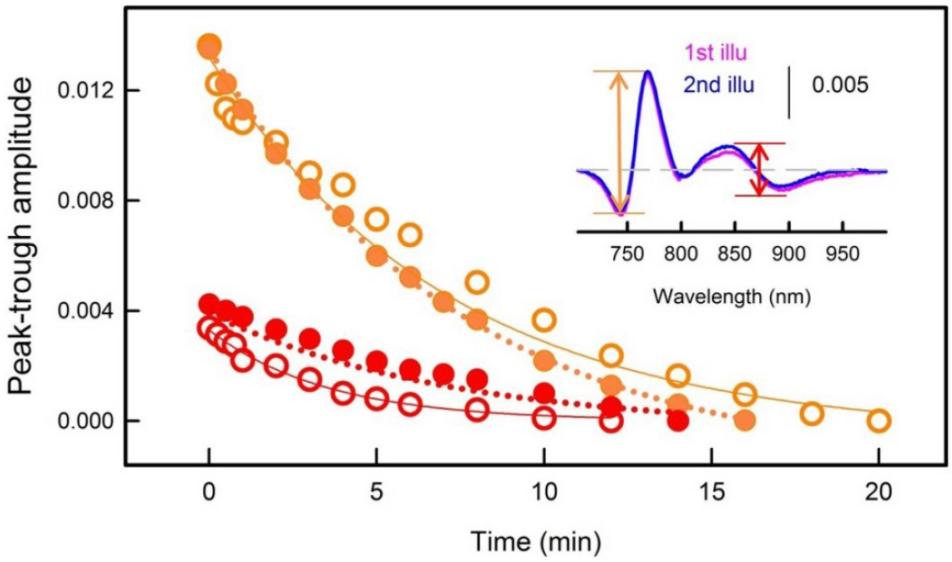

Figure 3.9: Recovery of the light-induced spectral changes after first and second illumination in the presence of manganese at low LDAO concentration. The insert shows the light - dark difference spectra promptly after first and second illumination was stopped. The orange and red double head arrows show where the peak-trough amplitudes are measured. Open and closed circles represent first and second illumination, respectively, while red and orange symbols represent peak-to-trough amplitudes of the 865 nm shift of the P band and the 757 nm shift of the Bpheo- band, respectively. Solid and dotted lines represent single exponentials yielding to rate constants at 865 nm and 757 nm, respectively: 4×10^{-3} s^{-1} and 2×10^{-3} s^{-1} for first illumination, 2.2×10^{-3} s^{-1} and 2.3×10^{-3} s^{-1} for second illumination. Conditions as for the traces in Figure 3.2.

We performed similar experiments in the presence of elevated LDAO concentration at pH 9.4, 9.0 and 8.7 to monitor the influence of altered dielectric environment on the binding and oxidation of manganese. After the first illumination in all probed pHs, the peak-to-trough amplitudes of two main spectral features of PQ^- state: the blue shift of the dimer peak around 865 nm and red shift of bacteriopheophytin peak around 760 nm were observed.(Figure 3.10, panels A-C) While the peak-to-trough amplitudes of red shift of bacteriopheophytins did not changed upon addition of LDAO, its recovery time increased by ~2-fold at pH 9.4. Additionally the peak-to-trough amplitudes blue shift of dimer around 865 nm is increased by 66% in presence of high LDAO. The main difference by addition of high LDAO concentration was that the recovery of blue shift of dimer. Similarly to low LDAO condition the blue shift of dimer was needed ~10

minutes to be fully recovered after first illumination. However, the change of dimer absorption band was not stopped at high LDAO condition, where the blue shift after recovery transformed to red shift. The amplitude of red shift of dimer increased until ~30 minutes and never fully recovered.

In order to reveal the effect of pH on the binding and oxidation of manganese in altered dielectric environment, the similar experiments were performed at low pH values. The peak-to-trough amplitudes of red shift of bacteriopheophytins and its recovery time did not changed upon lowering the pH. However, the blue shift of dimer recovered in ~5 and ~2 minutes at pH 9.0 and 8.7, respectively and then transformed to red shift. Further increase in the amplitude of red shift of dimer was observed by 41% at pH 9.0 and nearly 3-fold at pH 8.7, where the red shift reached to maximum amount in ~10-15 minutes after illumination was stopped, and then recovered in ~40 and ~80 minutes at pH 9.0 and 8.7, respectively. (Figure 3.10 B,C)

The recovery of the electrochromic signals of PQ^- state: namely the shift of the dimer peak and red shift of bacteriopheophytin peak after the first illumination at high LDAO concentration is fitted to single and double exponential functions, yielding to rate constants, which are shown in Table 3.1. It must be noted that during the course of observation the dimer shift observed after the first illumination changed sign at all three monitored pH values, namely the initial blue shifts (positive signals) were converted to red shifts (negative signals) reaching their maximum values 10-20 minutes after the illumination seized, depending on pH. This is an indication of a de-coupling between the diffusion of the oxidized Mn^{3+} from (characterized by k_3 rate constant) and the diffusion of the fresh, reduced Mn^{2+} to the weak binding site (characterized by k_4 rate constant). The extent of the reversal was increased as the pH was lowered indicating a weakening binding at lower pH values. This can only be interpreted if the bound LDAO

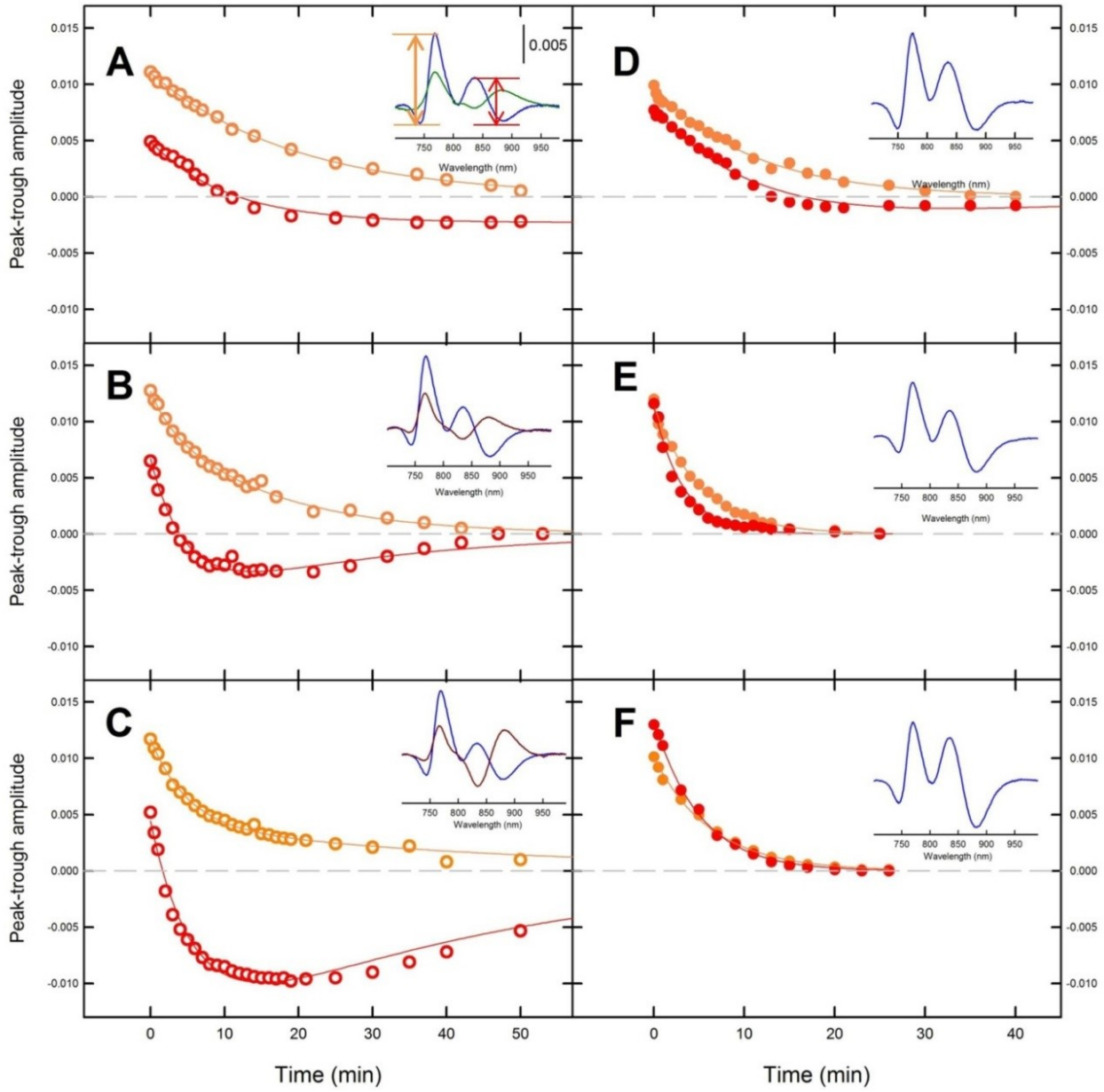

Figure 3.10: The recovery of peak-to-trough amplitude of two main spectral features of PQ- state after first and second illuminations in R-26 BRCs in the presence of manganese at high LDAO concentration. A, B, C: First illumination and D, E, F: second illumination at pH 9.4, 9.0 and 8.7, respectively. The inset shows the light-dark difference spectra promptly after illumination was stopped (blue traces), 10 minutes later (brown trace) and 20 minutes later (green trace). Open and closed circles represent first and second illumination, respectively, while red and orange symbols represent peak-to-trough amplitudes of the 865 nm shift of the P band and the 760 nm shift of the H band, respectively. Solid lines represent fitted single or double exponential function. Conditions: 1 μM R-26 BRC in 1% LDAO, 80 mM BTP, 30mM Mn^{2+} at various pHs. Continuous illumination excitation of 0.95 W/cm^2

molecule also changes conformation upon illumination. After the second illumination the two monitored electrochromic signals recovered in similar rates and the reversal of the blue-shift of the P band was not observed, rather its amplitude has grown by 2-fold compared to that observed after the first illumination.(Figure 3.10 D,E and F panels)

pH	Red shift of Bpheo band at ~760 nm				Shift of P band at ~ 865 nm			
	A_1	k_1 (s^{-1}) $\times 10^{-4}$	A_2	k_2 (s^{-1}) $\times 10^{-3}$	A_3	k_3 (s^{-1}) $\times 10^{-3}$	A_4	k_4 (s^{-1}) $\times 10^{-4}$
9.4	0.011	8.3	_	_	0.007	1.6	_	_
9.0	0.010	10	0.002	6.4	0.016	3.4	-0.007	6.6
8.7	0.004	3.5	0.007	3.4	0.021	0.28	-0.016	4.0

Table 3.1: The relative amplitude and rate constants assigned to recovery of spectral features of PQ^- state, red shift of bacteriopheophytin peak at 757 nm and the shift of dimer band at 865 nm after first light excitation, fitted to double exponential function at different pH. In the recovery of red shift of Bpheo band at ~760 nm, the fast and slow components were assigned to oxidation of from the secondary (Q_A^-) or the primary (Q_B^-) reduced quinones, respectively. In the recovery of shift of P band at ~ 865 nm, the k_3 and k_4 rate constants were assigned to the diffusion of the oxidized Mn^{3+} and the diffusion of the fresh Mn^{2+} to binding site, respectively.

The recovery of peak-to-trough amplitude of spectral features of PQ^- the shift of the dimer peak around 865 nm and red shift of bacteriopheophytin peak around 760 nm after second illumination at high LDAO concentration could be well fitted to single exponential function.(see Table 3.2). As it can be seen, similarly to low LDAO concentration, both spectral features of PQ^- state after subsequent illumination decay with similar rate, which means they are coupled.

pH	Red shift of Bpheo band at ~760 nm		Shift of P band at ~865 nm	
	A_1	k_1 (s^{-1}) $\times 10^{-3}$	A_2	k_2 (s^{-1}) $\times 10^{-3}$
9.4	0.010	1.5	0.008	1.8
9.0	0.011	3.1	0.013	5.0
8.7	0.010	2.6	0.013	3.1

Table 3.2: The relative amplitude and rate constants assigned to recovery of spectral features of PQ^- state, red shift of bacteriopheophytin peak and the shift of dimer band after second light excitation, fitted to single exponential function at different pH.

3.7 EPR data

3.7.1 Replacing manganese with non-redox active metal

It is shown here that by coordination of the manganese ion with BTP into a complex with much lower redox midpoint potential, the manganese ion was able to act as secondary electron donor to the native BRCs. Upon light excitation of Mn-BRC system, the oxidation is triggered and the resulting spectroscopic signatures are the combination of those of binding/unbinding and oxidation of manganese ions. In order to study exclusively the signatures of binding to BRCs, Cu(II) was chosen as a suitable substitute for manganese as it is unable to undergo further oxidation, therefore any observed change in the Cu-BRC system could be interpreted as a signature

of binding. Coordination geometry of the copper ion is not as strict as it is for manganese and the change of coordination can be detected by EPR spectroscopy. Only limited distortion from the octahedral geometry is allowed when Mn(II) is coordinated by different ligands. As a consequences, the EPR spectra of the various mononuclear manganous complexes are very similar to each other (see Figure 3.11). Cu(II) can have many different coordination geometries ranging from octahedral in water to trigonal plane and tetrahedrally distorted square planar in type I and type II Cu-proteins, respectively [68]. The change of coordination geometry can be studied by EPR spectroscopy as the electronic structure of the coordinated Cu(II) can be correlated with the chemical composition. Additional benefit of exploring Cu coordination is that Cu(II) is the only transition metal ion besides iron that is involved in long-range electron transfer in proteins [68].

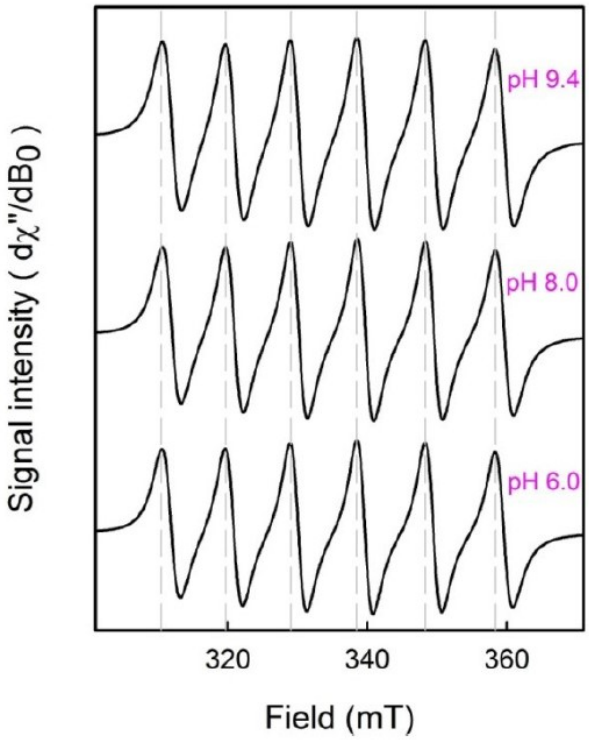

Figure 3.11: The X-band EPR spectra of Mn-BTP complex at room temperature at different pH values. Condition: 10 mM Mn^{2+}, 80 mM BTP, 0.03% LDAO at various pH values. Recorded at ~9.51 GHz.

3.7.2 Formation of the Cu-BTP complex

As explained in Section 3.4, BTP has three protonable states, separated by pK_a values of 6.8 and 9.0 determined in aqueous solutions. It has been reported that BTP is able to coordinate transition metal ions with its hydroxyl and amine groups [57]. Reports of BTP coordinated Cu, however, describe synthetized complexes that are used in biologically incompatible solvents [69]. Here we recorded the EPR spectra of Cu-BTP complexes at various BTP concentration and pH values in order to gain information on the change of coordination geometry of Cu upon association with BTP. BTP-coordinated metal complexes recently have been synthetized to model metal complexes in electron transfer proteins [70].

In the absence of BTP molecules, water molecules coordinate Cu^{2+} in the *hexa-aquo* complex involving six symmetrically arranged water molecules as ligands forming a perfect octahedral around the Cu^{2+} ion. The EPR signature of this complex was observed only at pH 4.0 a broad signal was observed, most likely due to the very short spin relaxation time in this complex. As the concentration of BTP increased, new spectral features were raised, indicating that the water molecules are replaced by BTP molecules, forming a Cu-BTP structure. In order to describe the coordination of Cu^{2+} ions with BTP molecules, the increment of the relative amplitude of the signal intensity at particular value of the magnetic field as a function of the added BTP was plotted. As it can be seen in Figure 3.12 this behavior followed the binding equation (2.3). Fit to this equation with two BTP ligands per metal, yielded K_D values of 5.54 mM, 5.52 mM and 4.90 mM at pH 5.0, 7.0 and 9.0, respectively. While at pH 9.0 the data fitted well to binding equation with 2 BTP/Cu^{2+} stoichiometry, at low pH the exact stoichiometry is not obvious. The observed pH dependency suggests that the coordination is changing as the amine groups successively deprotonate.

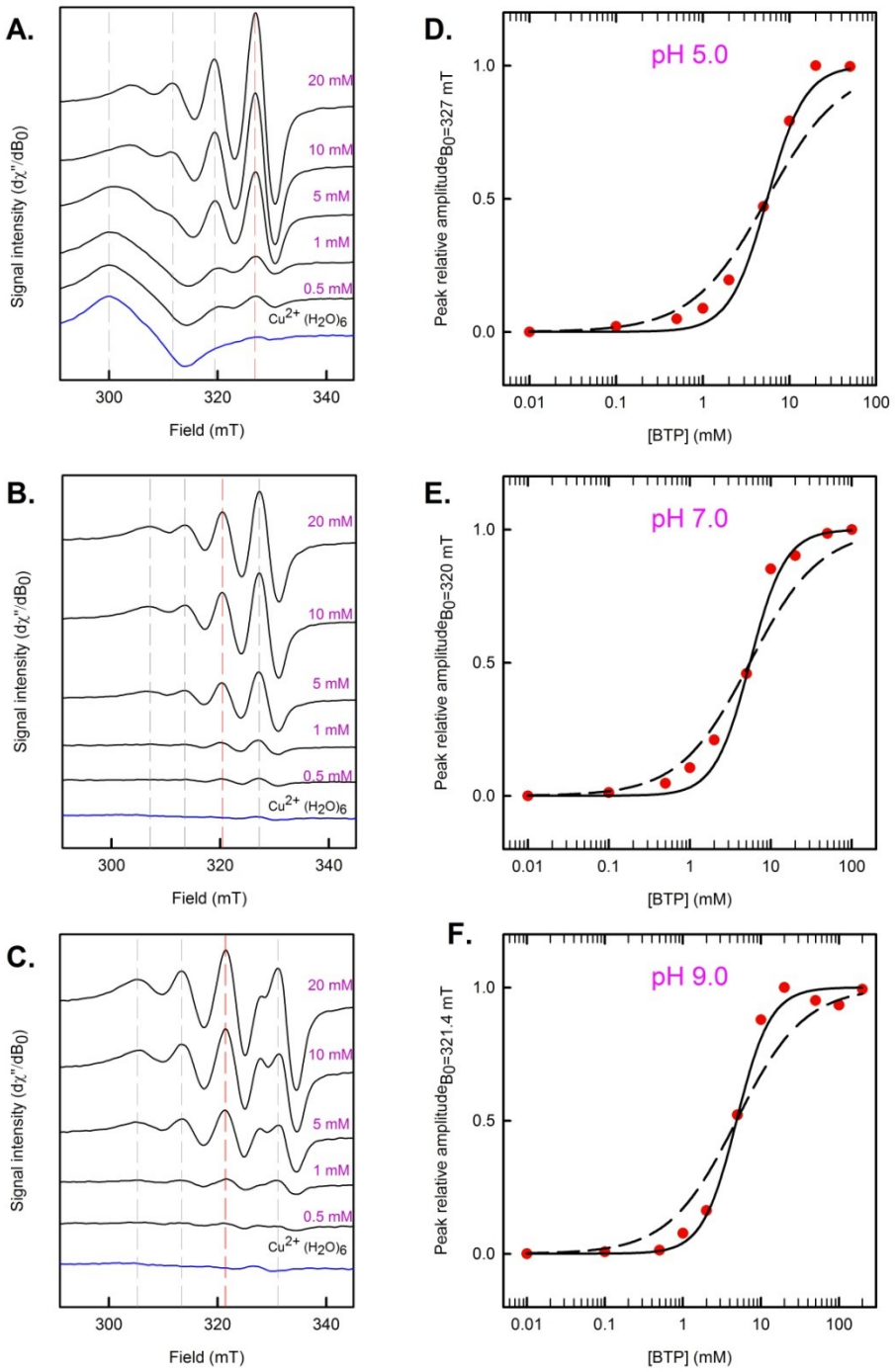

Figure 3.12: Change in coordination by addition of BTP to in hexa-aqua complex. Panels A, B and C represent the X band EPR spectra recorded at ~9.41 GHz of Cu-BTP complex at pH 5.0, 7.0 and 9.0, respectively. Dependence of the intensity of spectra on BTP concentration are shown in panels D to F. The solid circles in red represent the relative intensity of the signal at the magnetic field, which is indicated in panels A, B, C as vertical red dashed lines. The dashed and solid lines are fit to the data using the binding equation (2.3) assuming 1 BTP/Cu^{2+} or 2 BTP/Cu^{2+}, respectively .Condition: 10 mM Cu^{2+}, 0.03% LDAO at various BTP concentrations.

3.7.3 The effect of change in pH on coordination of copper in Cu-BTP complex as monitored by EPR

In order to reveal the effect of deprotonation of amine groups of BTP on coordination of copper ions, the pH dependency of Cu-BTP complex was studied by monitoring the EPR spectra of the complex from pH values of 4.0 to 9.5 at a high BTP concentration. Upon increasing the pH two transitions could be identified. These transitions were attributed to the deprotonation of the two secondary amine groups. The shift of the third peak position from ~319 mT to ~322 mT due to changes in the hyperfine coupling constant (a sensitive parameter that reflects change in coordination) is plotted as function of pH in Figure 3.13. The data were fitted by using Henderson-Hasselbalch model (equation 2.5). The obtained pK_a values are 5.8 and 8.7 for Cu-BTP complex. These values represent 1.0 and 0.3 pH unit shifts from the reported aqueous pK_a values of BTP. It can be seen that the steepness of the curve at low and high pH follows the deprotonation of one and two groups, respectively. This therefore suggests that at low and high pH, the Cu^{2+} is coordinated by one and two BTP molecules, respectively.

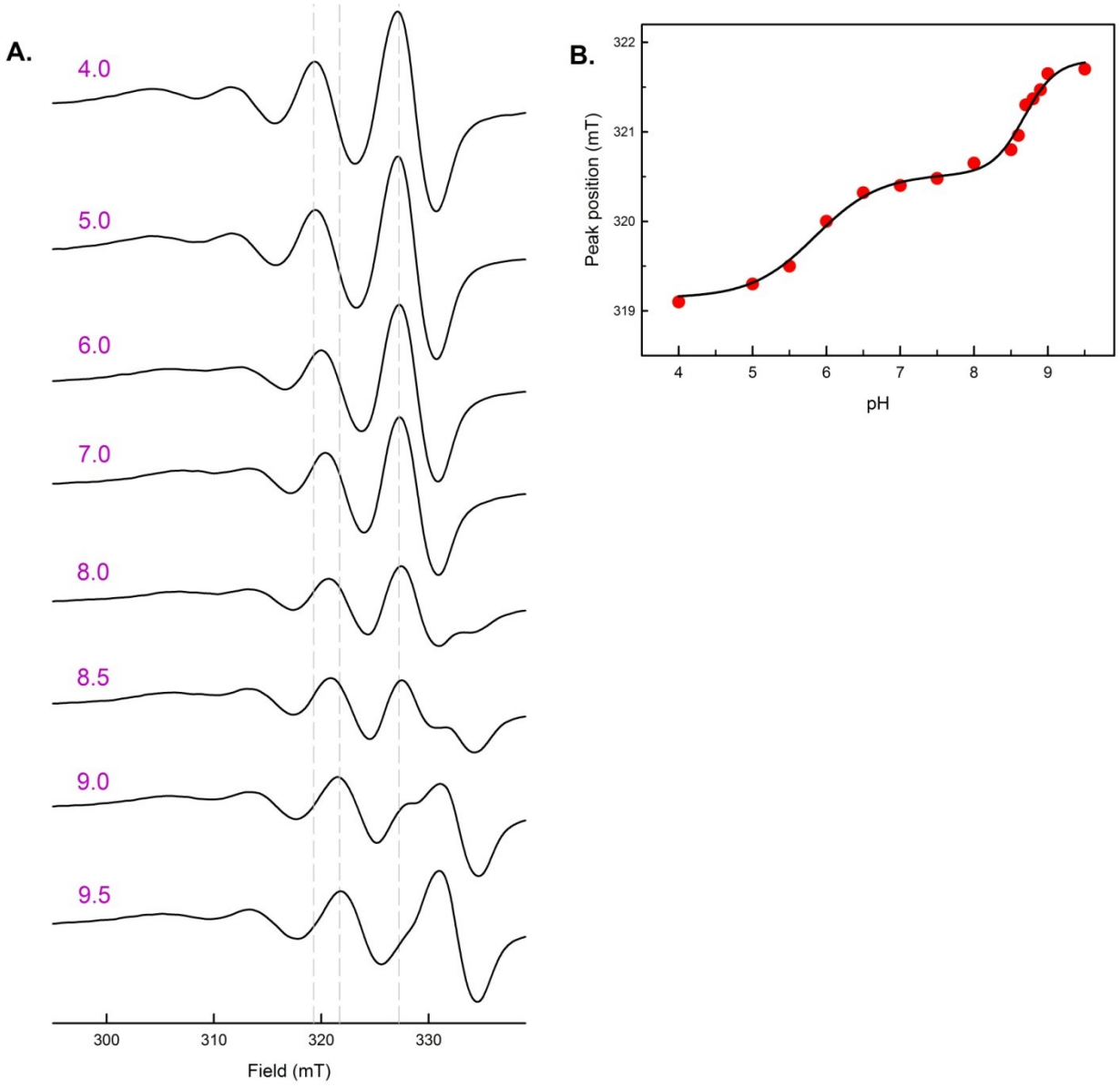

Figure 3.13: Change in coordination by deprotonation of amine groups in Cu-BTP complex. A: X band EPR spectra of Cu-BTP complex recorded at ~9.41 GHz at various pH. B: shift of third peak position from 319.1 mT to 321.7 mT. Black curve represents fitting to Henderson-Hasselbach model with 1 H^+/pH (equation 2.4) and 2 H^+/pH (equation 2.5) at low and high pH, respectively. The apparent pK_a values obtained were 5.8 and 8.7. Conditions: 10 mM Cu^{2+} in 0.5 M BTP, 0.03% LDAO.

3.7.4 Simulation of Cu-BTP complex EPR spectra

The simulated spectra for Cu-BTP complex for low and high pH values show different configurations of the complex. The simulation of EPR spectra was done by EasySpin software and the simulated spectra and the fitted parameters, along with the observed spectra, are shown in Figure 3.14 and Table 3.3, respectively. The spread of the wings at lower magnetic fields in the simulations are not reproduces as it is an effect associated with the tumbling in the liquid state whereas the simulations are done in the solid state (rigid limit) [78].

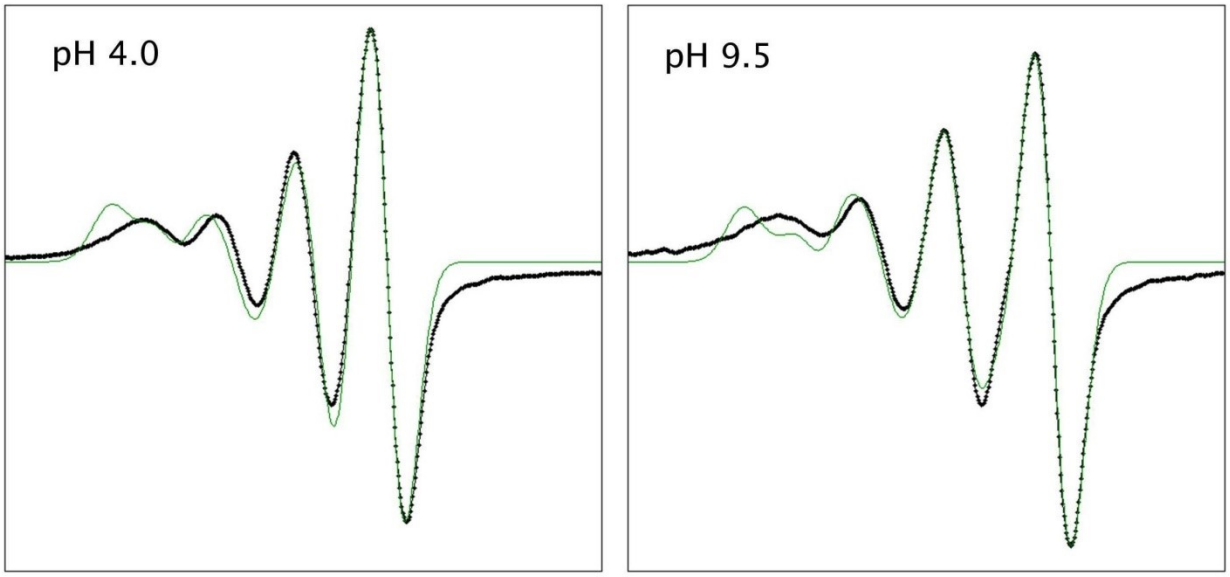

Figure 3.14: The simulated EPR spectra of Cu-BTP complex at low and high pH. The solid black and green spectra represent experimental and simulated spectra, respectively. The simulation shows the spectrum in the rigid limit (solid state), whereas the experimental spectrum is in liquid state at room temperature. As a consequence the low field lines are smeared out due to the tumbling motion of the complex, not simulated in the rigid-limit simulation.

pH	4.0	9.5
g(1)	2.1202	2.1274
g(2)	2.1004	2.1085
g(3)	2.1469	2.0585
A(1) (MHz)	218.86	305.68
A(2) (MHz)	145.87	215.13
A(3) (MHz)	270	110.47
$\bar{g}$	2.1225	2.0981
$\varepsilon^{\perp}$	0.0093	0.0090
$\varepsilon_{\parallel}$	0.0114	-0.0188

Table 3.3: The EPR parameters obtained from the simulated EPR spectra of Cu-BTP complex at low and high pH. The mean value of $\bar{g}$, axial ($\varepsilon^{\perp}$) and longitudinal ($\varepsilon_{\parallel}$) anisotropies are calculated by following equations: $\bar{g} = (g(1) + g(2) + g(3))/3$, $\varepsilon_{\perp} = |g(1) - g(2)|/\bar{g}$ and $\varepsilon_{\parallel} = (g(3) - \bar{g})/\bar{g}$.

The distortion of the Cu-BTP octahedron can be estimated by calculating the axial ($\varepsilon^{\perp}$) and longitudinal ($\varepsilon_{\parallel}$) anisotropies as listed in Table 3.3. If the axial ($\varepsilon^{\perp}$) and longitudinal ($\varepsilon_{\parallel}$) anisotropies are equal to zero, the geometry of the complex will be a symmetrical octahedron (Figure 3.15 A). In the present case the values of $\varepsilon_{\perp}$ are ~0.9%, indicating only a small departure from the axial symmetry, whereas the values of $\varepsilon_{\parallel}$ indicate less than 2% elongation or compression along the z-axis. The positive and negative values of the longitudinal ($\varepsilon_{\parallel}$) anisotropy indicate compression and elongation along the z-axis of octahedron, respectively (Figure 3.15 B, D). The value $\varepsilon^{\perp}$=0 shows the presence of square-planer geometry of the octahedron. From Table 3.3 the calculated axial ($\varepsilon^{\perp}$) anisotropy of Cu-BTP complex for both pH 4.0 and 9.5 are positive values,

indicating that the geometry of complex is distorted from square planer (Figure 3.15 C). Additionally the longitudinal ($\varepsilon_{\parallel}$) anisotropy is positive at pH 4.0 and negative at pH 9.5, which indicates that the Cu-BTP complex has been compressed and elongated along the z-axis of the octahedron at low and high pH values, respectively.

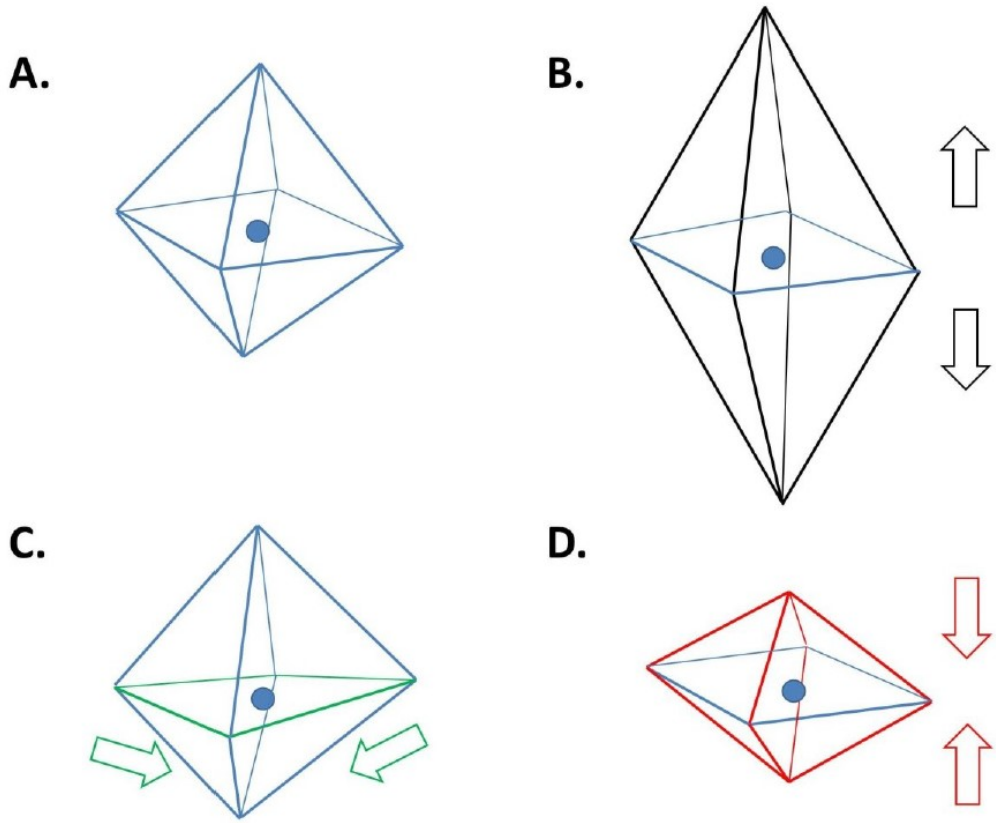

Figure 3.15: Plausible geometries for Cu-BTP complex. The perfect symmetrical octahedron is represented in panel A. The distortion from this symmetrical octahedron could occur as elongation (B), distortion of square plane (C) and compression (D). The arrows show the directions of the distortions. The location of the Cu(II) ion inside the octahedron is indicated as a blue solid circle.

Chapter 4

Discussion

In this work we extended the study of BTP coordinated metal binding and oxidation to involve broadened pH regime and dielectric tuning. Recently it was shown that upon spontaneous coordination of Mn^{2+} with hydroxyl and amine groups of bis-tris propane, the Mn^{2+} /Mn^{3+} midpoint potential was lowered to ~400 mV at pH 9.4, and allowed it to bind and serve as secondary electron donor to native BRC [43]. The rate of electron transfer from Mn^{2+} to P^{+} was successfully competed with charge recombination.

This is particularly interesting as environmental factors were required to incorporate Mn^{2+} as secondary electron donor to native BRC, freeing the system from genetic modification. Additionally from evolutionarily point of view, this process serves as proof of alternative transition mechanism for the development of oxygen producing photosynthesis.

We mapped the pH dependency of the diffusion of manganese ions to binding site. The influence of pH on the electron donation process highlights the importance of the deprotonated amine groups of BTP in the proper coordination of the complex.

In our current work we revealed that the binding is facilitated by light-induced conformational changes. In order to characterize the accessibility of the binding site, the local dielectric constant was altered by incorporating hydrophobic molecules, such as detergents to the vicinity metal binding site.

4.1 Pre-illumination history influences the diffusion of Mn^{2+} to metal binding site 1 and its oxidation

Photoactivation, namely subsequent illumination has been shown to be required for the photoassembly of the Oxygen Evolving Complex (OEC) in PSII [65]. The electron transfer form Q_A^- to Q_B in BRC has also been demonstrated to require structural changes [66]. In genetically modified BRCs, where tyrosine oxidation was enabled by highly elevated P/P^+ potential and the introduction of Tyr residues to positions analogous to the redox active Tyr residues of PSII. The Tyr oxidation was also found dependent on the light-induced structural changes near P [40].

Here we found that both the rate of oxidation of the bound Mn^{2+} and its diffusion to the proposed binding site were dependent upon the conformational state of the BRC (Figures. 3.2-3.4). In the light-adapted conformation (induced by pre-illumination prior to addition of Mn^{2+}) the rate of electron transfer was found to be 50% to 3-fold higher depending on the pH than in the dark-adapted conformation at the same pH value (Figures 3.2-3.4). It is anticipated that the electron transfer rate from manganese to P^+ decreases with decreasing pH. If one assumes change only in the driving force over the pH, generally one order of magnitude change of the rate constant is expected over one pH unit indicating the involvement of one proton that likely determines the oxidation potential of one of the reacting entities [55]. This would mean that the difference in mid-

point potentials should be changing with a slope of ~60 mV/pH at room temperature [38]. This value corresponds to the pre-logarithmic term in the Nernst-equation at room temperature assuming the transfer of one electron. The pH dependency of the P/P^+ potential was reported to be very modest with a value of only ~6 mV/pH between pH 7.0 and 10 [67]. It should be noted, however, that this value was determined in the absence of any metal. Our group also found nearly identical potentials for the P/P^+ potentials in the presence of Manganese at pH 8.0 and pH 9.4 [48,43]. The modest pH dependence was interpreted by the electrostatic stabilization of P^+ by the nearby amino acid side chains that deprotonate, and thus provide an accumulation of negative charges near P^+. The pH dependence of the oxidation potential of Mn^{2+}/Mn^{3+} in BRCs when coordinated with bicarbonate was reported to have a slope of -63 mV/pH in the same range between pH 7.0 and 10 [38]. There the manganese was not bound to the BRC, so the strong pH dependence is attributed to the lack of strong association and interaction between the manganese and the BRC. Here the observed 0.9 order of magnitude/pH slope change of the rate constant in the dark-adapted BRCs (Figure 3.7 panel A) also indicates that there must not be a strong binding between manganese and the BRC. This slope is also indicative of the transfer of only one electron that must be electrostatically compensated by the loss of one proton, hence the difference of mid-point potential should have a ~-60 mV/pH slope. Contrarily, in the light-adapted BRCs that were subjected to light-induced conformational changes before addition of manganese we only observed a -0.70 order of magnitude/pH slope in the pH dependence of the electron transfer from manganese to P^+ (Figure 3.7 panel A). Since the P/P^+ potential in the presence of Mn^{2+} in this pH regime is nearly independent of pH this dependence must be attributed to the elevation of the potential of Mn^{2+}/Mn^{3+} as the pH was lowered. This pH dependency, however, is weaker than the one expected without association (1 order of magnitude/pH), thus binding to BRC electrostatically stabilizes the manganese cofactor.

The pH-dependence of the rate of diffusion to the active site is nearly pH independent in the dark-adapted BRCs and shows a two-phase dependence in the light-adapted BRCs (Figure 3.7 panel B). The lack of strong pH dependence in the dark-adapted BRCs is consistent with the lack of strong interaction, whereas the two phases in the light-adapted BRCs can clearly be related to the two protonational states of BTP. Below pH ~9 in the semi-deprotonated form BTP provides weaker coordination to manganese and thus moderate dependence on pH is observed. Diffusion to the binding site slows down above pH 9.0 as the BTP loses another proton from its second amine group.

As it was explained in Section 1.6 Introduction, light-induced conformational changes of the BRC, which have been shown to occur in the cavity of protein, near B_B, precisely where the manganese binds to BRC. The light-induced conformational changes are consequence of deprotonation of M210 Tyr. The maximum influence of light-induced structural changes on increasing the local dielectric constant of the hydrophobic cavity of BRCs was observed at low pH values such as pH 6.0, since most of the residuals are still protonated [9]. At higher pH values the probability of deprotonation of amino acid side chains nearby P increases, therefore the effect of light-induced structural changes on increment of local dielectric constant decreases as the pH is raised. This in line with our observation that the effect of light-induced conformational changes on acceleration of Mn^{2+} diffusion to metal binding site of BRCs was decreased upon increasing the pH. At low pH the effect of pre-illumination on acceleration of Mn^{2+} diffusion to the binding site is pronounced, but the observed difference is diminished at higher pH values between the dark- and light-adapted conformations.

4.2 Two possible electron donating manganese

We observed further evidence of diffusion of manganese to metal binding site of BRC when reaction centers were incorporated with various Mn^{2+} concentrations. The nearly ~2-fold difference in the observed ET rate from decomposition of kinetics manganese oxidation using continuous saturating illumination (Figure 3.5 panel B) clearly suggest two different reaction are taking place. The faster process observed in Figure 3.5 suggests a rapid, first-order kinetics from a bound Mn^{2+}, while the slower process can be attributed to a second-order reaction, where the electron donation is limited by the slow diffusion of the Mn^{2+} to and from the vicinity of P.

At low concentration of manganese due to low driving force, manganese is unable to bind to proteins and Mn-BRC complex (bound Mn^{2+} to BRC) cannot be formed. The minimum concentration of ~2 mM manganese was needed to observe the initial evidence of manganese at bound state to BRC. It was particularly interesting that manganese ions even at free state were able to reduce oxidized dimer, but at slow rate. The slow component of rate constant linearly increased with concentration of added Mn^{2}, indicating that the driving force of manganese diffusion to vicinity of P has been increased due to increased number of collision between Mn^{2+} and BRC. However, the relative amplitude of slow component slower component fell, in favor of the faster component, as the concentration of Mn^{2+} increased. The concentration of 5 mM manganese was enough to convert ~50% of BRCs to Mn-BRC complex. At high concentration of manganese, the faster ET from Mn^{2+} to P^{+} totally originates from bound manganese, indicating a rapid first order manganese oxidation process.

The rate constant for ET from Mn^{2+} to P^{+} assuming originates from bound manganese to BRC is 1.22 s^{-1}, leads to time constant of 0.81 s, which can compete with wasteful $P^{+}Q_B^{-}$ charge

recombination with lifetime of ~1-10 s. This time constant for cyt c_2 (natural secondary electron donor), ferrocene and 3,6-diaminodurene (DAD) are ~ 1 µs, ~250 µs and 1 ms, respectively [9]. The association between Mn^{2+} and the BRC has been determined by assuming binding of two manganese ligand, leads to dissociation constant of 6.5 mM. This observation is in line with pervious study, which the dissociation constant of 6.5 mM was determined by monitoring flash-induced kinetics of Mn-BRC system [43].

The second order rate constant for Mn^{2+} has been measured at 3.5×10^2 $M^{-1}s^{-1}$. The second order rate constant for Mn^{2+} with mutant BRC was reported 9×10^4 $M^{-1}s^{-1}$ [38]. Much faster second-order rate constant was measured, 10^9 $M^{-1}s^{-1}$ for reduction of P^+ by cyt c_2 [58].

4.3 Influence of LDAO on tuning the local dielectric environment of metal binding site 1

Besides prolonged illumination the conformation of the BRC near P can also be altered by selective use of detergent molecules. Two decades ago it was demonstrated that the use of sulfobetaine detergents, such as SB12 resulted in shifts the optical absorbance spectrum of P from 865 nm to 850 nm in *Rhodobacter sphearoides* [71]. This shift was accompanied by the spin density ratio of P^+ between P_L and P_M, namely the probability of the localization of the electron hole on either the L or M half of the dimer, to change from 2:1 ratio to 4:1 ratio [72]. This spin density change indicates that the bacteriochlorophyll dimer behaves more monomeric in the presence of these detergents. The molecular origin of these detergent-induced conformational changes were not identified that time but our group has recently found similar shifts in the absorption band of P in *Rhodobacter capsulatus* (a very similar strain to *Rhodobacter*

sphaeroides) in the presence of LDAO detergent [8]. The spin density distribution and the position of the P band was systematically altered by the use of detergents with positive (CTAB, cetyltrimetylammonium-bromide), zwitterionic (LDAO) and negative (DOC, deoxycholate) headgroups. The detergent-induced conformational change was combined with light-induced conformational change to identify that the shift of the optical absorbance band of P was caused by the out of plane rotation of the 2-acetyl group of P_L [8]. This shift did not influence the oxidation potential of P/P^+ in the dark-adapted conformation but provided an additional ~70 mV drop in the potential in the light-adapted conformation on top of the ~80 mV drop detected in BRCs without the blue-shift of the P band. Here using BTP coordinated Mn as electron donor to BRC we found that the large blue-shift of the P band can only be seen upon the light-induced oxidation with manganese if the BRCs were in the light-adapted conformation ([43], Figure 3.10). This is consistent with the presence of an entity with an extra positive charge along the Qy transition moment of P, similarly to the presence of a detergent molecule with positive charges [71]. By increasing the LDAO concentration and thus, increasing the population of LDAO molecules in the vicinity of the binding site in the cavity (please see Figure 4.1 for reference) the shift of the P band can be increased as evidenced by the larger derivative signal in the optical spectra around 865 nm (Figure 3.10 panels D, E, and F inserts). High LDAO concentration, however, also means that the cavity must be shared by free Mn ions and LDAO molecules and the replacement of the oxidized Mn^{3+} to Mn^{2+} via diffusion became slower (Figure 3.10 panels A, B, and C). At low LDAO concentrations in both dark- and light adapted conformations of the BRCs the recovery of Q^- (measured as the time dependent difference of the signals measured at 770 nm and 745 nm) was found to be the rate limiting step to make the BRC open again for a new photocycle [43]. Here at high LDAO concentration in the dark-adapted conformation the replacement of the oxidized Mn^{3+} with a fresh Mn^{2+} became the rate limiting step (Figure 3.10 A, B, and C panels). The positively

charged manganese ions were displaced (hence the reversed electrochromic shift of the P band) and were replaced with Mn^{2+} on a long timescale, which is in line with our observation that the Mn^{2+} is needed 40-60 minutes to completely diffuse to its binding position in dark-adapted BRCs (see Figures 4.2 and 3.4).

The maximum observed reversed electrochromic shift of the P band corresponds to a de-coupling between the diffusion of the oxidized Mn^{3+} from and the diffusion of the fresh, reduced Mn^{2+} to the weak binding site. This decoupling can only be explained if one allows the bound LDAO molecule to be part of the light-induced conformational change as proposed earlier [8, 72, 73]. At this point the spectroscopic signature of bound manganese to RC is lost. The amplitude reversed electrochromic shift of the P band corresponds to distance which Mn^{3+} is being thrown out from initial binding site. At high pH due to higher affinity of manganese binding this distance is too short, and increased by nearly 41% and 3-fold by lowering the pH to 9.0 and 8.7, respectively.

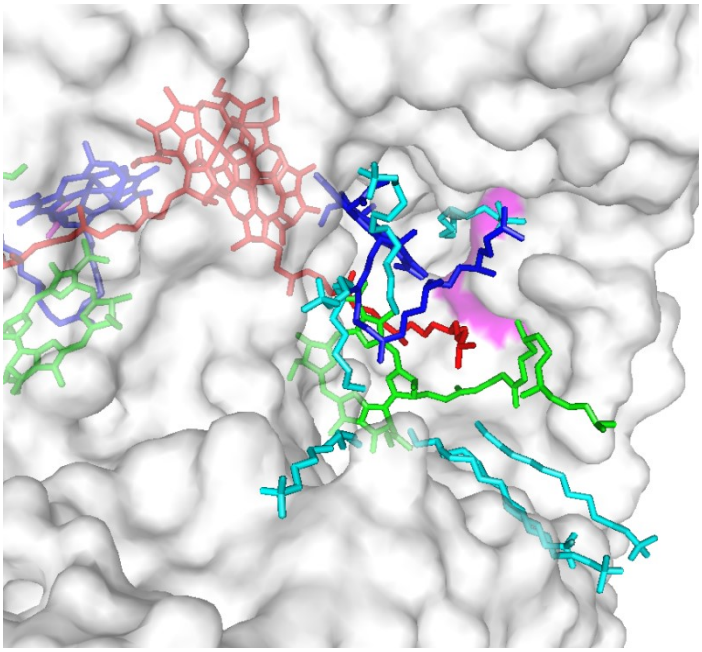

Figure 4.1: X-ray crystallographic image of showing LDAO molecules in the vicinity of the site 1. The protein is shown with gray semi-transparent surface, and the metal binding site is colored pink. The cofactors of reaction center are colored red, blue and green for bacteriochlorophyll dimer, bacteriochlorophyll monomer and bacteriopheophytins, respectively. In R-26 multiple LDAO molecules (cyan) have been observed to bind to the BRC in this region, with one bound precisely to Site 1. Atomic coordinates taken from PDB code: 2UXK.

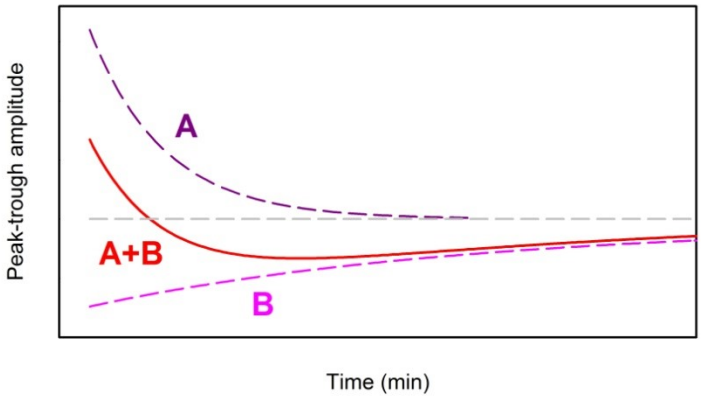

Figure 4.2: Decomposition of peak-trough amplitude recovery of shift of P band at pH 9.0. The A and B processes are assigned to displacement of Mn^{3+} and diffusion of Mn^{2+} to binding site, respectively. The composition of these two processes (A+B) is recovery of shift of the P band.

As explained in Section 1.2.2 Introduction, the binding sites of Q_A and Q_B, the primary and secondary electron acceptors are very different in nature, where the Q_B is located near the hydrophobic cavity of RC, and Q_A is shielded inside hydrophobic region of protein, tightly bound to the complex in contrast to Q_B.

Due to this difference in binding environment the recovery of the PQ_A^- state requires the reduced quinone to find an electron acceptor from its hydrophobic surroundings, and thus takes much longer time than the recovery of PQ_B^- state, where Q_B binding site provides limited accessibility to plausible oxidizers inside the solvent, such as Mn^{3+} in our case.

The binding affinity of Q_B strongly depends on environmental conditions, such as presence of metal ions and variation of pH. At higher pH the Q_B is loosely bound and its binding affinity increases by lowering the pH [75]. It has been reported that at pH 9.4 manganese ions are able to access to Q_B binding site and trigger the displacement of Q_B from its binding site [46]. This process could be intensified upon presence of a detergent molecule with positive charges such as LDAO, where the binding affinity of Q_B decreases due to enhancement of the dielectric constant of hydrophobic cavity of RC.

Briefly we anticipate that at high LDAO concentration, presence of manganese and high pH, due to displacement and limiting electron transfer to Q_B, the recovery of Q^- state takes much longer time, since the only reduced quinone is Q_A. However the contribution of faster recovery of Q_B^- must be observed, as the pH lowers.

This in line with our observations, where at high LDAO concentration in the dark-adapted conformation the recovery of Q^- was found to be biphasic, with the faster component due to BRCs in the PQ_B^- state, and the more slow component due to those in the PQ_A^- state (see Table 3.1)

At high pH only contribution of slow component in the recovery of Q^- was observed, since primary quinone Q_A is only active electron acceptor. As the pH decreased, the fraction of the fast

component that accounts for the fraction of BRCs that have active secondary quinone Q_B increased.

Additionally the kinetics of recovery of shift of P around 865 nm (measured as the time dependent difference of the signals measured with a peak at ~835 nm and a trough at ~885 nm) was found to be biphasic, the component with negative amplitude due diffusion of Mn^{2+} to binding site, and the component with positive amplitude due to removal of the oxidized Mn^{3+}. (see Table 3.1, Figure 3.10 B and C panels)

This indicates that the slow component in recovery PQ^- state, and the component with negative amplitude in recovery of shift of P were yielded to similar rate constants, suggesting that the recovery of reduced primary quinone (Q_A^-) to its neutral state and Mn^{2+} diffusion into binding site are two coupled physical processes.

Contrarily, the recovery of both spectral features of PQ^- state at pH 9.4 are monophasic, where the shift of P band recovers by 2-fold faster $^-$. It could be possible that in the high pH due to high affinity of manganese binding to RCs the oxidized manganese Mn^{3+} does not leave completely the binding site, similarly to low LDAO condition the exchange of Mn^{2+} to Mn^{3+} process takes place coincidentally and we are not able to track Mn^{2+} diffusion to binding site. (see Table 3.1, Figure 3.10 panel A)

As the spectroscopic features fully recover at pH 9.0 and 8.7, the Mn^{2+} can come to binding site and PQ:Mn^{2+} state is re-established.

The larger electrochromic shift of dimer after second illumination does not necessarily means that the replaced Mn^{2+} is now in a more optimal position (Figure 3.10 panels D, E, and F inserts), since we are still in dark-conformation due to fast electron donation of manganese. Before measuring the spectra in subsequent illumination, baseline correction was done for all spectra

measurements. Therefore the effect of reversed electrochromic shift of due to displacing oxidized Mn^{3+} in previous illumination has been added to emerged electrochromic shift of P band. However, as explained in Section 3.5.3, the fraction of P is increased by lowering the pH. Therefore at low pH values some RCs which have not involved in manganese oxidation could be converted to light-adapted conformation. As it can be seen in Figure 3.10, at pH 8.7 the ~90% of RCs are reduced by manganese, therefore they follow the dark-conformation and the rest small fraction could turn to conformationally altered state, therefore manganese could be located in much more closer optimum binding position.

After the subsequent illumination the recovery of peak-to-trough amplitude of spectral features of PQ^- the shift of the dimer peak around 865 nm and red shift of bacteriopheophytin peak around 757 nm were become monophasic, yielding very similar rate constants (see Table 3.2). Similarly to low LDAO condition, it seems that the subsequent illumination facilitate charge displacement, eliminating the rate-limiting replacement of Mn^{2+} to Mn^{3+} process, where it couples to recovery of reduced quinone (Q^-) to its natural state.

The changes in behaviour of the Q^- recovery could be related to light-induced structural changes occur near the Q_B binding site. Based on crystallographic data, it was reported that Q_B could be located either in a so-called distal position in the dark-adapted state of the RC or in a proximal position in the illuminated state. Distal and proximal refer to the Q_B position relative to the non-heme iron. Q_B was proposed to undergo a light-induced shift of ~4.5 Å towards the non-heme iron, accompanied by a 180° propeller twist around the isoprenoid tail [73].

Also the population of proximal bound Q_B in light state is pH dependent, while at pH 7.0 100% of the Q_B are in proximal position, this population decreased to ~25% at pH 10 [74].

These results support our observation, since at high pH the subsequent illumination did not help to activation of Q_B, and the Q^- recovered in long time scale similar to initial illumination due to recovery Q_A^- to its natural state.

However, at low pH the effect of light-induced conformational changes on acceleration of Q^- state recovery is pronounced, where the Q^- recovered ~50 % earlier, likely due to illumination the Q_B is activated and only Q_B^- contribution is observable.

4.4 Three types of manganese binding at metal binding site 1

In the current work we probed the accessibility of metal binding site of RCs by tuning the dielectric constant of hydrophobic cavity of BRC. The structure of metal binding Site 1 is shown in Figure 4.3. The residues make up this site are Ser M119, Met M122, and Tyr M177. At low LDAO concentration, the Mn^{2+} could be well coordinated by these three residues, if the BRC has undergone light-induced conformational change. This binding position could be labeled as the most optimal binding geometry, corresponding to fast oxidation of manganese with a rate constant of 1.22 s^{-1} Light-induced structural changes are required for enabling this site. At high LDAO concentration, the bound LDAO molecule in this region interferes with Mn^{2+} binding, due to sharing of binding site between two entities, and forces manganese to be coordinated at position further away, known as sub-optimal binding geometry. The ~18% reduction in rate of manganese oxidation for light-adapted BRCs at pH 9.4 is the consequence of changing manganese location from optimum to sub-optimum binding geometry, as the bound LDAO in vicinity of binding site 1 prevented formation of optimum photo-activated metal binding site.(see Figure 3.4)

Under strong continuous illumination the rate constant of 0.8 s^{-1} for manganese oxidation has been reported in wild type (WT) BRC, which contains carotenoid in the binding site [46]. This rate is exactly equal to the maximum observed electron donation rate in carotenoid-less strain (R-26) BRCs, when they were in dark-adapted conformation. This level of binding is the worst in terms of Mn^{2+} ability to donate electron to P^{+}, and can be labeled as passive binding site.

On the other hand presence of excess LDAO had no effect on the rate of Mn^{2+} oxidation in wild type (WT), where this site was already occupied by carotenoid [46].

This set of observation suggests that manganese binding position in R-26 at dark-conformation is similar to wild type (WT), which is further away from sub-optimum binding position. It seems that we can force this sub-optimum binding geometry be restored without pre-illumination of R-26, if high LDAO is added. The excess of LDAO improved the dielectric constant of metal binding site of dark-adapted R-26 RCs, and the rate of manganese oxidation is increased by ~25%, very close to the level of manganese oxidation rate in light-adapted R-26 in presence of high LDAO, where the manganese located at sub-optimum binding geometry.

While at high LDAO concentration the rate of Mn^{2+} incubation did not changed in dark-adapted RCs, this rate decreased by ~73% in light-adapted RCs to the level of RCs in dark-adapted conformation. As we expected, due to tuning the dielectric constant of metal binding site of BRCs by incorporating detergent molecules, upon manganese presence at sub-optimum binding position the observed differences for manganese binding and oxidation were diminished between the dark and light-adapted conformations.

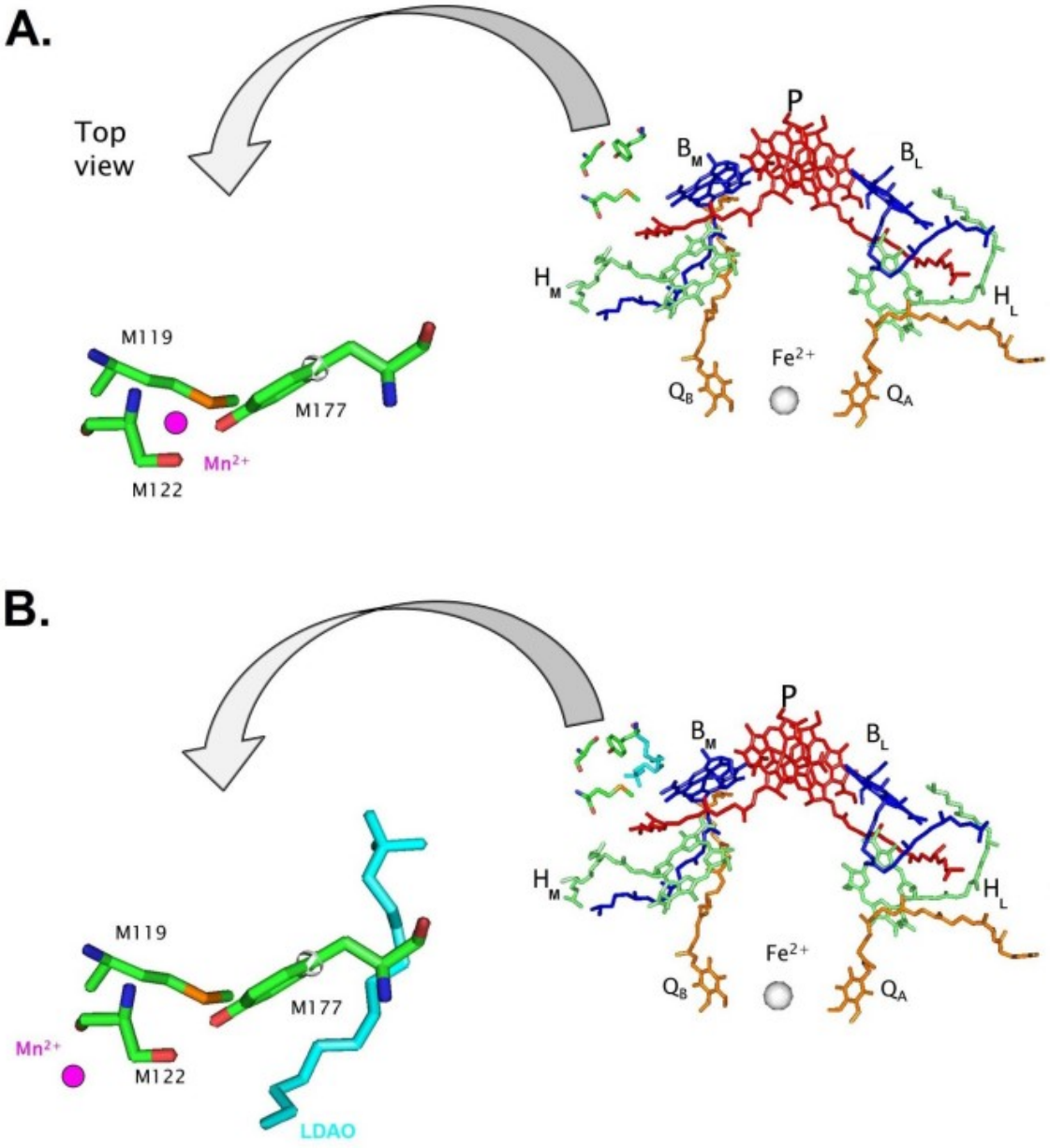

Figure 4.3: Structural views of the BRC showing metal binding site 1 at low and high LDAO concentration. Close up top view of the predicted metal binding site near B_M is shown in left panels. The surrounding cofactors were removed for clarity. This site is composed of the residues: Ser M119, Met M122, and Tyr M177. At high LDAO concentration the binding site 1 is being shared with LDAO molecule and manganese Atomic structures are taken from PDB code: 1PCR.

4.5 The EPR Spectroscopic evidence for structural changes of Cu-BTP complex

The influence of the protonational state of the amine groups on Cu(II) coordination in Cu-BTP complex was studied by EPR spectroscopy for various pH values as the electronic structure of the coordinated Cu(II) ion is correlated with the chemical composition. The Cu(II) ion in the *hexa-aquo* complex is coordinated with six symmetrically arranged water molecules, forming a perfect octahedral around the Cu(II) ion. Upon addition of BTP, new spectroscopic signatures were observed indicating changes in the ligand configuration of the complex as discussed in Section 3.7.4. Increasing the pH of Cu-BTP complex from 4 to 9.5 resulted in changes in the EPR spectra that were modeled assuming the participation of the secondary amine groups of BTP as new ligands as they become available upon their deprotonation.

The shift of the third peak position from ~319 mT to ~322 mT due to changes in the hyperfine coupling constant as function of pH were fitted by using Henderson-Hasselbalch model, where two apparent pK_a values 5.8 and 8.7 were obtained for Cu-BTP complex. The model revealed that at low and high pH, the Cu^2+ ion is coordinated by one and two BTP molecules, respectively (Figure 3.12 and 3.13). This observation is in line with the reported stoichiometry of Mn-BTP complex, where coordination with BTP involves two amine groups per Mn(II) ion [43].

In this study we also determined the *in situ* pK_a of Mn-BTP complex when in association with BRCs. The fraction of the residual P^+ as function of pH was fitted by using Henderson-Hasselbalch model involving 2 protons, and the obtained pK_a value was ~8.2 (Figure 3.8). While the obtained pK_a values of the Cu-BTP complex and Mn-BTP complex associated with BRCs are quite different, involvement of two protonable groups of BTP per metal was observed.

The Cu-BTP EPR spectra change with pH, and are characterized by two different sets of spectra at pH 4.0 and 9.5. The intermediate pH values, particularly for pH values in the 8.0 to 9.0 region, the spectra are admixtures of those corresponding to pH 4.0 and 9.5 (Figure 3.13). For the pH 4.0 to 7.0 the spectra are almost the same. The change in spectra shows that the configurations of Cu-BTP complexes change.

The distortion of the Cu-BTP octahedron was estimated by calculating the axial ($\boldsymbol{\varepsilon}$+) and longitudinal ($\boldsymbol{\varepsilon}_{\|}$) anisotropies, indicating that the geometry of complex is distorted from square planer both at low and high pH values. Additionally, the calculated longitudinal ($\boldsymbol{\varepsilon}_{\|}$) anisotropy indicated that the geometry of the Cu-BTP complex has been compressed and elongated along the z-axis of octahedron at low and high pH values, respectively (Table 3.3 and Figure 3.15).

Chapter 5

Conclusions

This study unraveled many aspects of the interactions between manganese ions acting as a secondary electron donors to native bacterial reaction centers. First, we mapped the pH dependency of the diffusion of manganese ions to binding site 1, which previously the presence of bound manganese at this site had been confirmed experimentally. It was observed that the rate of diffusion to the binding site was at least 3-fold higher for BRCs that underwent light-induced structural changes.

Then the pH dependency of electron transfer from Mn^{2+} to P^{+} in dark-adapted and pre-illuminate BRCs was studied. We determined the rate constant of this electron transfer in light-induced conformationally altered BRCs was 50 % faster than the dark-adapted conformation. Next, we found evidence for slight variations of manganese locations at metal binding Site 1.

The local dielectric constant of metal binding site was altered by incorporating hydrophobic molecules, such as detergents. Tuning the dielectric properties of the binding site by incorporating detergent molecules diminished the observed differences between the electron transfers in the dark- and light-adapted conformation.

This set of observations reveal that the two ways to influence the local dielectric constant of metal binding site of BRCs are: subjecting the BRCs to conformational changes and adding molecules that have access to the cavity. Spectroscopic signature of increasing local dielectric constant of the binding site in presence of detergent molecules was studied and a molecular mechanism for the interaction of Mn^{2+} with BRCs was proposed.

The Cu-BTP EPR spectra change with pH, and are characterised by two different sets of spectra for pH 4.0 and 9.5. The intermediate pH values, particularly in pH 8.0 to 9.0 region the spectra are the mixture of the corresponding to pH 4.0 and 9.5. For the pH 4.0 to 7.0 the spectra are almost the same. The change in spectra shows that the configurations of Cu-BTP complexes are different from each other. As for the Mn-BTP complex, the spectra did not change with pH in the liquid state, because only the central hyperfine sextet was observed, which is rather insensitive to the environmental change when the pH of the solution is changed.

Chapter 6

Future work

The ability of manganese to serve as secondary electron donor to BRC must be tested in preparations that more closely resemble the natural environment of living cells. It is obvious that BTP was not readily available in the Archean ocean. Therefore it is more useful to find more natural compounds to form low potential manganese complexes.

As discussed in Section 3.3, tuning the dielectric properties of the binding site by incorporating molecules, which has access to cavity of RC, such as detergent molecules, the rate of electron donation from manganese was increased for RCs in dark-adapted conformation. The effect of tuning the dielectric constant of metal binding site of RCs must be tested in presence of other electron donors, such as ferrocene and cyt c_2, natural secondary electron donor. Probing the influence changing the dielectric constant of binding site on charge recombination in RCs is recommended as well. Studying the diffusion of manganese ions to binding site of wild type (WT) RC, which contains carotenoid in its binding site will reveal new aspect of interaction of manages with RCs.

It is desirable to measure EPR spectra in the frozen state to be simulated in the rigid limit.

Bibliography

[1] Cavalier-Smith T., Proc. Biol. Sci. 361(1470), 969-1006 (2006)

[2] Nisbet EG, Fowler CMR., Proc. Biol. Sci. 266(1438), 2375-2383 (1999)

[3] Des Marais D., Science. 289(5485), 1703-1705 (2000)

[4] Bittl R, Kawamori A. Photosystem II: The Light-Driven Water: Plastoquinone Oxidoreductase. Springer; p. 390-402 (2006)

[5] Dismukes GC, et al., PNAS. 98(5), 2170-2175 (2001)

[6] Hunter CN, Daldal F, Thurnauer MC, Beatty JT. The Purple Phototropic Bacteria. Dordrecht, The Netherlands: Springer Verlag (2008)

[7] Deshmukh SS. et al., Biochem. 50(3), 340–348 (2011)

[8] Deshmukh SS. et al., Biochem. 50(23), 5249–5262 (2011)

[9] Deshmukh SS. et al., Biochem. 50(16), 3321–3331 (2011)

[10] Koepke J. et al., J. Mol. Biol. 371, 396 (2007)

[11] Umena Y. et al., Nature. 473, 55 (2011)

[12] Nicholas Cox. et al., Science. 345, 804-808 (2014)

[13] McElroy J. D. et al., Biochim. Biophys. Acta. 172, 180-83 (1969)

[14] Norris J. R. et al., Proc. Natl. Acad. Sci. U.S.A. 68, 625-628 (1971)

[15] Feher G. et al., Ann. N. Y. Acad. Sci. 244, 239-259 (1975)

[16] Feher G. et al., Biochim. Biophys. Acta. 267, 222-26 (1972)

[17] Okamura M. Y. et al., Proc. Natl. acad. Sci. U.S.A. 72, 3491-3495 (1975)

[18] DeWinter A., Boxer S.G., J. Phys. Chem. B 103, 8786 (1999)

[19] Pan J. et al., J. Phys. Chem. B 115, 7058 (2011)

[20] Axelrod H.L. et al., Photosynth Res. 85, 101 (2005)

[21] Nugent J. Eur. J. of Biochem. 237(3), 519-531 (1996)

[22] Deisenhofer J. et al., Trends in Biol. Sci. 10(6), 243-248 (1985)

[23] de Paula JC. et al., Biochem. 24, 8114-8120 (1985)

[24] Maxwell R. Biology Newsletter Archive. [Internet]. (2013) Available from: http://biomoocnews.blogspot.ca/2013/10/daily-newsletter-october-9-2013.html

[25] Clayton RK., Photosynth Res. 73, 63-71 (2000)

[26] Parson WW. Modern Optical Spectroscopy. Seattle, WA: Springer; 2009. p. 182-186.

[27] Donohue T. J., et al., J. Bacteriol. 152, 595-606 (1982)

[28] van Mourik F. et al., Biochim. Biophys. Acta 1504, 311 (2001)

[29] Trotta M. et al., Mat. Sci. Eng. C 22, 263 (2002)

[30] Sperotto M.M., Mouritsen O.G., J. Biophys. 59, 261 (1991)

[31] Bowie J.U., J. Mol. Biol. 272, 780 (1997)

[32] Piazza R. et al., Phys. Rev. Lett. 90, 208101 (2003)

[33] Kálmán L. et al., Biochem. 36, 4489-4496 (1997)

[34] Rosen M. J. Surfactants and Interfacial Phenomena. 3, 105-136 (2004)

[35] Roth M., et al., Biochem. 30, (1991)

[36] Deshmukh S., Ph.D. thesis, Concordia University (2013)

[37] Kálmán L. et al., Nature. 402, 696 (1999)

[38] Kálmán L. et al., Biochem. 42, 11016-11022 (2003)

[39] Dismukes GC. et al., Tyryshkin A. PNAS. 98(5), 2170-2175 (2001)

[40] Kálmán L. et al., Biochem. 43, 12905-12912 (2004)

[41] Thielges M. et al., Biochem. 44, 7389 (2005)

[42] Khorobrykh A. et al., Chem. BioChem. 14, 1725 (2013)

[43] Deshmukh SS. et al., BBA Bioenergetics. 1859(4), 227-233 (2018)

[44] Feher, G. and Okamura, M. Y. The photosynthetic bacteria. NewYork: Plenum Press pp. 349-386, (1978)

[45] Maróti P., Wraight C.A., Prog. Photosynth. Res. 2, 401 (1987)

[46] Williams J.C. et al., Research in photosynthesis. Dordrecht, The Netherlands: Kluwer, p. 377-380 (1991)

[47] McPherson P.H. et al., Biochim. Biophys. Acta. 1144, 309 (1993)

[48] Ivanescu M.A., M.Sc. thesis, Concordia University (2014)

[49] Laurie A.T.R., Jackson R.M., Bioinformatics 21, 1908 (2004)

[50] Protheroe Ch., M.Sc. thesis, Concordia University (2016)

[51] Yeates T.O. et al., Proc. Natl. Acad. Sci. U.S.A. 85, 7993 (1988)

[52] Wraight, C.A., Israel J. Chem. 21, 348 (1981)

[53] Ferguson A. et al., Dalt. Trans. 40, 334 (2011)

[54] Kálmán L, et al., Porphyrins Phthalocyanines 11(3-4), 205–211 (2007)

[55] Hay S. et al., Biochem. 44, 35, 11891–11902 (2005)

[56] Utschig LM, et al., Biochem. 37(23), 8278– 8281 (1998)

[57] Utschig LM, et al., Biochem. 44(43), 14131–14142 (2005)

[58] Paddock ML, et al., Proc Natl Acad Sci. USA 96(11), 6183–6188 (1999)

[59. Axelrod HL, et al., Proc Natl Acad Sci. USA 97(4), 1542–1547 (2000)

[60] Gerencsér L, Maróti P., Biochem. 40(6), 1850–1860 (2001)

[61] Kalman L. et al., Biochem. 45, 13869-13874 (2006)

[62] Tang K, et al., Biophysical. 96, 3295–3304 (2009)

[63] Gábor S. et al., Photosynth Res. 136, 379–392 (2018)

[64] Deshmukh SS. et al., American Chemical Society. 133(40), 16309 (2011)

[65] Wydrzynski T., Satoh K. Reviewed in Photosystem II, Ed. The light driven-water: Plastoquinone Oxidoreductase. Springer-Dordrecht (2005)

[66] Xu Q., Gunner M.R., Biochem. 41, 2694-2701 (2002)

[67] Maroti P., Wright C., Biochim Biophys Acta. 934, 329-347 (1988)b

[68] Flores M, et al., J. Phys. Chem B. 119(43), 13825-13833 (2015)

[69] Murrie M., Polyhedron. 150, 1-9 (2018)

[70] Najafpour, Chem. Rev. 116, 2886 (2016)

[71] Muh F. et al., Photosynth Res. 55, 199–205 (1998)

[72] Muh F. et al., Biochem. 36, 4155–4162 (1997)

[73] Stowell, M. H. et al., Science. 276, 812–816 (1997)

[74] Koepke, J. et al., J. Mol. Biol. 371, 396–409 (2007)

[75] McComb J.C. et al., Biochim Biophys Acta. 1015, 155–161(1990)

[76] Van Holde, K. E., Johnson, W. C. & Ho, P. S. Chapter 8: Quantum Mechanics and Spectroscopy. in *Principles of physical biochemistry* (Upper Saddle River, 2006)

[77] https://en.wikipedia.org/wiki/Electron_paramagnetic_resonance

[78] Misra S.K, J. Magnetic. Resonance. 189, 59–77 (2007)